



Fakultät für Physik  
Physics of Energy Conversion and Storage

# **Identification of active sites at model platinum electrocatalysts**

Marcus Dominic Pohl

Vollständiger Abdruck der von der Fakultät für Physik der Technischen Universität München zur Erlangung des akademischen Grades eines

Doktors der Naturwissenschaften

genehmigten Dissertation.

Vorsitzende(r): Prof. Dr. Martin Zacharias

Prüfer der Dissertation:

1. Prof. Dr. Aliaksandr Bandarenka
2. Prof. Dr. Radim Beranek

Die Dissertation wurde am 04.09.2017 bei der Technischen Universität München eingereicht und durch die Fakultät für Physik am 21.09.2017 angenommen.

# Table of Content

<b>1</b>	<b>Abstract</b> .....	<b>3</b>
<b>2</b>	<b>Acknowledgements</b> .....	<b>4</b>
<b>3</b>	<b>Publications and conference presentations</b> .....	<b>5</b>
<b>3.1</b>	<b>Publications</b> .....	<b>5</b>
<b>3.2</b>	<b>Conference contributions</b> .....	<b>6</b>
<b>4</b>	<b>Introduction</b> .....	<b>7</b>
<b>4.1</b>	<b>Current situation and future challenges</b> .....	<b>7</b>
<b>4.2</b>	<b>Aim of this Thesis</b> .....	<b>13</b>
<b>5</b>	<b>Theory</b> .....	<b>14</b>
<b>5.1</b>	<b>Heterogeneous Catalysis and electrocatalysis</b> .....	<b>14</b>
<b>5.2</b>	<b>The Sabatier principle and scaling relations</b> .....	<b>15</b>
<b>5.3</b>	<b>The concept of active sites</b> .....	<b>17</b>
<b>5.4</b>	<b>Activity descriptor</b> .....	<b>18</b>
<b>5.5</b>	<b>The role of single crystal model systems in electrocatalysis</b> .....	<b>21</b>
<b>5.6</b>	<b>The electrochemical interface</b> .....	<b>24</b>
<b>5.7</b>	<b>Fundamental electrochemical equations</b> .....	<b>26</b>
<b>5.8</b>	<b>Effect of the electrolyte composition on the activity</b> .....	<b>28</b>
<b>5.8.1</b>	<b>Effect of cations</b> .....	<b>28</b>
<b>5.8.2</b>	<b>Effect of anions &amp; pH-Effect</b> .....	<b>29</b>
<b>5.9</b>	<b>Electrocatalytic reactions</b> .....	<b>31</b>
<b>5.9.1</b>	<b>Hydrogen evolution reaction (HER)</b> .....	<b>31</b>
<b>5.9.2</b>	<b>Oxygen reduction reaction (ORR)</b> .....	<b>35</b>
<b>5.9.3</b>	<b>Carbon monoxide oxidation (CMO)</b> .....	<b>42</b>
<b>5.10</b>	<b>Electrochemical techniques</b> .....	<b>44</b>
<b>5.10.1</b>	<b>Three-electrode setup</b> .....	<b>44</b>
<b>5.10.2</b>	<b>Cyclic voltammetry</b> .....	<b>45</b>
<b>5.10.3</b>	<b>Rotating-disk electrodes and hanging meniscus – rotating disc electrode measurements</b> .....	<b>46</b>
<b>5.10.4</b>	<b>Electrochemical impedance spectroscopy</b> .....	<b>49</b>
<b>6</b>	<b>Experimental</b> .....	<b>51</b>
<b>6.1</b>	<b>The electrochemical cell</b> .....	<b>51</b>
<b>6.1.1</b>	<b>Preparations before electrochemical measurements</b> .....	<b>52</b>
<b>6.1.2</b>	<b>Evaluation of the hydrogen evolution – activity</b> .....	<b>53</b>
<b>6.1.3</b>	<b>Evaluation of the oxygen reduction – activity</b> .....	<b>54</b>
<b>6.1.4</b>	<b>Evaluation of the carbon monoxide – oxidation activity</b> .....	<b>54</b>

6.1.5	Evaluation of the role of the spectator species on the performance of active sites..	54
6.2	Modification of single crystal electrodes.....	55
6.2.1	Copper underpotential deposition (Cu UPD) and stripping .....	55
6.2.2	Dealloying of Pt(111)/Cu surface alloys .....	55
6.2.3	Galvanic displacement experiments .....	56
6.2.4	Electrochemical destruction procedures .....	56
6.2.5	Experimental assessment of *OH adsorption energies.....	56
6.3	EIS-measurements .....	57
6.3.1	Assessment of the adsorbate surface coverage .....	57
6.3.2	Equivalent electric circuit for the surface limited reversible adsorption .....	57
6.3.3	Assessment of the uncompensated resistance .....	60
6.4	List of equipment, materials and chemicals .....	60
6.4.1	Equipment.....	60
6.4.2	Materials .....	60
6.4.3	Chemicals .....	61
6.4.4	Software.....	61
7	Results and discussion .....	62
7.1	The generalized coordination number as an activity descriptor .....	63
7.2	The Hydrogen evolution reaction on model stepped platinum surfaces .....	65
7.3	Oxygen reduction reaction at Pt surfaces elucidation of the nature of active sites .....	73
7.3.1	Oxygen reduction reaction on Pt(111).....	74
7.3.2	Adsorbate surface coverage of stepped single crystals .....	86
7.3.3	The role of Introduction of steps in the electrochemical reduction of oxygen.....	94
7.3.4	Nanoparticles and complex structures for the electrochemical reduction of oxygen	100
7.4	Carbon monoxide oxidation on model stepped platinum surfaces: the nature of active catalytic centers.....	103
7.5	Oxygen reduction reaction on polycrystalline Pt-based alloys.....	109
7.6	The role of the electrolyte composition on the performance of active sites.....	114
8	Conclusion and outlook .....	120
9	References.....	123

# 1 Abstract

Nowadays, the computational or experimental assessment of the activity of catalysts for the oxygen reduction reaction, the hydrogen evolution reaction and the carbon monoxide oxidation is a material and time-consuming task. The state-of-the-art electro-catalysts still do not show the optimal adsorption properties. A simple possibility to influence and evaluate these properties for various materials is by the targeted introduction of surface defects or quasi-periodic highly coordinated surface structures like steps or concavities. In this work, their effect was experimentally investigated using single crystal model systems. As a theoretical framework, recently developed concept which is based on so-called generalized coordination number was applied.

It has been shown that on stepped surfaces, hydrogen evolution and oxygen reduction reaction shows increased activities. Our joint theoretical and experimental study showed that the highly coordinated concave sites force the adsorption properties closer to the optimal conditions. However, the introduction of such defects coincides with the formation of less coordinated convex defects, which adsorb key oxygen intermediates too strong. Their influence on the adsorbate structure was investigated by “in situ” potentiodynamic electrochemical impedance spectroscopy and cyclic voltammetry measurements. The results indicated that already at early potentials (0.06 V vs RHE) hydroxide species adsorb at the surface and that at the working potential of 0.9 V vs RHE the convex defects are covered by oxygen adsorbates (\*O). The latter influences (weakens) the bonding strength of the sites at the adjacent terraces and improves the overall activity of the surfaces for the oxygen reduction reaction. On the other hand, the early adsorption of hydroxide species on the step edges also accelerates the oxidation of carbon monoxide.

An alternative method to efficiently influence the adsorption properties of active sites towards the oxygen reduction reaction intermediates is the formation of polycrystalline alloys with lanthanides. As a suitable descriptor, the atomic diameter of the alloyed metal which was recently proposed for the polycrystalline surfaces of alloys was used. Its predictive power was experimentally proven in this work to discover new highly active towards the oxygen electroreduction alloy, namely Pt<sub>5</sub>Pr.

Finally, it is shown that the choice of the cation in alkali metal solutions influences the adsorption properties of the active sites at the catalyst surface based on their changed interaction with the first water-layer. Thereby, the nature of the alkali metal cations can drastically change the activity of electrocatalysts, depending on their surface structure.

## 2 Acknowledgements

*This thesis would have not been possible without the contribution of many people.*

*First of all, I would like to thank my supervisor Prof. Dr. Aliaksandr S. Bandarenka for giving me the opportunity to work on this interesting topic, his guidance and support.*

*I want to thank my student David Reinisch for helping me with the measurements, his results in alkaline media, proof reading my abstracts and part of my thesis.*

*I also would like Jonas H.K. Pfisterer for helping me in many aspects of the daily laboratory life and helping me familiarizing myself with everything at the university at the beginning of my PhD.*

*I also want to thank our theoretician Dr. Federico Calle-Vallejo (University of Leiden, The Netherlands) for providing the theoretical framework of our results and his fruitful collaboration on many papers. In this respect, I also want to thank Prof. Dr. Philipp Sautet (University of California LA, USA) and David Loffreda (University of Lion, France) in successful efforts to expand this theoretical framework even further.*

*I would like to thank Daniel Scieszka and Dr. Faheem Butt for the collaboration, time for discussions and feedback on my thesis.*

*Special thanks go to Siegfried Schreier and Markus Haß for always helping me to improve the setups and in other technical requirements. In this context, I would like to thank Manuela Ritter for her help in dealing with the bureaucratic challenges of TUM. Of course, I would like to thank Mareike Stoller for helping me with the obstacles of the IT in the chair and for the nice discussions.*

*Also, I would like to thank Dr. Batyr Garlyyev, Yunchang Liang and Dr. Victor Colic for the successful joint experiments.*

*Another thanks go to Dr. Jakub Tymoczko, Dr. Quang Huy Vu, Prof. Dr. Karina Morgenstern and Prof. Dr. Wolfgang Schuhmann (Ruhr-Universität Bochum, Germany) for the productive collaboration on the activity increase of Pt(111) surfaces and their measurements.*

*I also would like to thank Philipp Marzak, Sebastian Watzel and Alexander Wiczorek for their help, support, feedback on my thesis and enjoyable discussions in the office.*

*Finally, I would like to thank the whole chair ECS and all people belonging to it during this time, which I have not mentioned, for the last three years and the enjoyable times. Without all of you it would have been such a great time.*

### 3 Publications and conference presentations

This thesis is based on the following published and submitted manuscripts as well as contributions at the international conferences:

#### 3.1 Publications

8. M.D. Pohl, V. Čolić, D. Scieszka, A. Bandarenka, *Elucidation of adsorption processes at the surface of Pt(331) model electrocatalysts in acidic aqueous media*. **Physical Chemistry Chemical Physics** (2016) 18, 10792-10799. DOI: 10.1039/C5CP08000B.

7. F. Calle-Vallejo, J. Tymoczko, V. Čolić, Q.H. Vu, M.D. Pohl, K. Morgenstern, D. Loffreda, P. Sautet, W. Schuhmann, A.S. Bandarenka, *Finding optimal surface sites on heterogeneous catalysts by counting nearest neighbors*. **Science** (2015) 350, 185-189. DOI: 10.1126/science.aab3501.

6. V. Čolić, M.D. Pohl, D. Scieszka, A. Bandarenka, *Influence of the electrolyte composition on the activity and selectivity of electrocatalytic centers*. **Catalysis Today** (2015) 262, 24-35. DOI: 10.1016/j.cattod.2015.08.003

5. F. Calle-Vallejo, M.D. Pohl, D. Reinisch, D. Loffreda, P. Sautet and A.S. Bandarenka, *Why conclusions from platinum model surfaces do not necessarily lead to the enhanced nanoparticle catalysts for the oxygen reduction reaction*. **Chemical Science** (2017) 8, 2283-2289. DOI: 10.1039/C6SC04788B

4. F. Calle-Vallejo, M.D. Pohl and A.S. Bandarenka, *Quantitative Coordination-Activity Relations for the Design of Enhanced Pt catalysts for CO Electro-Oxidation*, **ACS Catalysis** (2017), 7, 4355-4359, DOI: 10.1021/acscatal.7b01105

3. M.D. Pohl, F. Calle-Vallejo and A.S. Bandarenka, *Electrocatalytic active sites for the hydrogen evolution reaction at Pt electrodes in acidic media*, 2017, **ACS Omega**, revision is requested

2. M.D. Pohl, B. Garlyyev, V. Čolić, Y. Liang, F. Butt, A. Holleitner, A.S. Bandarenka, *Oxygen reduction reaction activity of Pt<sub>5</sub>Pr in acidic and alkaline media*, submitted

1. B. Garlyyev, M.D. Pohl, D. Reinisch and A.S. Bandarenka, *The effect of alkali metal ions on the oxygen reduction reaction on stepped surfaces*, 2017, in preparation

## 3.2 Conference contributions

### Oral presentations

ECHEMS 2017, Milano Marittima, 6<sup>th</sup> to 9<sup>th</sup> June 2017, “Elucidating the relation between surface structure and electrocatalytic activity of platinum surfaces by the generalized coordination number”

### Poster presentations

6th Colloquium of the Munich School of Engineering, Munich, 7<sup>th</sup> July 2016, “Can fuel cell-catalysts be designed by simply counting nearest neighbors?”

Symposium Electrochemical Energy Conversion and Storage in honor of Prof. Ulrich Stimming’s 70th Birthday, Munich, 20<sup>th</sup> October 2016, “Structure-Activity Relations in Electrochemical Oxidation of CO Molecules at high- and low-index Pt Electrodes”

## 4 Introduction

### 4.1 Current situation and future challenges

Nature is essentially based on closed material cycles. In these systems, the resources undergo several chemical transformations and at the end, revert to the starting product, so that a future supply of the materials is ensured. Several examples of this principle can be found in nature, for example for oxygen, carbon and nitrogen cycles [1-3]. Unfortunately, humankind cannot nowadays follow this natural concept in many cases [4, 5]. Especially since the beginning of industrialization and urbanization, increasing amounts of resources have been mined without remorse [6, 7]. Figure 4-1 exemplarily illustrates energy-consuming fuel production of today's society.

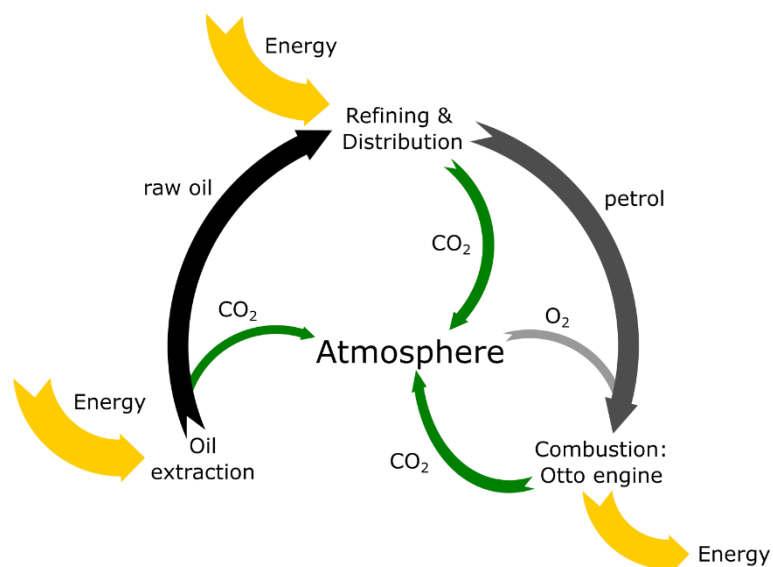


Figure 4-1: Exemplary human consumption of oil and the connected extensive emission of carbon dioxide (green) disturbing the natural carbon cycle.

As a result, humankind needs to master several challenges. A major obstacle is that today's economy strongly depends on fossil fuels like gas and oil, the supply of which will only last for a maximum of 50-60 years at the global production of 2016 [8]. Additionally, the combustion of fossil fuels causes high emission of carbon dioxide, resulting in an imbalance in the natural carbon cycle (see Figure 4-1) [9]. Moreover, carbon dioxide as a greenhouse gas most likely contributes to the climate change [10]; although the total impact remains under discussion [11]. Nevertheless, fossil fuels satisfy a significant amount of today's energy demand [12]. Additionally, the energy consumption will increase steadily in the near future (see Figure 4-2A). From one side, this is caused by the so-called third-world countries'

steadily growing population. On the other hand, in general, the population in so-called first-world countries is decreasing; some show however a positive tendency (see Figure 4-2B) [13, 14]. Further countries on the verge of industrialization depend, like their predecessors, on the consumption of fossil fuels to become developed nations [15]. Especially the transport sector is challenging, as nearly all transportation in some way depends on the consumption of oil [16]. This energy cannot be supplied by fossil fuels permanently.

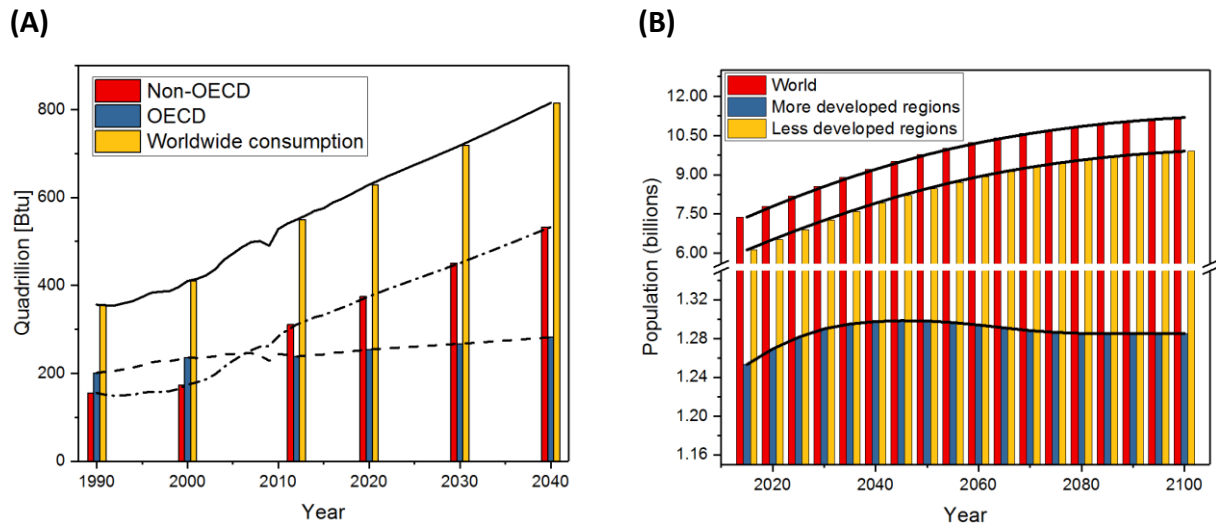
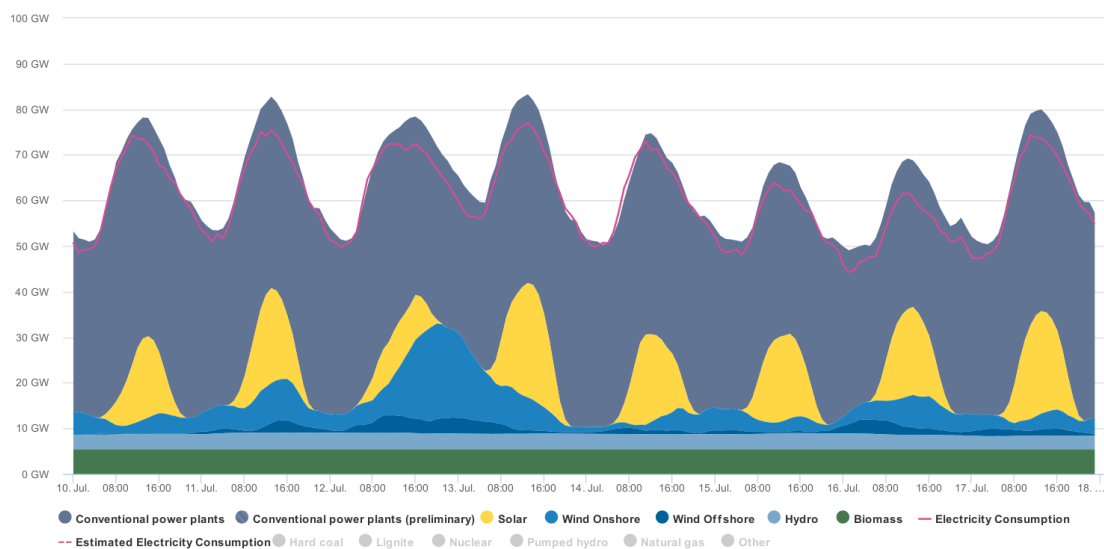


Figure 4-2: (A) Increasing world energy demand until 2040. It is based on the projections by the American Energy Information Administration. (B) Increasing world population in total and for the more- and less-developed countries until 2100. Projections are based on data published by the United Nations Population Division Department of Economic and Social affairs. The black lines are added as a guide for the eye.

Permanently replacing the environmentally unfriendly energy sources worldwide by less harmful alternatives is mandatory [10, 17]. This is a global effort, which is especially challenging with the increasing tendency toward protectionism in the developed nations [18-20]. However, non-developed countries require their assistance to bypass an economy based on fossil fuels. An additional effect of implementing renewables is an independent energy economy, which eliminates fossil fuels as a political factor [21, 22]. Preliminary steps are international political directives like the Paris agreement, which orders the permanent decrease of carbon dioxide emission by 2% until 2050 and is signed by 194 countries [23].

Unfortunately, the most prominent renewables like solar and wind energy allow no steady supply of electricity [24-26]. Their performance depends on the hours of sunshine and the wind velocity, respectively (see Figure 4-3). This results in two opposing scenarios. Under ideal conditions, an overproduction of electricity occurs, which momentarily can be neither consumed nor stored. In the opposite situation, the supply is insufficient and the deficiencies

need to be compensated [26, 27]. The prevalent nuclear power plants are not a suitable compensation as they face severe issues like high related carbon dioxide emission, unresolved waste management and limited supply of uranium [28-31]. Unfortunately, the environmentally friendly “reverse” process, nuclear fusion, is still far from an economical implementation [32, 33].



Agora Energiewende, Current to: 19.07.2017, 17:10

Figure 4-3: Exemplary representation of the energy output for the conventional power plants and renewables wind and solar energy over several days from 10<sup>th</sup> to 17<sup>th</sup> July 2017. The produced energy of the latter strongly depends on the weather conditions. Taken from [34].

The surplus electricity mentioned above could be stored using an efficient and reversible storage device like batteries. Unfortunately, their current capacity and efficiency is insufficient [35, 36]. Already in the transportation sector, as a replacement for combustion engines, their limited operational range is problematic [37, 38]. Alternatively, the surplus could be used for the electrochemical production of hydrogen, which would be stored or used as the fuel [39, 40]. Already in the 1970s, Bockris proposed this concept in the so-called hydrogen economy [41]. While this was not forgotten for several decades, the interest has significantly increased recently based on the decreasing availability of fossil fuels [8].

Since its first proposal, the hydrogen economy was significantly refined and updated towards the so-called hydrogen cycle as shown in Figure 4-4A [28, 42, 43]. According to this concept, water is electrolyzed with excess electricity from renewable sources to hydrogen (hydrogen evolution reaction) and oxygen. The former is either stored or distributed to fueling stations. The distribution remains challenging as the existing gas station network is not equipped with appropriate gas pumps and gas storage [28, 42]. Appropriate measures

were introduced worldwide recently with Germany pioneering by planning to install up to 400 stations until 2023 [44]. Unfortunately, the safe and reversible storage of hydrogen remains another bottleneck [45, 46]. Currently, the best approach is to store it in pressurized gas tanks like in the Toyota Mirai fuel cell cars [40]. To regain the stored energy in the fuel cell, the hydrogen is electrochemically oxidized at the anode side of the fuel cell, while oxygen from air is simultaneously reduced at the cathode side (oxygen reduction reaction) to form water as exhaust [47, 48].

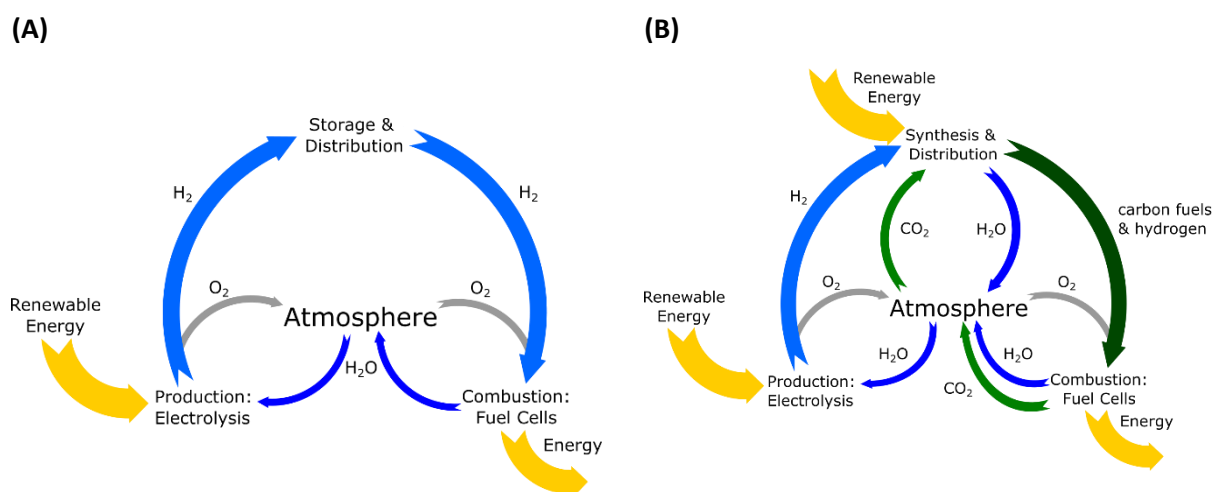


Figure 4-4: Visualization of (A) the hydrogen- and (B) Hydrogen/SynthFuel-cycle. Both pictures and concepts are adapted from [42].

Additionally to the hydrogen cycle, the so-called Hydrogen/SynthFuel-Cycle, as shown in Figure 4-4B, could be established where alcohol or hydrocarbons replace hydrogen. To ensure its climate neutrality, all organic reactants need to be prepared from environmental carbon dioxide by, for example, Fischer-Tropsch synthesis. Additionally, the received long-chained hydrocarbons can be used for petroleum-based conveyance as climate-neutral fuel. This allows a slow and economically feasible modernization of the transportation sector over the impending years [28, 42].

A fundamental aspect of the hydrogen economy is the electrochemical energy conversion in fuel cells and electrolyzers. For the latter, the increase in efficiency for the hydrogen evolution reaction (HER) is an important aspect. Nowadays, the current state-of-the-art catalysts consist of high quantities of expensive platinum or other precious metals to compensate for their moderate activity [49]. Although the metals show a rather high activity, their adsorption properties are not optimal. For instance, on Pt(111) hydrogen intermediates are adsorbed too strongly, namely by  $\sim 0.1$  eV stronger than the optimum. A binding energy

reduction would allow to significantly increase the activity of the catalyst [50]. Similar problems are observed for the carbon monoxide oxidation (CMO) and oxygen reduction (ORR) on platinum in fuel cells [51, 52]. The higher amount of catalyst increases the price for the devices and hinders an economic feasible implementation in the energy storage or transportation sector. An important angle for this crucial optimization is the identification and subsequent increase of the amount of sites with optimal adsorption properties. The importance of catalysis for the modern society notwithstanding, the assessment of these catalytic centers on materials remains, however, challenging [53]. For instance, the influence of the surface structure on the activity is shown in Figure 4-5 for the electrochemical reduction of oxygen on stepped platinum single crystal surfaces. Theoretically, the introduction of steps should change the activity significantly due to the different adsorption properties. However, the activity was not easily explainable by the models presented before in the literature [54].

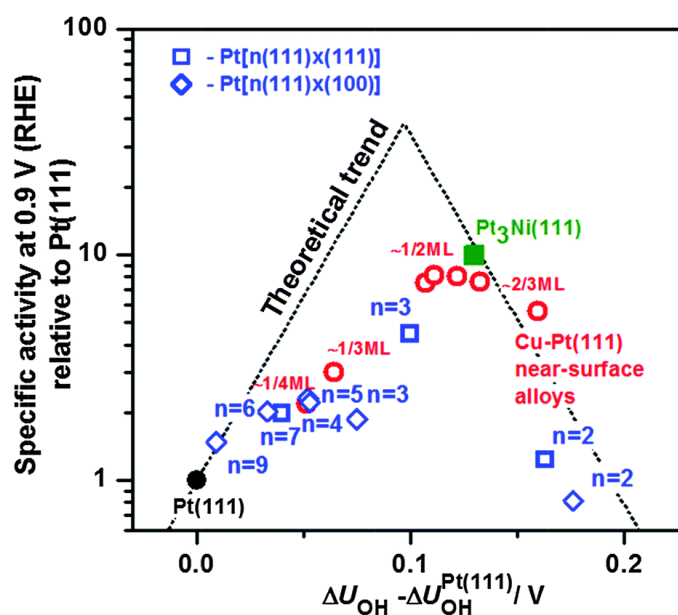


Figure 4-5: So-called volcano plot for the oxygen reduction reaction at different platinum and platinum based electrocatalysts in 0.1 M perchloric acid. The introduction of certain steps into the surface changes the adsorption properties of the surface towards the optimum and increases the activity. The picture is taken from reference [54].

The development of new catalysts by time and material consuming trial-and-error approach does not offer any insight into the catalyst structure [55, 56]. An alternative experimental approach is, prior to the preparation, to investigate model, often single crystal surfaces in pure electrolytes and derive adequate design principles. The model surfaces offer the advantage to reveal the structure / activity relations [57]. Although these surfaces are mere

models, the resulting principles are suitable to derive design concepts for new nanostructured catalysts.

However, a simple and direct theoretical framework explaining their activity is essential. Many computational approaches, like density functional theory calculations, are time-consuming and therefore not always powerful enough for high-throughput screening of a large array of surfaces for optimal catalysts [53, 58]. Additionally, their predictive power is limited and, for instance, fails to explain the activity of various nanoparticles [53, 59]. Alternatively, recently developed approach, which is based on the so-called generalized coordination number ( $\overline{CN}$ ), is a simple mathematical geometric descriptor taking into account the concept of the coordination number in chemistry. It correlates the activity of a potential catalytic site with its geometry by considering coordination numbers of its neighboring atoms. The derived structural information can be used for the development of new catalysts [53].

Another popular catalyst optimization approach is the use of alloyed catalysts, e.g. using alloys based on platinum. The introduced alloying atoms allow tuning the adsorption properties depending on their size and electronic structure [52, 60, 61]. Thereby, the observed changes in properties are influenced by so-called ligand, strain and ensemble effects; in many cases at the same time [62-64]. A prominent example of this class of catalysts is Pt<sub>3</sub>Ni(111) with the highest measured activity for the electrochemical reduction of oxygen [56]. Nevertheless, such catalysts still face several disadvantageous and require further optimization.

An additional important factor influencing the activity is the electrolyte composition. In pure solutions, which are used for electrochemical investigations on single crystals, the nature of the introduced species is "limited", i.e. the number of different adsorbates affecting the activity is low. Still a noteworthy influence of these few kind of ions is observed. Accordingly, the adsorption properties can be optimized by quantifying the interactions between the electrolyte components and the electrode surface [65, 66]. On the other hand the activity can be influenced through the non-covalent interactions when the properties of the first water layer are influenced by spectator species like alkali metal cations [67, 68]. This might allow tuning the adsorption properties closer to the optimal value in some cases.

## 4.2 Aim of this Thesis

In this dissertation, the activity of single crystal model surfaces is investigated to identify the active sites for energy relevant reactions such as the hydrogen evolution reaction, the oxygen reduction reaction and the carbon monoxide oxidation. A fundamental aspect of the active sites is their optimal adsorption properties for all relevant reactants, intermediates and, in some cases, the spectator species. In this context, the effect of several factors influencing the adsorption properties are investigated:

1. Introduction of quasi-periodic defects (all three reactions)
2. Effect of long-lived adsorbates (oxygen reduction reaction and carbon monoxide oxidation)
3. Targeted introduction of under-coordinated defects and defects with higher coordination (oxygen reduction reaction and carbon monoxide oxidation)
4. Alloying of Pt with lanthanides (oxygen reduction reaction)
5. Electrolyte composition, i.e. introduction of various spectator species (oxygen reduction reaction)

## 5 Theory

### 5.1 Heterogeneous Catalysis and electrocatalysis

Heterogeneous catalysis is a fundamental part of the chemical industry [69, 70]. However, already before the industrial implementation of catalytic processes, first examples are found in early stages of human development like the fermentation of alcohol. The documentation and observation of these processes was sporadic and there was no effort to actually explain these phenomena [71].

In 1835 J. J. Berzelius was one of the first scientist to systematically address this topic and coined the term “catalysis” [72]. The following years changed the perception of catalysis significantly. Especially, as it became clear that all reactions can be catalyzed, the interest in this new field peaked based on the possible savings in energy and, consequently, money [71]. The assumed working principle of a catalyst at that time was described by Wilhelm Ostwald. He stated that catalysts just by their presence accelerate the chemical process without changing the thermodynamic equilibrium [71, 73]. This paved the way for the establishment of catalysis as an important economical factor and the development of key catalytic processes. The most important result of those efforts might be the discovery by Fritz Haber and Carl Bosch, which showed that  $\text{NH}_3$  can be prepared from two constituents, hydrogen and nitrogen. Consequently, this allowed the industrial production of fertilizers and, thus, nowadays, to feed most of humankind [74].

Nowadays, the basic concept of catalysis is understood as follows. A chemical reaction requires a specific energy barrier to overcome, the so-called activation energy. The catalyst decreases this energetic demand by taking part in the reaction and forming an energetically lowered complex. Subsequently, the latter further reacts towards the product, possibly via several intermediates, while the catalyst in the end is reverted to its initial state [70].

Catalysis can be divided into two basic research fields: In the so called homogenous catalysis the catalyst and reactant are in the same phase (liquid or gaseous), which requires time and energy consuming separation of both materials. In contrast, in heterogeneous catalysis, the reactants and catalysts are in different phases. This simplifies the separation of the catalytic material and allows to increase of the highly active surface layer [70].

The catalyst has to fulfill three main requirements: First of all, it needs to be highly active for the reaction. Its activity is described by the so-called turnover frequency which is derived from the number catalytic cycles occurring at the active site per time unit under reaction conditions. Secondly, the catalyst should show a high selectivity towards one product. A selective catalyst directs the reaction towards a specific product preventing side reactions. Additionally, the catalyst should be ideally solely active towards the reactant and not react with other species in the reaction media. The selectivity often remains a bottleneck in today's catalyst development. Thirdly the catalyst needs to be highly stable under reaction conditions for a long period of time. Depending on the catalyzed reaction, the material needs to be able to withstand harsh conditions like high/low pH's, temperatures and strongly oxidizing or reductive environments [58, 75].

An important part of heterogeneous catalysis is electrocatalysis, which focuses on the catalytic effect of electrochemical reactions on an electrode surface in devices such as fuel cells or electrolyzers [75, 76]. The interest in this field increased recently based on the efforts to establish a climate and environmentally neutral transportation sector and energy storage [75]. In electrocatalysis, the reactions are limited to the electrode surface and are driven by an electron transfer from the electrode towards the reactant inside the electrolyte. The applied excessive electrical charge, which can be referred to so-called electrode potential, allows to control the reaction path. It is an additional variable which influences the reaction in many cases more effectively than the temperature in "conventional" catalysis [48, 76]. In the following section, the basics and challenges of electrocatalysis will be discussed in more detail.

## 5.2 The Sabatier principle and scaling relations

A fundamental process in heterogeneous catalysis as well as electrocatalysis is the adsorption of reactants to the catalyst active centers. Basically, adsorption can proceed via two different mechanisms: The first type is the so called physisorption based on van der Waals forces between the catalyst centers and adsorbates (reactants). These forces are one of weakest interatomic interactions; but they work over a great distance and can occur in several layers. The second, stronger type of adsorption and the most relevant in catalysis is

so-called chemisorption. It includes bond breaking in the adsorbate and the formation of an intermediate complex with the surface, which reacts further towards the product [77].

For a reactive surface species, the adsorbate and the catalytic center need to bind to each other neither too strong nor too weak as qualitatively described by Sabatier in 1911. In case of a too weak interaction between the center and the intermediate, the intermolecular bonds are insufficiently weakened and the center is too inactive to catalyze the reaction. In contrast, too strongly bound species simply block the active sites. However, these observations by Sabatier were only of qualitative nature [78].

Other important consequences become clear from a closer look at the reaction mechanisms. Most chemical reactions proceed *via* several intermediates and transition states at the surface. Therefore, the optimal adsorption properties for all these states need to be realized on the electrode surface. The resulting computational efforts to assess all new interactions would be not feasible for each potential catalyst. Fortunately, various intermediates binding with the same atom to the surface show linearly scalable adsorption properties on distinct surfaces. Figure 5-1 shows this concept for the conversion of carbon monoxide and hydrogen towards ethanol limiting the calculation to a few descriptive intermediates. For the reactions with several different and relevant adsorbates, like the oxidation of carbon monoxide, the adsorption properties of all species need to be considered [79].

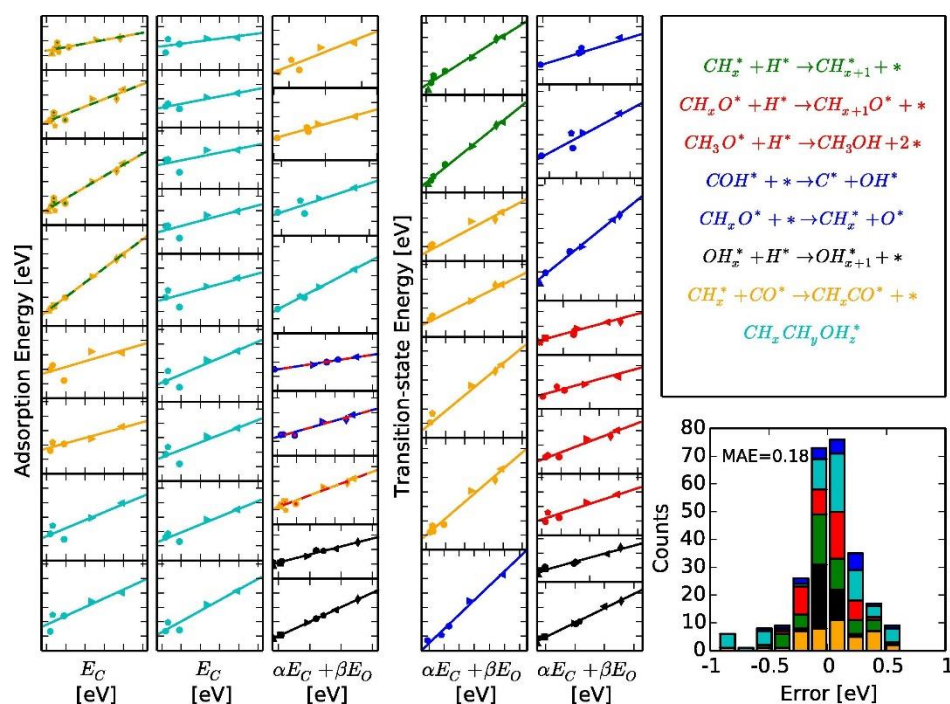


Figure 5-1: Scaling relations for 26 intermediates and 16 transition states in the conversion of CO and H<sub>2</sub> to ethanol (left) as a function of carbon and oxygen adsorption energies on transition-metal (211) surfaces. Taken from reference [79].

This relation is mathematically expressed as follows:

$$\Delta E_1 = \gamma \Delta E_2 + \xi \quad 5-1$$

with  $\Delta E_1$  and  $\Delta E_2$  being the adsorption energies of adsorbate and adsorbents and  $\gamma$  and  $\xi$  are constants given for adsorbates on a specific crystal facet [80, 81].

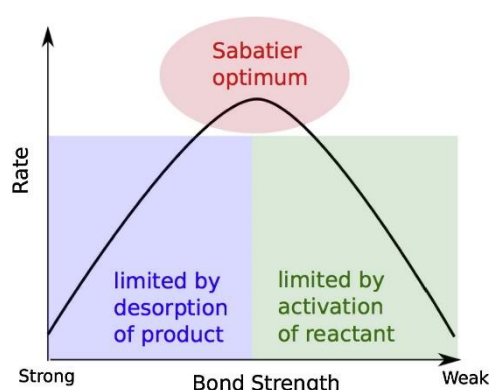


Figure 5-2: Schematic illustration of the Sabatier principle by a volcano plot. Taken from reference [79].

The combination of the Sabatier principle with the scaling relations in the so-called volcano plot allows quantifying the optimal adsorption properties as shown in Figure 5-2 with the optimum at the top. In this graph, a representation of the activity for a surface is plotted against a descriptor related to the surface/interface properties. Thereby, it needs to sufficiently describe in the best case all surface properties like the surface binding energy or heat of adsorption. The determination of a suitable descriptor will be discussed later in detail [79].

### 5.3 The concept of active sites

In the Langmuir's first approach to explain the catalytic activity of surfaces, he assumed that the surface consists of identical and non-interacting sites. This way the whole surface would be equally active for the reaction. This assumption still holds true for the so-called structure insensitive reaction.

Langmuir's idea was further elaborated by H.S. Taylor who proposed in 1925 that not the complete surface would be active for the reaction. Only sites with specific adsorption properties, the so-called active sites, would support the reaction [82]. These so-called

structure sensitive reactions require sites with ideal adsorption properties. Additionally, they should show a specific electronic and/or geometrical structure supportive for the reaction. Such sites can be easily distinguished on single crystals as defects, kinks, holes or steps [57].

## 5.4 Activity descriptor

Identification of active sites requires determination of a suitable descriptor representing the basic properties of specific sites. While the experimental detection of intermediates and elucidation of reaction mechanisms are essential, they are not enough for the successful design of efficient catalysts. A suitable descriptor is the adsorption energies for the reactants. The volcano plot allows quantifying this property by plotting the latter against the activity for a reaction. Although this descriptor can be assessed experimentally it is nowadays mainly determined by quantum mechanical calculations or using other, semi-empirical approaches. This allows to circumvent time and material consuming trial-and-error-experiments by following computational achieved design principles. However, even the computational determination of the activity of rather simple surfaces is still demanding method.

One of the first computational approaches to quantify the interaction between surface structures and adsorption strength was published by Hammer and Norskov. Their d-band model used the energetic level of the d-bands to determine the bonding strength towards the specific surfaces [83].

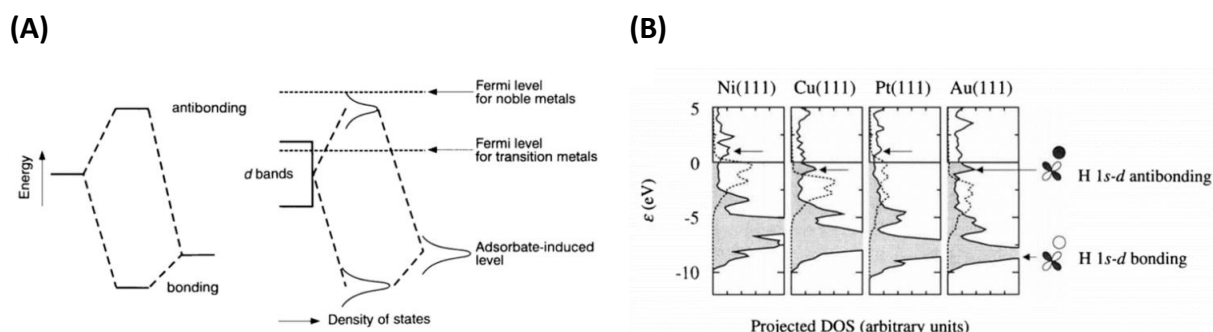


Figure 5-3: (A) Schematic illustration of the bonding between two electronic states for two sharp states (left) and bonding between the state of an adsorbate and metal surface (right). The states have been broadened based on resonance from the interaction between metal *s* band and metal *d* band. (B) Density of one electron state for atomic hydrogen chemisorbed to the indicated (111)-surfaces (solid lines). The dashed line represents the density of states (DOS) of the clean metal surfaces. The Fermi energy is set as zero. The antibonding states resulting from the interaction between chemisorbed hydrogen and surface are indicated by arrows. Taken from reference [83].

According to this theory, for transition metals the variations in adsorption energy are determined by coupling of the adsorbate valence states and the narrow metal d-states (see Figure 5-3A). A key factor is the energetic level of the antibonding states resulting from the interaction between adsorbates and surface sites. For instance, for gold and copper these states are below the highest electronically occupied state, the Fermi energy. Therefore, they are filled and cause a repulsive force towards the adsorbates. For platinum and nickel, the antibonding states are above the Fermi level and empty, resulting into a stronger bonding. In this case, the hybridization energy counters the orthogonalization costs and energy can be gained. The energetically higher the d-states are, the stronger the bonding will be (see Figure 5-3B) [83, 84].

An alternative extremely simple concept to quantify the adsorption on surfaces of metallic lattices is the coordination number used in chemistry. This concept describes the amount of direct neighbors of a central atom. The maximum coordination for e.g. metals depends on the crystal structure with 12 for *fcc*, 8 for *bcc* and 12 for *bcc* and is realized inside the bulk of the metal. On a pristine *fcc*-surface surface, atoms are typically nine times coordinated with six surrounding atoms and three in the bulk of the material. The decreased coordination, in respect to the bulk, can be compensated by the binding towards adsorbates. The lower the coordination is, the stronger the central atom will bind most of the adsorbates. The resulting proportional relationship describes the trend between the lack of direct neighbors and the tendency to form new bonds based on bond-order conversation [85].

A recently introduced first-order extension of conventional coordination numbers are the generalized coordination numbers ( $\overline{CN}$ ) by Calle-Vallejo et al. [53, 59]. In addition to the direct neighbors, for  $\overline{CN}$  also the neighboring atoms are weighted by their coordination numbers with the factor  $n_j/cn_{max}$ . The generalized coordination numbers are calculated as follows:

$$\overline{CN}(i) = \sum_{j=1}^{n_i} \frac{cn(j)n_j}{cn_{max}} \quad 5-2$$

with  $cn(j)$  being the conventional coordination number,  $n_j$  the number of atoms and  $cn_{max}$  the maximum atom coordination of the crystal structure. The generalized coordination

number can simply be adapted to a different crystal structure like *bcc* or *hcp* by changing  $cn_{max}$  towards the maximum coordination of the structure in the bulk. Figure 5-4 illustrates the calculation for a typical site on a *fcc* Pt(111) single crystal [53].

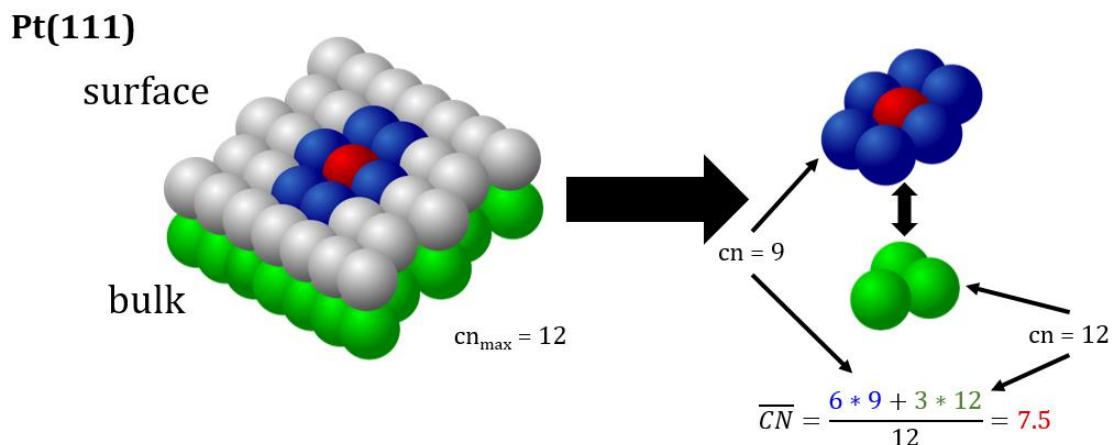
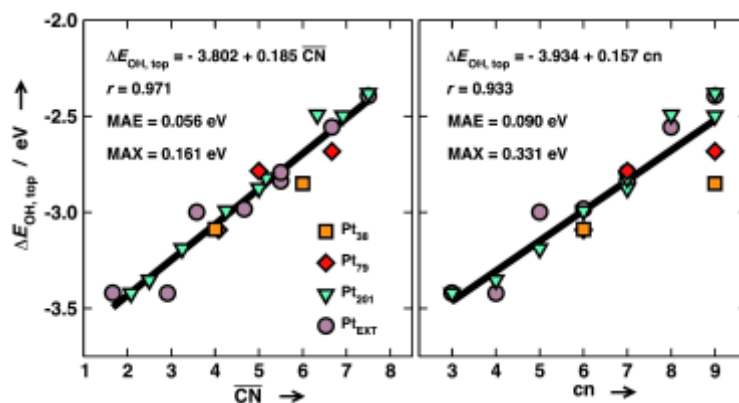


Figure 5-4: Illustration of the calculation of  $\overline{CN}$  exemplary for an "on top" surface adsorption site at Pt(111) surface.

The generalized coordination number can be calculated for other adsorption sites on metallic and non-metallic surfaces like bridge, three- and fourfold hollow sites with a maximum coordination of  $cn_{max}$  of 18, 22 and 28, respectively.

The proportionality of the adsorption energies for numerous media for different adsorbates is plotted in Figure 5-5 for various adsorption sites. As can be seen the linear regression coefficient in the case of the generalized coordination number is higher in comparison to the alternative descriptors [53].

(A)



(B)

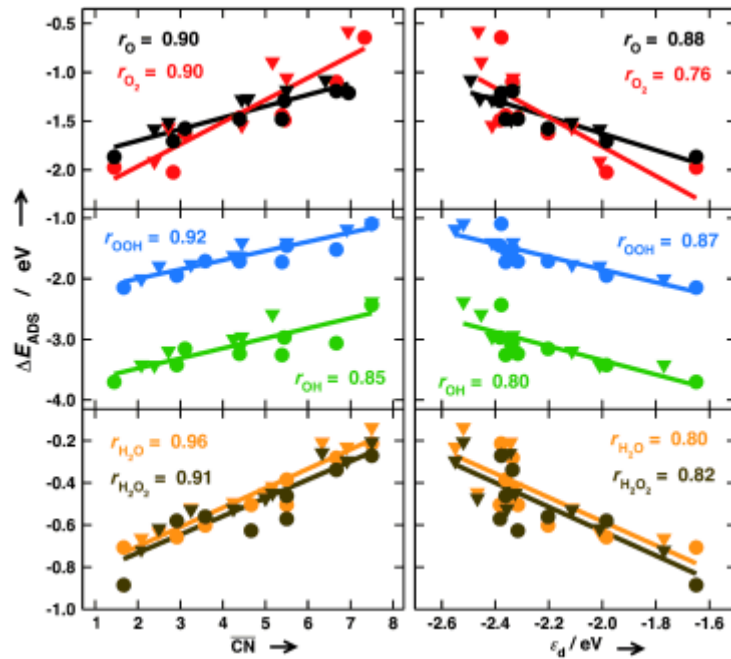
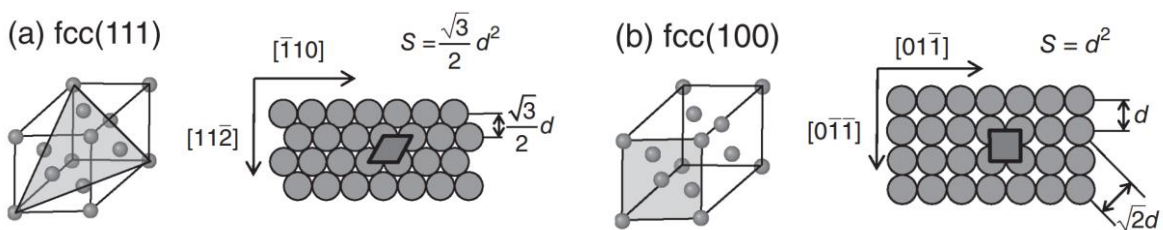


Figure 5-5: (A) DFT calculated adsorption energies for  $\text{OH}^*$  as a function of the generalized coordination number (left) and conventional coordination number (right) for different adsorption sites. Linear fits and regression coefficients are also given. (B) Adsorption energy trends for reaction intermediates in the case of the electrochemical reduction of oxygen on  $\text{Pt}_{201}$  ( $\blacktriangledown$ ) and extended surfaces ( $\bullet$ ) as a function of  $\overline{\text{CN}}$  (left) and the d-band center position. Least-square lines and regression coefficients are also given for each adsorbate. Taken from reference [53].

## 5.5 The role of single crystal model systems in electrocatalysis

A possibility to determine influence of the surface geometry on the resulting activity experimentally is the use of well-defined single crystal surfaces with a limited amount of different adsorption sites. Understanding the basic principles of such systems allows to better understand more complex systems like polycrystalline materials or nanostructured systems.



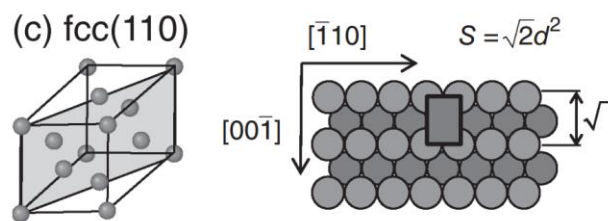
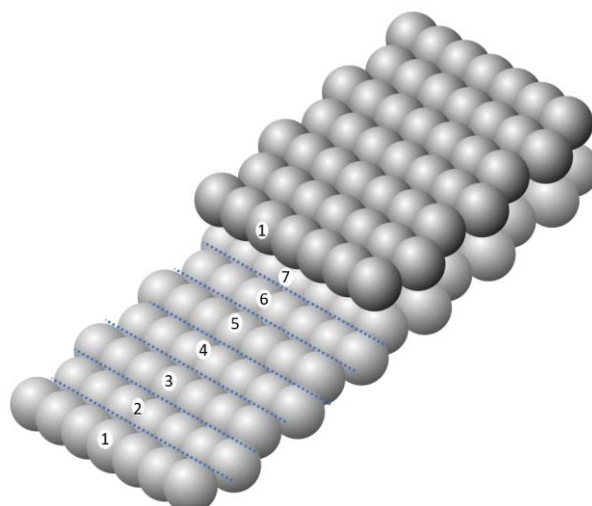


Figure 5-6: Possible atomic structures of the basal planes for platinum (fcc-configuration). Taken from reference [57].

For fuel cell applications, the most prominent example is platinum, which is a face centered cubic (fcc) – metal. Its surface configuration is described by the so-called Miller-indices. Platinum can have three fundamental basal planes (111), (100) and (110) as shown in Figure 5-6. In this context, the simplest surface is the *fcc*(111)-configuration with only few adsorption sites aside from random defective sites, which are always present at the surface of real electrodes[57].

For a long time, cyclic voltammograms of these simple single crystal surfaces were under discussion. Based on the lack of a suitable cleaning procedure, the measurements by several groups showed dissimilar and even contradictory results. For polycrystalline samples, the cleaning of the surface was done by polishing with alumina powders and subsequent electrochemical activation. Such a technique is not suitable for the well-defined surfaces as it would introduce disorder and roughening of the surface of the single crystals. A fundamental step forward was done by the French scientist Jean Clavilier, who introduced the flame annealing method. This allowed a general reproducibility of the measured voltammograms for the single crystal surfaces. Prior to the measurement, the electrode is annealed in a hydrogen flame to remove possible (e.g. organic) contaminations and increase the surface mobility of the metal atoms to allow a better reordering. Subsequently, it is cooled in ultrapure water, covered with a water droplet on the surface and introduced into the electrochemical cell. The droplet protects the surface from contaminations and other surface damaging. It was later realised, that specifically more complex surface such as (100), (110), stepped or kinked surfaces require a reducing atmosphere after annealing due to their increased sensitivity to oxygen and potential surface disordering [57].



*Figure 5-7: Pt(775) with indicated atoms making up the seven atom wide (111)-terrace and one atomic (111)-step. The blue lines are added as a guide for the eye to visualize the single rows.*

The more complex surfaces permit to introduce well-defined and periodical adsorption sites into the surface. This allows revealing of the geometric effects on the adsorption properties. Interestingly, the introduction of periodic steps has a noteworthy influence on the electrocatalytic activity of e.g. platinum surfaces towards several reactions like the hydrogen evolution or oxygen reduction reactions.

The stepped single crystals are also designated using the Lang-Joyner-Somorjei (LJS)-notation, which was developed to allow an easier description of the surface structures. For instance, a surface denoted as Pt[7(111)x(111)], consists of seven atoms long (111)-terraces separated by a monoatomic (111)-step as shown in Figure 5-7. Such periodic features significantly change the adsorption properties of the surfaces by introducing higher and lower coordinated defects. To analyse the voltammograms of the stepped single crystals, it needs to be considered that not all adsorption voltammetric features (peaks) necessarily originate from different absorbing species. They can also stem from the adsorption of the same species at different surface sites [57].

## 5.6 The electrochemical interface

This section is based on references [86, 87] and references therein. Immersing metallic electrodes into an electrolyte consisting of inert species results in the formation of the so-called electrolytic double-layer. In 1853, the first model was proposed to illustrate this behavior. The electrode and electrolyte sides can in principle be approximated by a parallel plate capacitor model; this capacitor stores charge electrostatically. Charge carriers arrange at the phase boundary between the electrolyte and electrode: for the external observer, the behavior of such a system would remind a “normal capacitor”.

According to the simplest assumptions by Helmholtz shown in Figure 5-8A, the first layer is formed inside the electrode consisting of the “electrons beneath the electrode surface”. In direct proximity, counter-ions from the electrolyte arrange to compensate for this excess charge. While this model describes the constant differential capacitance dependent of the dielectric constant and the thickness of the double layer to some extent, it completely neglects the effect of diffusion at the electrolyte side and the specific adsorption of ions at the electrode surface.

L. G. Gouy and D. L. Chapman complemented the above-mentioned Helmholtz model by the introduction of a diffuse layer, which took into account the Brownian movement of the ions in the electrolyte. The distribution of the ions is influenced by the applied potential and the ion concentration. It changes with the distance from the electrode surface. However, their model completely neglected the Helmholtz plane as shown Figure 5-8B.

The model shown in Figure 5-8C was proposed by Stern who combined both approaches [88]. Depending on the ion, the distance between the electrode surface and the Helmholtz plane will vary with their nature. While some ions can lose their solvation shells and get closer to the electrode, other may remain at some distance due to its hindrance. These layers were termed as the inner and outer Helmholtz planes. Following the latter are (i) the diffuse layer and (ii) the electrolyte bulk.

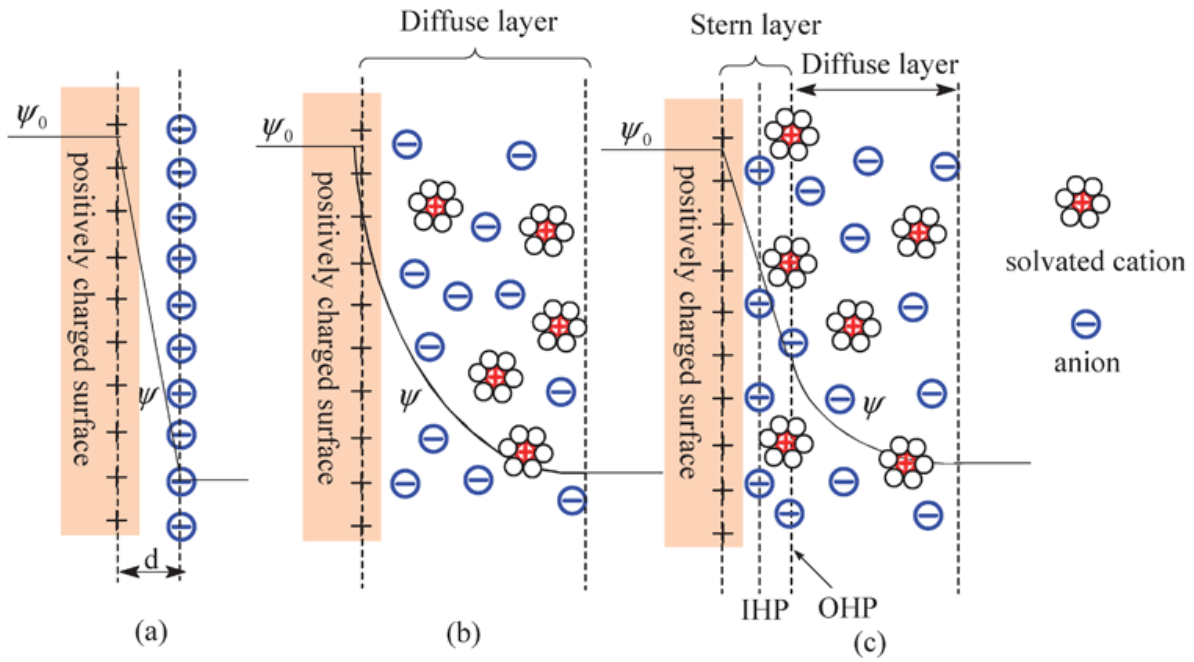


Figure 5-8: Schematic representing the electric double layer at a positively charged anode: (A) the Helmholtz model, (B) the Gouy-Chapman model, and (C) the Stern model. Reproduced from reference [89].

Potentially, ions, solvent molecules and any species inside the electrolyte are able to adsorb at the electrode surface. The ions can either adsorb due to coulombic forces as a result of the applied potential, van-der-Waals-forces, or chemisorption. While to some extent the potential influences the adsorption of anions from the electrolyte to the electrode, some ions adsorb readily on the surface (so-called specific adsorption, Figure 5-9). Hereby, the adsorption is stronger for weaker solvated ions.

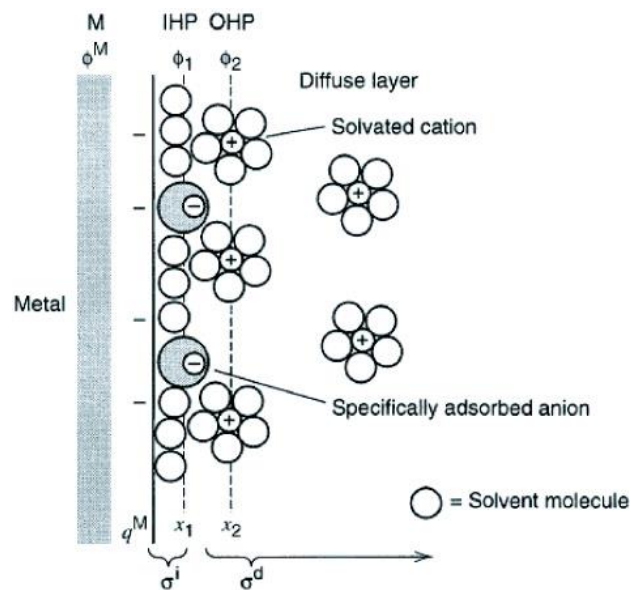


Figure 5-9: Generally accepted model of the double-layer region under conditions where anions are specifically adsorbed. Taken from reference [90].

The capacitance of the double layer can be calculated from the capacitance of the Stern layer and the diffuse layer by:

$$C_{dl} = \left( \frac{1}{C_H} + \frac{1}{C_{dif}} \right)^{-1} \quad 5-3$$

The capacitance of the Helmholtz double layer can be calculated like for a plate capacitor by:

$$C_H = \frac{\varepsilon_r \varepsilon_0 A}{d} \quad 5-4$$

where  $\varepsilon_r$  is the relative permittivity,  $\varepsilon_0$  the permittivity of the vacuum,  $A$  the electrode surface, and  $d$  the thickness of the “dielectric layer”. The capacitance of the diffuse layer is calculated, for a binary symmetric electrolyte, under the assumption of a constant relative permittivity, from

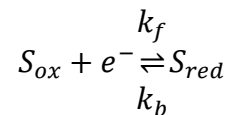
$$C_{dif} = \frac{4zeN_A\lambda_D c_\infty}{\psi_D} \sinh\left(\frac{ze\psi_D}{2k_b T}\right) \quad 5-5$$

where  $z$  is the valence of the electrolyte species,  $e$  is the elemental charge,  $N_A$  is the Avagadro number,  $c_\infty$  concentration in the electrolyte bulk,  $\psi_D$  is the electric potential in the diffuse layer,  $T$  is the temperature,  $k_b$  is the Boltzmann constant, and  $\lambda_D$  is the Debye length [86].

## 5.7 Fundamental electrochemical equations

### **Butler-Volmer-Gruz equation**

For a simple electrochemical reaction



where  $k_f$  and  $k_b$  are the rate constant of the forward and backward reactions, these rates can be estimated by the Arrhenius equation:

$$k = A' e^{\frac{-\Delta G^*}{RT}}$$

Where  $R$  is the universal gas constant,  $T$  is the temperature,  $-\Delta G^*$  is the standard free energy of activation, and  $A'$  is the constant frequency factor. From this equation, the Butler-Volmer-Gruz Equation can be derived, which is fundamental for the electrode kinetics. It describes the influence of a change in the electrode potential on the electrochemical current

and allows determining the current density ( $j$ ) as a function of the electrode potential in many cases:

$$j = j^- + j^+ = j_0 * \left( e^{\frac{\alpha_a n F \eta}{RT}} - e^{-\frac{\alpha_c n F \eta}{RT}} \right) \quad 5-6$$

Where  $j_0$  is the exchange current density,  $\eta$  is the overpotential,  $R$  is the universal gas constant,  $T$  is the temperature,  $n$  is the number of electrons involved in the reaction,  $F$  is the Faraday constant, and  $\alpha_c/\alpha_a$  are the dimensionless cathodic/anodic charge transfer coefficients [90].

### **Tafel equation**

A fundamental aspect of electrochemical kinetics is the observed overpotential for electrochemical, in the most cases inner-sphere reactions. It is considered as a kinetic effect; and it describes the potential difference between the thermodynamic redox-potential of a half-reaction and the actual potential at which the reaction occurs. It is defined as:

$$\eta = E - E_r \quad 5-7$$

Where  $E$  is the electrode potential under reaction conditions, and  $E_r$  is the electrode potential at formal equilibrium. For instance, while in an electrolyzer water splitting requires more energy for the production of the pure gases, in a fuel cell the produced energy is decreased relative to the thermodynamically predicted one. By taking the exchange current density into consideration ( $j_0$ ) and reforming the Butler-Volmer equation, the Tafel equation can be derived, which helps to correlate the reaction rate and the overpotential:

$$\eta = \frac{k_B T}{e \alpha} \ln \left( \frac{j}{j_0} \right) \quad 5-8$$

where  $k_B$  is the Boltzmann constant,  $T$  is the temperature,  $j_0$  is the exchange current density,  $j$  is the current density,  $e$  is the electron charge, and  $\alpha$  is the charge transfer coefficient [90].

## Nernst equation

The open circuit-voltage of an electrochemical cell is determined by the electrochemical potential of two connected half-cells with

$$E = E_{red} - E_{ox} \quad 5-9$$

where  $E_{red}/E_{ox}$  are the potentials of the half cells in which the reduction and the oxidation occur, respectively. For a simple electrochemical reaction:



The Nernst equation describes the dependence of the electrode potential of the redox-couple on the activity of ionic species.

$$E = E^0 + \frac{RT}{nF} \ln \left( \frac{a_{ox}}{a_{red}} \right) \quad 5-11$$

Where  $E$  is the electrode potential,  $E^0$  is the standard electrode potential of the reaction,  $T$  is the temperature,  $R$  is the universal gas constant,  $n$  is the number of electrons involved in the reaction, and  $a_{ox}/a_{red}$  are the activity of the oxidized and reduced species [90].

## 5.8 Effect of the electrolyte composition on the activity

The following description of the cation and anion effects will be limited to the relevant adsorption of reaction intermediates, which can be met in the investigated systems. This section is based on reference [91] and references therein.

### 5.8.1 Effect of cations

The most prominent example for the effect of the cations is the alkali metal cation solutions because of their broad application spectrum in industry and laboratory practice [92]. The effect of the nature and concentration of these ions was already observed in 1930s for several reactions [93]. In the following years, the research focus was shifted towards the electrode surface; the interest in the catalytic effect of these species was almost completely vanished. It was assumed that they were just mere spectator species, which do not influence the reactions. Recently, the interest in the cation species increased due to the improved understanding of the electrochemical systems and better experimental methodologies [91].

For instance, an important effect of the alkali metal cations is the changes in the activity for the electrochemical reduction of oxygen on Pt(111) at higher pHs. Hereby, the activity of the electrodes increases from lithium containing towards cesium containing electrolytes [94]. As was shown by the activity measurement and cyclic voltammetry, the ions seem to directly influence the adsorption of hydroxide on the surface and the formation of oxygenated species [95]. While this interaction is strong for lithium, it significantly decreases in the case of cesium. This can be attributed to the different interaction strength of the cations with the first-water layer. As a suitable descriptor, the hydration energy of the ions was proposed by Katsounaros et al, which decreases from lithium to cesium [96, 97].

The presence of alkali metal cations influences the adsorption of many reaction intermediates also in acidic solutions. For instance, the activity of Pt(111) electrodes towards the electrochemical oxygen reduction is changed, but follows no obvious trends. Interestingly, the cations seem to have a strong influence if e.g. sulfate anions are present in the solution. A prominent influence is also observed for the hydrogen evolution reaction on Pt(111); this electrode shows its highest activity in the presence of  $\text{Rb}^+$  [98].

### 5.8.2 Effect of anions & pH-Effect

Most of the anion-effects can be accounted for them to be specifically adsorbed as poisons for the surface [99-101]. For instance, sulfates strongly adsorb at various surfaces and block the active sites. Consequently, the oxygen reduction reaction activity of platinum in sulfuric acid media is significantly decreased [102-104]. On the other hand, the negatively charged perchlorate and sulfate do not hinder the cathodic hydrogen evolution reaction on Pt-electrodes but change the electrode properties related to the oxygen evolution reaction in acidic media. The strongly adsorbed sulfates suppress the reactions at the electrode, while for the only weakly adsorbed perchlorate higher activities are observed [105].

However, it remains challenging to explain some pH effects [106, 107]. In general, the change in the pH can be attributed to the anion effect, as it is limited to the interaction between the surface and the negatively charged hydroxide [108]. Based on the contribution of protons and hydroxide as interacting species, the influence of those should be able to be described by the Nernst equation [109]. This is not observed even for the hydrogen

oxidation and evolution reactions at different electrodes and is even more complicated for many other reactions [110-112]. It should be noted that it is rather difficult to separate the pH-effect and the contributions originating from the alkali metal cations. The latter are unavoidably used to create highly alkaline environment. The differentiation of these contributions requires a suitable model which has yet to be found.

To make correction with respect to the reversible hydrogen electrode in alkaline media, the hydrogen evolution/oxidation reaction mechanism at the electrode surface must be taken into consideration. As the first approximation, it proceeds as follows:



This gives for the redox-potential according to the Nernst equation:

$$E = E^0 + \frac{RT}{nF} \ln \left( \frac{a_{H^+}^2}{p_{H_2}} \right) \quad 5-13$$

Where  $E$  is the potential of the half-cell,  $E^0$  is the standard electrode potential of the reaction,  $T$  is the temperature,  $R$  is the universal gas constant,  $n$  is the number of electrons involved in the reaction,  $a_{H^+}$  is the activity of the protons in the solution, and  $p_{H_2}$  is the partial pressure of the produced hydrogen gas. The equation can be rewritten as follows:

$$E = E^0 + \frac{RT}{nF} (\ln(a_{H^+}^2) - \ln(p_{H_2})) \quad 5-14$$

For this equation, several simplifications can be made:

- $p_{H_2}$  becomes 1 as hydrogen is bubbled over the platinum at atmospheric pressure  
 $\rightarrow \ln(p_{H_2}) = 0$
- $E^0$  as the standard potential is by definition zero

$$E = \frac{RT}{nF} \ln(a_{H^+}^2) \quad 5-15$$

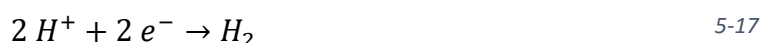
Converting  $\ln$  towards  $\log_{10}$  and taking into account all constants gives the pH-dependence of the potential with  $pH = \log_{10} a_{H^+}$  [90]:

$$E = -0.059 V * pH \quad 5-16$$

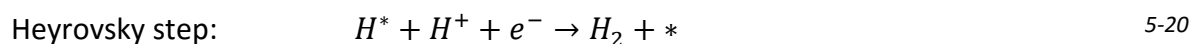
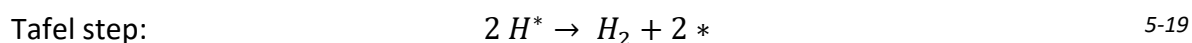
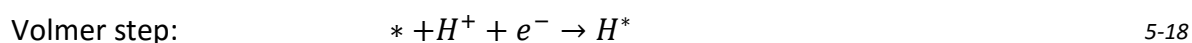
## 5.9 Electrocatalytic reactions

### 5.9.1 Hydrogen evolution reaction (HER)

This chapter is based on reference [113] and references therein. Nowadays hydrogen, although it is most likely an important future green energy carrier, is mostly produced as a rather impure waste product of steam cracking under high carbon dioxide emissions [114]. An alternative production method is the electrochemical splitting of water, giving highly pure hydrogen. The reaction can be simplified as follows:



An important factor is the reaction mechanism with its intermediates. This reaction can be described by the following steps (\* denotes a surface site or a species adsorbed to the surface) [113]:



While the proton adsorption from the electrolyte to the surface proceeds *via* a single step, the so-called Volmer step, the subsequent reaction step can proceed through two independent ways. In the Tafel reaction two adsorbed hydrogen react with each other and form hydrogen. In contrast, in the Heyrovsky step the adsorbed hydrogen reacts under the addition of an electron and a proton from the electrolyte towards molecular hydrogen [113]. The Tafel slope can give valuable insight into the underlying reaction mechanism. In contrast to more complex reactions such as the oxygen reduction reaction, this reaction seems to proceed only through one intermediate, which simplifies the assessment of the optimal adsorption properties.

#### **Noble metal based catalysts**

The high price and scarcity of platinum, the typical commercial catalyst for many reactions in the field of renewable energy, there is a demand for the optimization of Pt-based catalysts.

For it, the amount of catalyst can be decreased using either nanostructured and/or porous materials. Based on their advantageous surface to volume ratio the quantity of catalyst can be decreased in the case of nanoparticles. An alternative approach along the same road is replacing platinum by less costly alternatives. For instance, a thin layer of the precious metals (e.g. Pd, Au, Pt) on tungsten carbide or molybdenum carbide shows similar bulk electronic properties and activities to the pure metal and keeps the stability under reaction conditions [115-118]. On the other hand, highly active catalytic alloys based on precious metals can be designed with optimized adsorption properties for the intermediates [119].

### **Non-precious metals and their alloys**

An alternative to precious metals are catalysts based on nickel, which show a high activity and stability in alkaline media [120]. Such catalysts however undergo reversible hydride formation, which deactivates the electrode surface and decreases their activity [121, 122]. This problem can be overcome by alloying of the nickel catalysts. The most prominent example of this class is the Raney®-Nickel, based on an alloy of nickel and Al. Varying the concentration of the elements allows to tune the catalytic properties of the surface [123, 124]. Similar effects were also observed for alloys with molybdenum, zinc, cobalt, iron or chromium [125].

A limiting factor for these catalysts in alkaline media is that they do not facilitate optimal water dissociation [126, 127]. Moreover, in acidic media this class of catalysts corrodes readily. This can be overcome by encapsulating the materials with e.g. graphene. This increases their stability in acidic media significantly, while keeping the high activity. This allows the catalysts to meet the performance of platinum in 0.05 M sulfuric acid [128, 129].

### **Transition metal chalcogenides**

The interest in transition metal chalcogenides increased significantly since 2011 [130-134]. The most prominent example of such materials is molybdenum sulfide with a layered structure analogous to graphite [135]. Therefore, it will be taken as an example for this class of catalysts. While the bulk material is catalytically inactive for the hydrogen evolution reaction, the sulfur-reached edges are highly active [136, 137]. However, most molybdenum

sulfide structures tend to form close shell fullerene-like structures which eliminate the active sites at the edges [138, 139]. To prevent this, significant efforts were spent in order to prepare the thin films and to introduce specific defects [140-143]. The activity of these catalysts can be further increased by the implementation of metal cations, Ni or Co, as promoters. These ions decrease the free energy of hydrogen adsorption at the catalyst edges [144, 145].

While molybdenum sulfide is the most prominent example, catalytic activity was also observed for tungsten sulfide, molybdenum selenide and tungsten selenide. These materials showed similar characteristics as molybdenum sulfide [146]. Additionally, non-layered chalcogenides such as cobalt sulfide, cobalt selenide, nickel sulfide and nickel selenide show activity for the hydrogen evolution reaction [147-151].

### **Transition metal carbides**

Another relatively cheap alternative to Pt are transition metal carbides with tungsten and molybdenum carbide as the most prominent examples [152]. According to density functional theory calculations, the hybridization between the carbides and transition metal results into a higher electronic density of states at the Fermi-level and a broad unoccupied d-band. This allows comparable electronic properties as observed for platinum [153, 154].

Based on their different characteristics, the materials show a lower tendency towards poisoning and deactivation [155, 156]. However, the preparation of tungsten carbide is quite challenging if considering up-scaling of this technology [157, 158].

### **Transition metal nitrides**

Transition metal nitrides such as molybdenum nitrides are considered to be promising as the d-band of the parental metal is “modified towards the right side” for the hydrogen evolution reaction and oxygen reduction reaction. Therefore, it appears similar to VIII–group precious metals [152, 154]. Like the chalcogenides, their activity can be increased by the introduction of late transition metals such as Co and Ni [152].

### **Transition metal borides**

Transition metal borides, such as zirconia boride ( $ZrB_2$ ), are known as hydrogen evolution catalysts for more than forty years [159]. A more recent example of this type of catalyst is amorphous nickel boride with good activity in alkaline and acidic media. Their activity is comparable towards Raney<sup>®</sup>-Nickel with an improved corrosion resistance [160-163].

### **Transition metal phosphides**

Transition metal phosphides were mostly used for hydrogenation or hydrodesulphurization and only recently became interesting as catalysts for the hydrogen evolution reaction [164, 165]. Nowadays, they belong to the most active catalysts. However, their preparation methods still require serious optimizations [113].

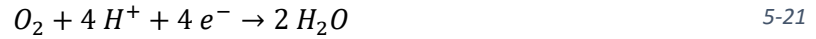
### **Metal-free catalysts**

Recently, carbon-based catalysts were established as electrocatalysts for the hydrogen evolution reaction. However, pristine carbon materials are inert as the catalysts [166]. They require modifications by chemical methods, such as heteroatom doping, to become catalytically active [167, 168]. Although, electrocatalytic activity was reported for undoped carbon nanotubes, it can be assumed that their rather moderate activity originates from the metal contamination due to the preparation method [113, 169-171]. In general, the activity of carbon based catalysts can be increased by doping with heteroatoms such as nitrogen, boron, oxygen, sulfur and fluorine which was demonstrated for graphene nanosheets [167, 168].

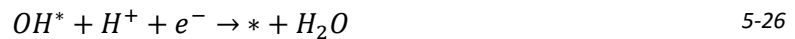
Additionally, carbon nitride, as two-dimensional crystal structure, is a recently reported electrocatalyst for the hydrogen evolution reaction. Although, nanorod arrays showed good catalytic activities, their specific current density is rather low [172]. It can be improved by hybridizing it with nitrogen-doped graphene nanosheets. The resulting high activity is explained by the separated reaction steps on the components provided (according to density functional theory calculations). Hydrogen adsorbs on the highly active adsorption sites provided by the nitride component and is subsequently reduced on the nanosheet [173].

## 5.9.2 Oxygen reduction reaction (ORR)

In contrast to the hydrogen evolution reaction, the electrochemical reduction of oxygen is significantly more complex in sense of the involved intermediates process. In general, the reaction in acidic media can be summarized as follows:



The reaction mechanism proceeds *via* either the dissociative or associative pathways, which are determined by the oxygen coverage. The dissociative mechanism was used for the modelling of the oxygen reduction reaction on platinum in this thesis [174]:



Hereby it has been determined that the two potential-determining steps are [174, 175]:

- Chemisorption of oxygen from the electrolyte and its subsequent protonation towards  $OOH^*$  (combination of step 5-21 and 5-22)
- Protonation of the hydroxide towards water (step 5-26)

A general problem of the oxygen reduction reaction on platinum surfaces is the too strong binding of all oxygen-intermediates:  $OOH^*$ ,  $OH^*$  and  $O^*$ . In this thesis, for the assessment of the generalized coordination number,  $OH^*$  is considered as the archetypical intermediate for this reaction. Due to the scaling relations shown in Figure 5-10, its adsorption properties can be used as a general descriptor for all the investigated surfaces. As  $E_{OH}$  and  $E_{OOH}$  are separated by 3.2 eV, the binding properties of the surface must be balanced out for all activation energies. Based on this non-ideal scaling, a catalyst with optimal  $\Delta E_o$  will have a non-zero overpotential [174, 176, 177].

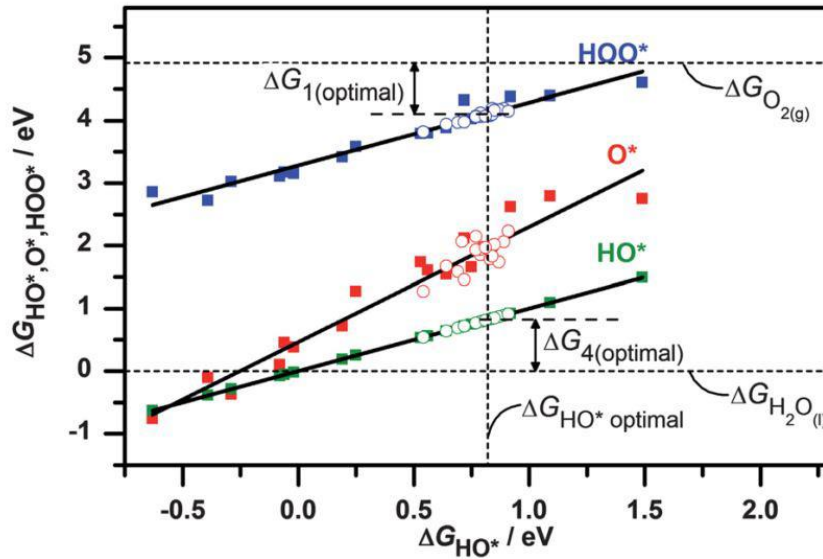


Figure 5-10: Binding energies of the oxygen-reduction reaction intermediates plotted against  $E_{OH}$  demonstrating their linear dependency. Taken from reference [52].

In alkaline media the reaction mechanism is not well understood due to the influence of pH, solvation and polarity of water [110, 178]. Already in 1987 Anastasijevic et al. postulated a rather complex model for the reaction mechanism on platinum based catalysts (see Figure 5-11) which is discussed elsewhere in detail [179, 180].

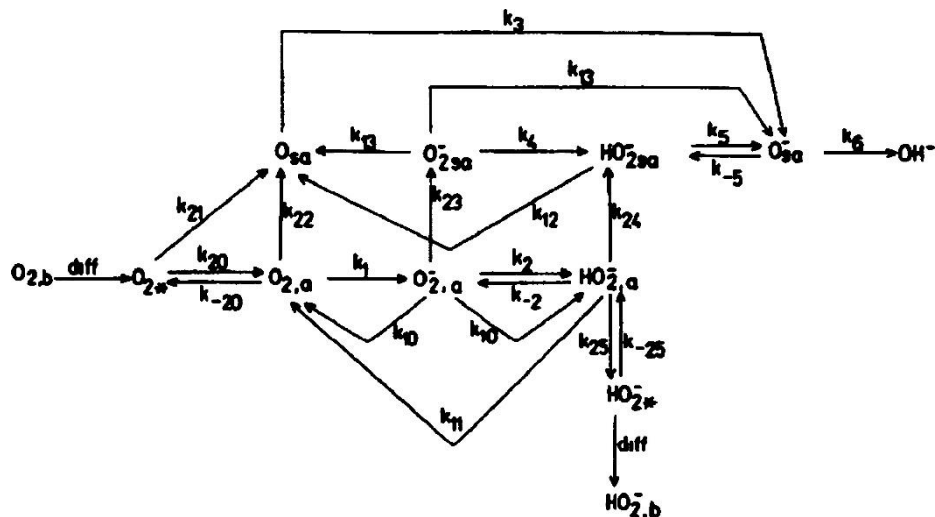


Figure 5-11: Reaction mechanism scheme for the electrochemical reduction of oxygen on Pt-based catalyst surface in alkaline media.  $k$  represents the rate constant of the  $i$ -th reaction step. The subscripts denote  $sa$  = strongly adsorbed,  $a$  = weakly adsorbed,  $b$  = bulk, and  $*$  = vicinity of disk electrode. Taken from reference [180].

The following section is based on reference [181] and references therein. For the activity of platinum towards the oxygen reduction reaction, the different low-index single crystal facets

rank in perchloric acid as follows: (110) > (111) > (100) [182]. In sulfuric acid, the activity of the (100)-facet is higher than the (111)-facet due to the adsorption of sulfate from the electrolyte [65]. This observed behaviour inspired the implementation of several complex nanoparticulate platinum based structures with specific main facets to increase the catalytic activity [183-185].

The following section is based on reference [61] and references therein. Alternative to the pure platinum, recently a new type of electrocatalyst became popular which consisted of platinum alloyed with 3d-transition metals and lanthanides.

The low-index surfaces show a high activity and are relatively stable under electrochemical conditions. The most prominent example is Pt<sub>3</sub>Ni(111) with approximately ten times high oxygen reduction reaction activity compared to the pristine Pt(111) and a nearly optimal binding of the reaction intermediates [56, 186, 187]. See the relative activity of various Pt alloy *fcc*(111) single crystals for the oxygen reduction reaction shown in Figure 5-12.

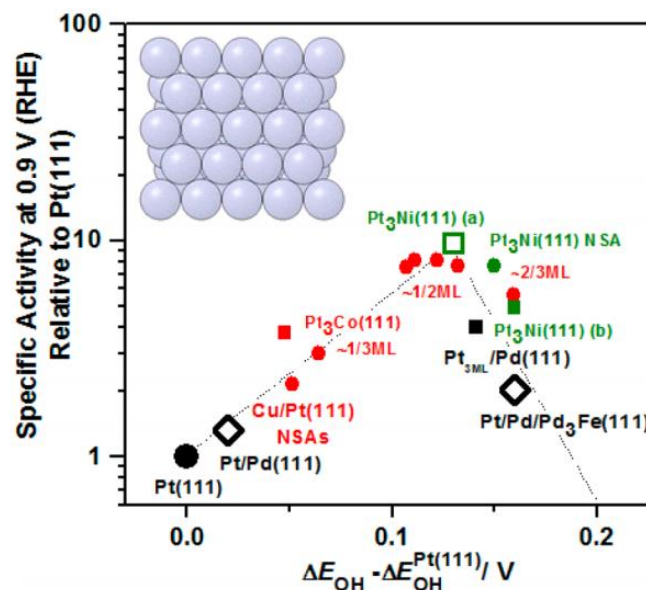


Figure 5-12: Relative activity of platinum alloys *fcc*(111) single crystals towards the electrochemical reduction of oxygen in 0.1 M perchloric acid at the working potential (0.9 V) of fuel cells against the hydroxide binding energies. Taken from reference [61].

The variations in composition introduce an additional degree of freedom to tune the adsorption properties by three main factors mostly at the same time:

- Strain-effect

Alloying of platinum with either transition metals or lanthanide results in the introduction of compressive strain inside the surface layer due to their different lattice parameter. This strain directly influences the adsorption properties of the intermediates by changing the electronic configuration of the sites. Interestingly, alloying Pt with either smaller or bigger atoms results in only compressive strain. The difference in size of the alloyed materials and the host lattice determines the extent of the introduced strain. While the effect is negligible for similar sized atoms, it becomes more prominent in more drastic cases [61, 62, 188].

- Ligand-effect

Independent to the introduction of strain, the different electronic characteristics of the alloyed elements influences the neighboring atoms. Hereby, the introduction of foreign atoms can significantly influence the electronic structure and change the adsorption properties of the neighboring atoms. In contrast to the strain effect, the influence of the ligand effect is limited towards one to maximum five atomic layers [63, 64].

- Ensemble-effect

An additional effect results from the arrangement of the atoms on the surface which can allow the specific adsorption of an intermediate from the electrolyte. The configuration of the elements on the surface can result into its activation. For instance, a bimolecular adsorbate can adsorb in two independent energetically preferential adsorption sites, like hollow sites, which allows them to be dissociated [64].

An alternative approach to modify the catalytic properties is the usage of more complex structural features like steps, which introduce periodic defects [54, 189]. While the limited adsorption sites on an *fcc*(111) surface allows estimating the binding energies of the reaction intermediates from both theoretical calculations and experimental data *via* a volcano plot, the influence of steps is not easy to differentiate as strain, ligand effect and steps influence the electronic properties of the surface at the same time. Hence, the theoretical identification of their active sites is challenging and the evaluation of the activity is mostly based on experimental activities. Based on their lower coordination, steps should bind the intermediates too strongly and deviate more from the optimal conditions. However, alloyed

stepped surfaces do not follow such trends (see Figure 5-13); most likely active sites are located at the concavities [61].

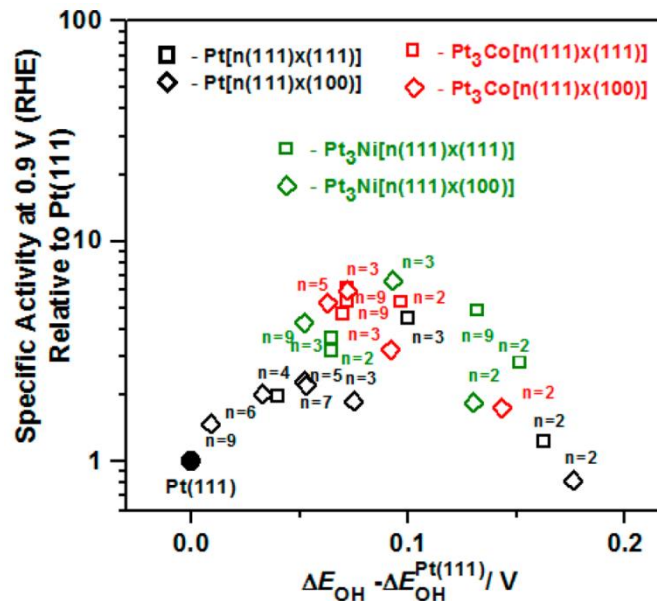


Figure 5-13: Relative activity of various stepped surfaces platinum alloys towards the electrochemical reduction of oxygen measured in 0.1 M HClO<sub>4</sub> at the potential (0.9 V, vs RHE) as a function of the estimated hydroxide binding energies. Taken from reference [61].

For practical catalytic applications, however, polycrystalline alloys (nanostructured thin films) or nanoparticles are used. However, their broad variety of sites, like various crystal facets, kinks, steps and defects hinders identification of active sites. Optimizations are normally done with an insufficient approximation that solely the *fcc*(111)-facets determine the activity. Additionally, these catalysts are less stable under electrochemical experimental conditions. In the case of alloys of platinum, the less noble materials are leached from the surface area or the near surface layers, especially at defect sites, resulting in the formation of an unaltered core and a platinum rich outer shell. The unaltered core causes different interatomic distance between the outer shell atoms which decreases the bond strength towards oxygen intermediates [188]. This can introduce a high amount of new catalytically active sites into the surface. The occurrence and complete effect of deploying of such a methodology will be discussed later in more detail.

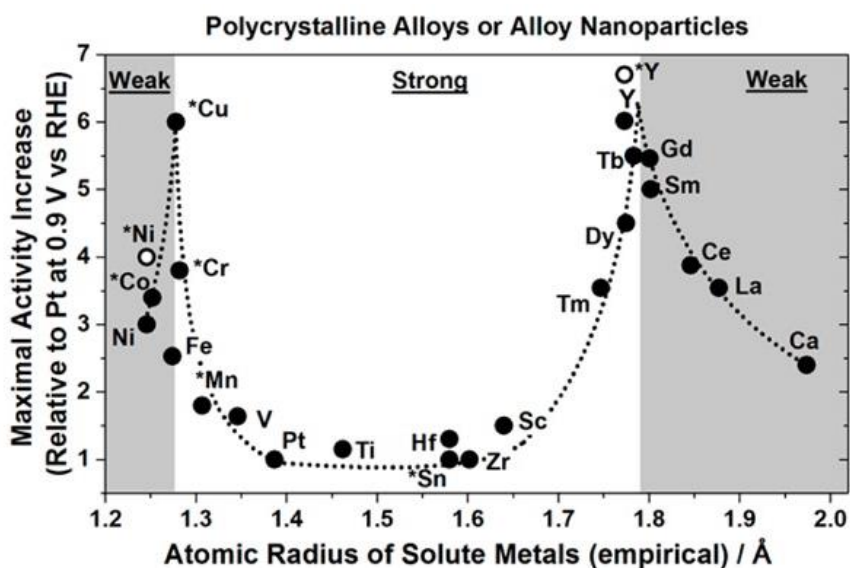


Figure 5-14: Activity increase for the electrochemical reduction of oxygen for nanostructured (indicated by \*) and polycrystalline Pt-alloy materials relative to pure platinum at 0.9V vs RHE in 0.1 M perchloric acid plotted versus the atomic radii of the solute elements. Taken from reference [61].

Elucidation of the origin of the activity of these types of catalysts is challenging and requires another suitable descriptor which is statistically connected to the binding energies of the key intermediates. Colic et al. proposed a so-called double volcano plot in which the maximal activity of an alloy catalytic system relative to polycrystalline platinum is plotted against the atomic radius of the alloyed metal as shown in Figure 5-14. For this approximation, the investigated polycrystalline alloys need to be put in respect to polycrystalline platinum and alloyed nanoparticles to platinum nanoparticles of the same size and shape (to account for the size effect). Additionally, the measurements are limited to 0.1 M perchloric acid to eliminate electrolyte effects and “conventional” nanoparticles of a convex shape. Hereby, the activity of the polycrystalline alloy and “their” nanoparticles can differ due to the potential partial delocalisation of d-electrons on the alloy nanoparticle [61].

The following section is based on reference [190] and the references therein.

### Palladium based catalysts

Based on the high price and scarcity of platinum, the research is also focused on palladium as more abundant and cheaper alternative. However, palladium is significantly less active for the electrochemical reduction of oxygen [191]. The highest activity was measured for (100) followed by a significantly less active (111)- and (110)-facet in perchloric acid [192]. The

activity of palladium can be increased by the generation of nanostructured palladium like nanocubes and octahedra [193]. However, their stability in perchloric acid is limited [194].

Like platinum, palladium alloys based on transition metals show higher activities but consist of palladium rich shells and alloyed cores [190, 195, 196]. Alternatively, more sophisticated structures such as complex nanoparticles and porous structures are also more active [197, 198].

### **Metal oxides**

A different class of catalysts are metal oxides based on group IV and V metals for acidic media. While they show limited activity for the electrochemical reduction of oxygen, they are mostly used as a catalyst support. However, another issue is their low electronic conductivity and lack of the adsorption sites for oxygen species. However, surface modifications, doping, alloying or highly dispersed nanoparticles allow an increase of their activity [199-202].

### **Metal nitrides and oxynitrides**

The negligible activity and electronic conductivity of nanoparticulate nitrides can be increased by doping with oxygen. Based on the “hybridization” of nitrogen with oxygen the adsorption properties of the formed oxynitrides are optimized [203, 204]. Additionally, tantalum, niobium and zirconium based oxynitrides are active for the oxygen reduction reaction [205].

### **Metal carbonitrides**

These catalysts are mostly based on transition metal carbonitrides which show the highest activities [206-209]. Interestingly, their onset potential for the oxygen reduction reaction can easily be influenced by the nitrogen content [200]. However, their activity is far behind the actually required values.

### **Metal chalcogenides**

The important metal chalcogenide catalysts consist of ruthenium selenides and sulphides, which demonstrated similar activities to platinum in sulphuric acid [210-213]. Through the coordination of bulk selenium with ruthenium, the semiconductor starts demonstrating metallic properties due to the electron transfer from the introduced metals [214]. The

introduced metals act as the active sites for the oxygen reduction reaction [215, 216]. However, problematic for the application of selenium as catalyst, is its toxicity [190]. In addition, for rhodium and iridium chalcogenides activities for the oxygen reduction reaction could be demonstrated [217, 218].

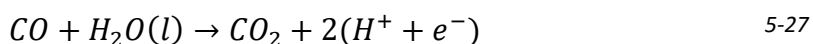
Chalcogenides with non-noble metals such as cobalt, nickel and iron are studied for more than a decade as potential catalysts for the oxygen reduction reaction [219-221]. Based on their low cost and high abundance, they are suitable candidates to replace platinum. Their activity ranks from sulphides, selenides towards tellurides [222].

### **Carbon-based catalysts**

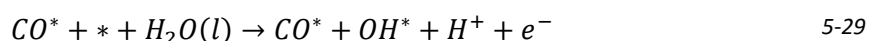
Interesting options as replacement of Pt could be iron catalysts based on carbon. The low price of such a material and its high abundance could make it a suitable alternative [223]. Based on the production method by pyrolysis it is assumed to be of the Fe/N/C type [224, 225]. This class of catalyst still faces several challenges such as low performance, durability and fast activity loss. This increases the price of fuel cells above platinum based ones. Main targets for their economical implementation are the improvements of the performance, durability (at least comparable to platinum) and a decrease in the production costs [190].

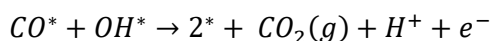
#### 5.9.3 Carbon monoxide oxidation (CMO)

The oxidation of carbon monoxide is an important anodic reaction in low-temperature fuel cells which use at the anode side mild oxidation of small organic molecules. However, carbon monoxide is a strong poison for platinum based catalysts and needs to be efficiently oxidized towards carbon dioxide. The reaction can be summarized as follows:



In contrast to the previously discussed mechanism for the electrochemical reduction of oxygen and the hydrogen evolution, this reaction proceeds *via* two entirely intermediates hydroxide and carbon monoxide. Hence, the reaction progress is limited by the adsorption of both species. For the underlying reaction mechanism, the so-called Langmuir-Hinshelwood model is assumed [226, 227]:





5-30

For the conducted experiments carbon monoxide was pre-adsorbed to the surface, so that the reaction is only limited by the adsorption of hydroxide from the electrolyte. Consequently, the adsorbates react readily with each other after the adsorption of hydroxide towards carbon dioxide.

The adsorption of carbon monoxide on the surface can be weakened with nanoparticulated platinum alloys with other elements like ruthenium, tungsten and iron. On ruthenium, oxygenated species are formed at lower potentials than on platinum. The formed hydroxide species then react with carbon monoxide *via* a bifunctional mechanism. The additional introduction of transition metals, like Mo, Ru or Sn, influences the electronic structure of the nanoparticles by electron transfer between platinum and alloyed element which weakens the bond towards the CO. These introduced metals further support the bifunctional mechanism by their oxyphilic groups [228].

While the use of the support is often limited to the increase of the catalyst dispersion or to increase mechanical and chemical stability of the material, it can also be used to influence the electronic properties of the deposited nanoparticles. The metallic support can change the electronic structure of the deposited electrocatalyst by introducing compressive strain and the ligand effect. The additional usage of metal oxides based on titanium, tungsten, cerium and iron allows to further increase the activity of platinum [228].

## 5.10 Electrochemical techniques

### 5.10.1 Three-electrode setup

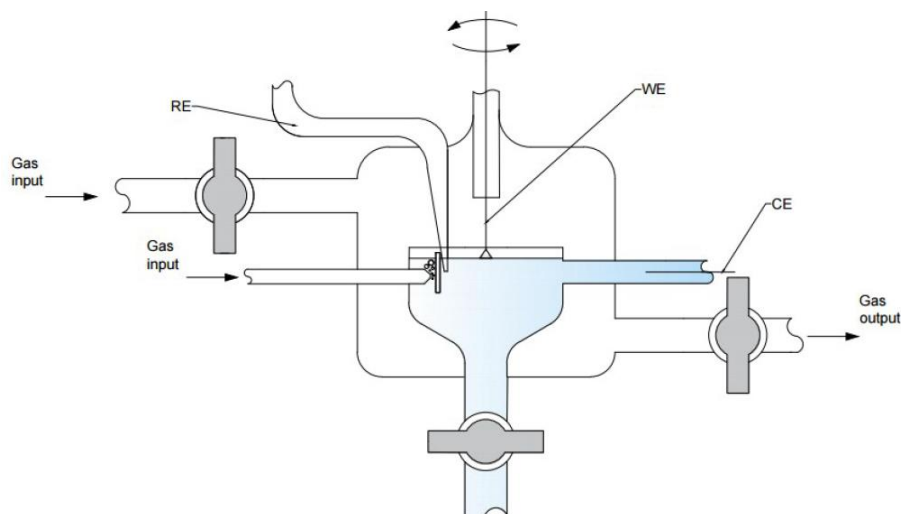
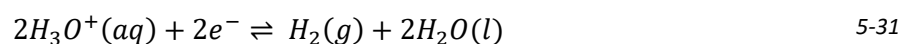
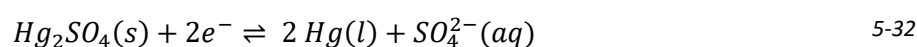


Figure 5-15: Schematic visualization of the three-electrode setup used in this thesis with a bead electrode as the working electrode (WE), a platinum wire as a counter electrode (CE) and the reference electrode (RE) connected to the cell via a Luggin capillary separated by a ceramic inlet. Taken from reference [229].

The voltage-current characteristics of two electrodes cannot be measured independently for each other. For instance, it is not possible to monitor the overpotential of the working electrode without the influence of the counter electrode. Therefore, it is necessary to implement a third electrode, the so-called reference electrode. The resulting setup used in this work is shown in Figure 5-15. This allows to measure the potential of the working electrode reproducibly. As the reversible hydrogen electrode was established as a common reference electrode in electrocatalysis all electrode potentials are reported versus this electrode in this thesis. In general, for hydrogen electrodes the following reaction is used on a platinum electrode:



For simplicity in experimental procedures, the reversible hydrogen electrode can be replaced by a commercial mercury-mercurous sulfate electrode with a determined conversion factor. This electrode consists of a platinum wire in a mixture of liquid mercury and nearly insoluble mercury sulfate with potassium sulfate as electrolyte and is separated by a ceramic inlet. The according reaction is:



To minimize the overpotentials at the reference electrode the current density should be kept at a minimum. Hereby the potential difference between working and reference electrode is

fixed by a potentiostat with the counter electrode adjusted so that the current is minimized at the reference.

### 5.10.2 Cyclic voltammetry

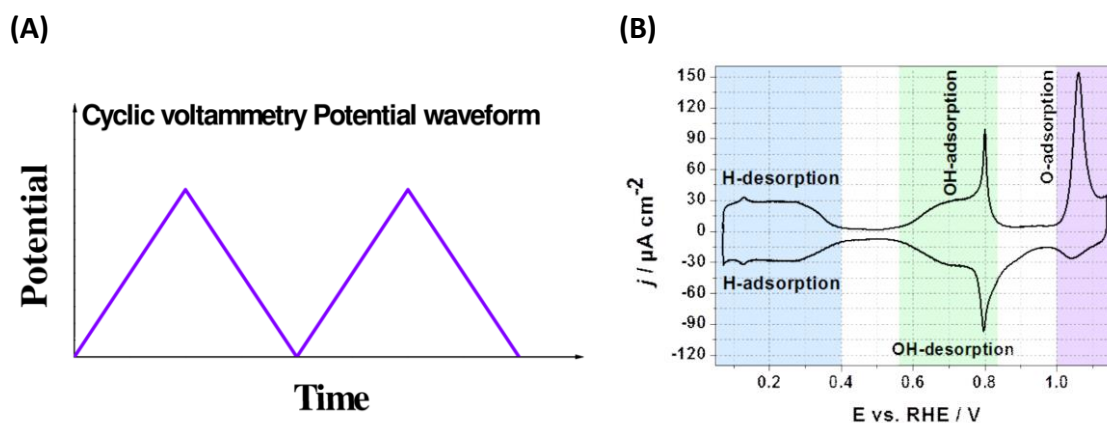


Figure 5-16: (A) Triangular waveform of the applied potential for the measurement of the cyclic voltammogram and (B) the resulting voltammogram for Pt(111) with the adsorption and desorption of species from the pure electrolyte. Taken from reference [230] and [59] supplementary, respectively.

This section is based on reference [90] and references therein. Cyclic voltammetry is a simple standard method to investigate the adsorption/desorption processes at an electrode surface. During the measurement, the potential at the working electrode is applied in a triangular waveform as shown in Figure 5-16A, while at the same time the current is monitored. With the potentials, also the dependent equilibrium state of the reaction is shifted linearly. This measurement is usually performed in the potential range from hydrogen and oxygen evolution reaction on platinum single crystal surfaces. In a pure aqueous electrolyte like perchloric acid (Suprapur), without any other electroactive species, only the adsorption/desorption of hydrogen and oxygen layers from the electrolyte is observed. The measurement is performed from anodic (positive going / lower vertex potential) to cathodic (negative going / higher vertex potential) currents whereby the potential is controlled by a potentiostat. Hereby the characteristics of the voltammogram are influenced by the

- Composition of the electrolyte
- Electrode material
- Potential region
- Scan rate (e.g. 50 mV/s)

- Scanning direction (anodic to cathodic or cathodic to anodic)
- For single crystals: surface facet

The simplest electrode surface is a single crystal surface. In this case, the surface facets play a key role in the adsorption of species from the electrolyte. Figure 5-16B shows a typical cyclic voltammogram for a Pt(111) electrode and its potential dependent adsorption of hydrogen and hydroxide from the electrolyte.

### 5.10.3 Rotating-disk electrodes and hanging meniscus – rotating disc electrode measurements

(A)



(B)

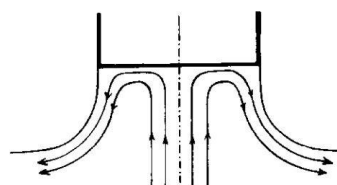


Figure 5-17: (A) Setup used in this work with installed rotating disk electrode. Taken from reference [231]. (B) Electrolyte flow towards a rotating electrode steadily supplying reactant-saturated electrolyte. Taken from reference [232].

The concentration of reactants changes during the investigation of, for instance, the electrochemical reduction of oxygen at the electrode interface. In this case, the oxygen has to diffuse from the surrounding electrolyte to the electrode surface. Therefore, the measured activity would be limited by the diffusion of oxygen. In general, there are three modes of mass transport in the electrolyte [47]:

#### 1. Diffusion.

Diffusion is plainly based on Brownian movement along a gradient in the absence of an electric field. The resulting flux ( $J_{ij}$ ) of a species  $i$  can be described by the first Fick's law:

$$J_{ij} = -D \partial c_i / \partial x_j \quad 5-33$$

with  $D$  being the diffusion coefficient for the ions in aqueous electrolytes,  $c_i$  being their concentration and  $x_j$  being their direction.

The resulting variations in concentration, due to e.g. consumption of a reactant, are taken into account by Fick's second law:

$$\frac{\partial c_i}{\partial t} = D_i \Delta c_i \quad 5-34$$

with  $t$  being the time and the difference in concentration. Due to the steady consumption of reactants at the electrode a concentration gradient is formed in this direction [47].

## 2. Migration.

Migration is caused by a potential gradient applied between two electrodes. This can be described by the Nernst-Planck-equation, an extension of the Fick's law:

$$J_{ij} = -D_i \left( \frac{\partial c_i}{\partial x_j} + z_i c_i \frac{F}{RT} E_j \right) \quad 5-35$$

with  $F$  being the Faradaic constant,  $z_i$  - the valence of the ionic species,  $R$  - the universal gas constant,  $T$  - the temperature and  $E_j$  - the applied electric field [47].

## 3. Convection.

Convection is forced movement based on natural or forced movement of the electrolyte species like small temperature differences and stirring (e.g. rotating disc electrode), respectively. It is described by:

$$J_{ij} = c_i v_j \quad 5-36$$

with  $v_j$  being the linear velocity in a specific direction [47].

Especially convection is often used to overcome the diffusion limitations. The steady rotation of the electrode moves its so-called hydrodynamic boundary. Additionally, it causes the electrolyte to be removed from the electrode surface by centrifugal forces. With increasing rotation, this force increases and the flux of saturated electrolyte towards the center of the electrode is increased. This ensures a steady supply of fresh electrolyte and ensures that the steady state current is controlled by the flow of the solution and not the diffusion towards the electrode [233].

A major problem of rotating disc electrodes is the encasing of the cylindrical samples in a polymer especially in case of single crystals. For the measurement, the encased sample is dipped a few millimeters into the electrolyte. In case of a not one hundred percent fitting

encasement, the electrode will experience lateral wetting, which can be seen in the voltammogram. Additionally, the installation requires taking the electrode out of the inert gas atmosphere. Thereby the surface of the electrode is easily oxidized and /or contaminated. An alternative approach is to use so-called hanging meniscus configuration. Thereby, the single crystal electrode is dipped into the electrolyte and pulled out to establish meniscus between the electrode surface and the electrolyte. This allows a higher rotation rate of up to ten thousand rotations per minute and keeping the freshly annealed electrode under “safe” conditions. Special emphasize needs to be put on the parallel alignment of the electrode surface to prevent destruction of the electrode and lateral wetting. The hydrodynamic behavior of the rotating disc electrodes in hanging meniscus-configuration are extensively discussed by Villulas et al. [232, 234-236]. Accordingly, the limiting current density ( $j_{lim}$ ) can be determined by this modified Levich equation:

$$j_{lim} = 0.62 nFD^{2/3}\nu^{-1/6}C^b\omega^{1/2}\left[1 - 2KR^{-1}\left(\frac{\nu}{\omega}\right)\right]^{1/2} \quad 5-37$$

with  $F$  being the Faradaic constant,  $D$  the diffusion coefficient,  $\nu$  the kinematic viscosity,  $C^b$  the bulk concentration of oxygen,  $\omega$  the rotation rate,  $R$  the geometric radius of the electrode and  $K$  the constant for the hanging meniscus. In this work, the influence of  $K$  can be neglected as only negligible values are achieved. Therefore, the kinetic current without mass transport limitation can be calculated by the Koutecky-Levich equation for first-order-reactions:

$$\frac{1}{j} = \frac{1}{j_k} + \frac{1}{0.62 nFD^{2/3}\nu^{-1/6}C^b\omega^{1/2}} \quad 5-38$$

Considering the definition of the limiting current density the equation becomes:

$$\frac{1}{j} = \frac{1}{j_k} + \frac{1}{j_{lim}} \quad 5-39$$

Accordingly, the kinetic current density can be calculated by [237]:

$$j_k = \frac{j}{1 - j/j_{lim}} \quad 5-40$$

#### 5.10.4 Electrochemical impedance spectroscopy

Electrochemical impedance spectroscopy is a technique which gives information about the kinetic parameters of a system and can help in forming deeper understanding of the electrochemical interface. An impedance is a total opposition of the system to ac-current. If one considers a simple reaction like:



The ac-probing reveals the situation that the interface responds like a “black box” with capacitors, resistors and other passive elements. The goal of the impedance analysis is to elucidate the physical model of such a black box and estimate its parameters. Electrochemical systems in general cannot be described by only linear differential equations. This limitation can be overcome by applying ac-probing signals of small amplitudes; the systems in this case behave quasi-linearly. According to the Butler-Volmer equation this range is limited to values below the thermal voltage defined by  $k_B T/e$ . An additional requirement is the “steady-state” during the measurement. This means the system needs to be stable during the acquisition of the data at stable pressure, temperature etc. Another important requirement is the causality. The observed response by the system should be solely caused by the excitation of the system.

In order to simplify the discussion of the models, instead of explicit equations related to the physical models, so-called equivalent electric circuits (EEC) are used. EEC is a compact representation of the physico-chemical equations describing the electrochemical systems. EEC normally consists of a certain number of relevant elements are resistors ( $R$ ), capacitors ( $C$ ), constant phase elements ( $CPE$ ), diffusional Warburg elements ( $W$ ), inductances ( $L$ ) and some other specific elements. To derive a physical model, the elements can only be connected according to only few rules originating from the so-called Randles-Dolin-Erschler approximation: there should be no arbitrary connections. An exemplary equivalent electric circuit for a single crystal platinum electrode in contact with perchloric acid is shown in Figure 5-18. The theoretical background of the assessment of the surface coverage will be discussed in detail later on. The discussion is based on references [238-241].

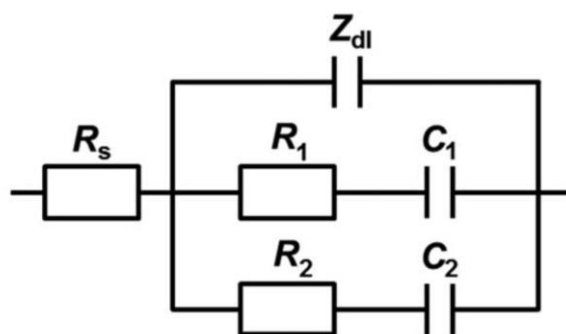


Figure 5-18: Equivalent electric circuit revealed for the surface adsorption on Pt(331) and utilized in this work. Taken from reference [229].

## 6 Experimental

### 6.1 The electrochemical cell

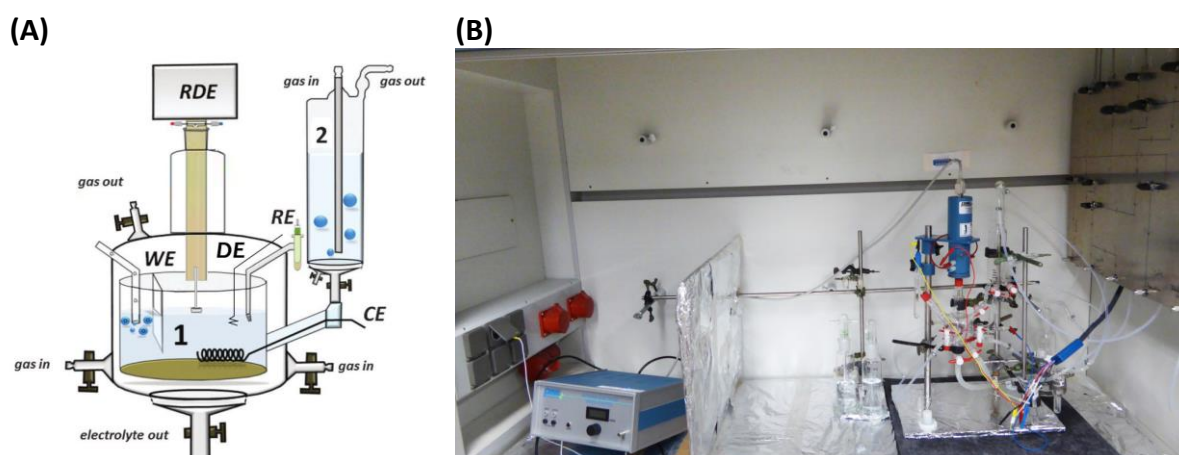


Figure 6-1: (A) Schematic and (B) photograph of the electrochemical cell used in this work (1 = electrolyte compartment; 2 = preconditioning compartment; WE = working electrode; DE = dummy electrode; RE = reference electrode; CE = counter electrode). Depending on the desired measurement the RDE could be disconnected. Pictures were taken from [231].

Figure 6-1 shows a schematic of the setup used in this work. It consists of a preconditioning cell (2) in which the electrolyte can be saturated with the necessary gases (with separate and independent gas in- and outlet), a Luggin capillary for the reference electrode (RE) and an electrolyte compartment for the measurements (1). The setup was protected from electromagnetic interferences from the rotator controller by a grounded metal shielding. The electrolyte compartment possesses two independent gas inlets to set up the necessary atmosphere in the compartment suited for the reactions and to continuously saturate the electrolyte. To prevent bubble formation at the electrode during continuous saturation of the electrolyte, the outlet inside the solution is separated by a glass wall. The gas flow was regulated with water locks at all outlets.

Prior to the measurements all glassware was cleaned regularly with a 3:1 mixture of sulfuric acid and hydrogen peroxide (both Suprapur, Merck, Germany). Subsequently the components were boiled out / rinsed multiple times using ultrapure water from an Evoqua Ultra Clear 10 TWF UV (Evoqua, Germany).

As the reference electrode (RE), a mercury-mercury sulfate (MMS) (SI Analytics, Germany) electrode was used. The reference electrode was separated by an ion conducting ceramic inlet or glass frit to minimize the ion exchange and kept in an extra compartment (Luggin capillary) filled with electrolyte solution. As counter electrode (CE), a platinum wire in direct

contact with the electrolyte was used. Before introduction of the electrode, the working electrode was kept at the potential control to prevent damage of the surface by potential spikes using a dummy electrode (DE). For this, a platinum wire connected in parallel to the working electrode in contact with the electrolyte was used. All measurements were performed using a VSP-300 potentiostat (Bio-Logic, France).

All potentials in this work were converted to the RHE scale by a factor determined with a self-made reversible hydrogen electrode (RHE).

### 6.1.1 Preparations before electrochemical measurements

As electrolytes, typically 0.1 M perchloric acid and 0.1 M alkali metal solutions were used. The purity of the chemicals is given at the end of this section. The acid solutions were prepared by diluting concentrated perchloric acid with ultrapure water. For the 0.1 M alkali metal solution, the according amount of lithium hydroxide monohydrate, sodium hydroxide and potassium hydroxide were dissolved in ultrapure water. For the measurement related to the effect of perchlorate, the electrolyte was prepared by mixing 0.2 M ultrapure perchloric acid and 0.4 M potassium hydroxide solution.

Before the measurements, the electrolytes were saturated for a minimum of 10 minutes with the necessary gases in the pretreatment compartment. During the experiment, the electrolyte compartment was continuously flooded with the same gas.

(A)



(B)



Figure 6-2: (A) Photograph of the setup used in this work and (B) the bead electrode in hanging meniscus configuration. Picture (A) is taken from reference [231].

## Pretreatment of the electrodes

As working electrodes, three different bead electrodes and three cylindrical electrodes were used. The specifications for all electrodes can be found in Table 1. For the experiments, the electrode surface was arranged in parallel to the electrolyte surface in the so-called hanging meniscus configuration (Figure 6-2B). Prior to each measurement, the platinum electrodes were annealed three times with an isobutane flame and let cool down for a minimum of 5 minutes in a reductive Ar/CO-atmosphere (1000 ppm CO (4.7) in Ar, 5.0, Air Liquide, Germany).

The quality of the surface was ensured by measuring the cyclic voltammogram of the freshly annealed electrode in 0.1M perchloric acid. For the measurements, the electrodes were introduced into the electrolyte under potential control at a potential of  $\sim 0.05$  V and measured in the electrochemically stable range from 0.05 to 0.9 V with a scan rate of 50 mV/s. To determine the quality of the surface, the measured voltammograms were compared with the state-of-the-art literature data.

Table 1: Measured electrode with their material, surface orientation and form.

<b>Electrode material</b>	<b>Surface orientation</b>	<b>Form</b>	<b>Literature CV</b>
platinum	$331 \triangleq 3[(111) \times (111)]$	Bead-type	[242]
platinum	$221 \triangleq 4[(111) \times (111)]$	Bead-type	[242]
platinum	$775 \triangleq 7[(111) \times (111)]$	Bead-type	[242]
platinum	$110 \triangleq 2[(111) \times (111)]$	Cylindrical	[242]
platinum	polycrystalline	Cylindrical	[243]
Pt <sub>5</sub> Pr	polycrystalline	Cylindrical	-

### 6.1.2 Evaluation of the hydrogen evolution – activity

After the quality assessment, the electrode was introduced under potential control into Ar-saturated 0.1 M perchloric acid electrolyte and arranged in hanging meniscus configuration. Subsequently the electrode was cycled in the potential range from -0.044V, -0.036 and – 0.086 V to 0.814 V with a scanning rate of 20 mV/s.

### 6.1.3 Evaluation of the oxygen reduction – activity

Prior to this measurement, the electrode was installed into a self-made RDE sample holder, and the surface was prepared like described above. Subsequently, the cyclic voltammogram of the electrode in the Ar-saturated alkali metal solutions was recorded. For the activity measurements, the main compartment and electrolyte were saturated with oxygen (4.6, Air Liquide, Germany) and the sample holder was installed in the rotator (Pine Eletronics, Grove City, PA, USA). Subsequently, the working electrode was introduced into the electrolyte under potential control at  $\sim 0.05$  V and arranged in hanging meniscus configuration. During the experiment, the electrode was rotated at different rotation speeds of 400, 625, 900, 1225 and 1600 rpm and cycled in the potential range from 0.05 to  $\sim 1.1$  V with a scan rate of 50 mV/s. After the activity measurements, the uncompensated resistance of the setup was determined under experimental conditions (see section 6.3.3).

### 6.1.4 Evaluation of the carbon monoxide – oxidation activity

After the pre-treatment, the electrode was introduced under potential control into Ar/CO-saturated (1000 ppm CO (4.7) in Ar, 5.0, Air Liquide, Germany) electrolytes. The electrode was installed using the hanging meniscus configuration and kept at a potential of  $\sim 0.1$  V for 40 minutes. During this time, the electrolyte and the compartment were steadily flushed with the Ar/CO-mixture. After forty minutes, the electrode was dipped into the electrolyte and the electrolyte was flushed for up to 15 minutes with argon to remove residual carbon monoxide. Subsequently, the CO stripping voltammogram was measured in a potential range of from 0.1 to  $\sim 0.9$  V with a scan rate of 50 mV/s.

### 6.1.5 Evaluation of the role of the spectator species on the performance of active sites

The pre-treated electrode was introduced into an Ar-saturated 0.1 M solutions under potential control and measured in the potential range from 0.1 to 1.1 V with a scan rate of

50 mV/s. Subsequently the activity was measured in the oxygen saturated solution at a rotation speed of 400, 625, 900, 1225 and 1600 rpm.

## 6.2 Modification of single crystal electrodes

Based on their defined surface structure single crystal electrodes allow reproducible introduction of defects onto the surface or other very controllable modifications.

### 6.2.1 Copper underpotential deposition (Cu UPD) and stripping

On the pre-treated electrode surface, a pseudomorphic overlayer of copper ions can be deposited from a 0.1 M perchloric acid containing 0.004 M  $\text{Cu}^{2+}$  ions. The electrode was introduced under potential control at 0.33 V and kept at this potential for three minutes.

For the measurement, the electrode potential was scanned to a potential of 1.0 V with a scan rate of 20 and 50 mV/s. The  $\text{Cu}^{2+}$  containing solution was prepared by dissolving CuO (99.99 %, Sigma Aldrich, Germany) in ultrapure perchloric acid solution and adding 1 ml of this solution to Ar-saturated perchloric acid.

### 6.2.2 Dealloying of Pt(111)/Cu surface alloys

These experiments were performed in Ruhr-Universität Bochum by Dr. J. Tymoczko. Briefly, on the Pt(111)-electrode copper was underpotentially deposited as described-above. Subsequently the monolayer was annealed for ~2 minutes at 400 °C in Ar-atmosphere containing 5% hydrogen (6.0, AirLiquide, Germany). Then the electrode was annealed twice in Ar/CO-atmosphere (0.1% CO in Ar) for two minutes at 400 °C. Afterwards it is cycled up to 1.0 V to remove the copper from the surface.

### 6.2.3 Galvanic displacement experiments

These experiments were performed in Ruhr-Universität Bochum by Dr. J. Tymoczko. A pseudomorphic overlayer of copper was deposited like mentioned above. The spontaneous displacement of copper by platinum was achieved by keeping the pretreated electrode at open-circuit potential in a 0.1 M perchloric acid solution containing 1 mM potassium tetrachloroplatinate(II) (99.99 %, Sigma Aldrich, Germany) at room temperature for ten minutes.

### 6.2.4 Electrochemical destruction procedures

The pre-treated electrode was cycled 10 times up to 1.72 V in Ar-saturated 0.1 M perchloric acid solutions.

### 6.2.5 Experimental assessment of \*OH adsorption energies

Cyclic voltammograms characterising certain adsorbate coverages can help to derive the adsorption isotherms for certain reaction intermediates (illustrated in Figure 6-3) [54, 244]. Cyclic voltammograms are integrated and the derived charge is correlated to the quantity of the adsorbed species. This requires a well-defined electrode surface and rather separated voltammetric features.

The difference in binding energy can be derived from the isotherms at the fractional surface coverage of  $\Theta=0.5\Theta_{\max}$ . To ensure the validity of this approach several things need to be neglected:

1. Changing adsorbate-adsorbate interactions
2. Heterogeneity of adsorption sites
3. Changes in the real surface area with the steps density

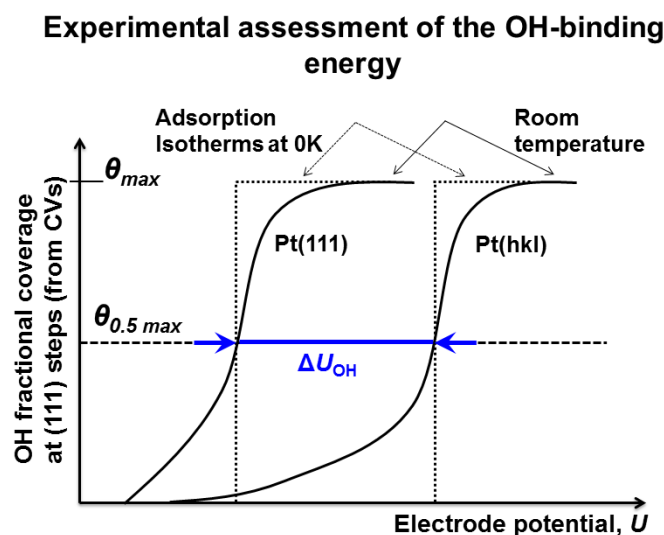


Figure 6-3: Schematics of the estimation of the relative change in \*OH energy from the integrated anodic parts of experimental voltammograms.  $\Delta U_{OH}$  stands for the change in the OH-binding energy of the surface under investigation relative to Pt(111)

## 6.3 EIS-measurements

### 6.3.1 Assessment of the adsorbate surface coverage

EIS measurements were conducted in the frequency range between 30 kHz and 10 Hz using a 10 mV amplitude of the probing signals in O<sub>2</sub>-free and O<sub>2</sub>-saturated (5.0, Air Liquide, Germany) 0.1 M perchloric acid. Aspects related to modeling and fitting of large experimental EIS datasets are reported in detail elsewhere [245] and briefly described below. To ensure the quality of the measured impedance spectra, the “linear” [246] and “logarithmic” [247] Kramers–Kronig check procedures were used. The legitimacy of the model and the accuracy of the fitting were assessed by the root-mean-square deviations and estimated individual parameter errors using the “EIS Data Analysis 1.0” software (described in references [248, 249]).

### 6.3.2 Equivalent electric circuit for the surface limited reversible adsorption

According to Dolin, Ershler [250] and Randles [251], a general model of the electrode/electrolyte interface is comprised of:

1. Impedance of the electrolyte ( $Z_{el}$ ), which is often approximated by a (uncompensated) resistance ( $R_U$ ) [252].

2. The impedance based on the interfacial charge transfer ( $Z_F$ ) influenced by mechanism and kinetics of the electrochemical reactions or mass transport modes [252].
3. The capacitive nature of the impedance of the interface itself ( $Z_i$ ), which is in many cases described by  $Z_i = C'_{DL}{}^{-1}(j\omega)^{-\phi}$  with  $C'_{DL}$  being proportional to the double layer capacitance,  $C_{DL}$ , and  $\phi \leq 1$ . When  $\phi = 1$   $C'_{DL}$  becomes true double layer capacitance  $C_{DL}$ .

Furthermore, they assume for the total impedance,  $Z_{tot}$ :  $Z_{tot} = Z_{el} + (Z_i^{-1} + Z_F^{-1})^{-1}$  as illustrated in the general equivalent circuit shown in Figure 6-4.  $Z_F$  and  $Z_i$  in parallel account for the current due to electrochemical processes considered as a “leakage” of the interfacial “capacitor”.

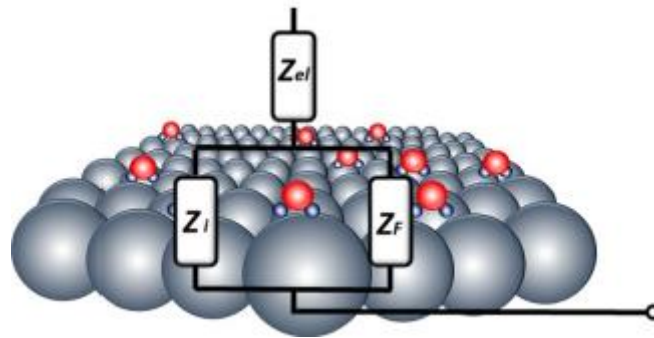


Figure 6-4: Dolin-Ershler-Randles generalized physical model relating the electrode/electrolyte interface.

Important adsorption/desorption processes in the investigated electrode potential region are  $*H$ ,  $*OH$  and  $*O$  adsorption/desorption. These species originate from water. At high concentrations of perchloric acid, the diffusional mass transport can be neglected. The application of small ac-probing signals to a system with reversible single-stage surface limited adsorption causes the adsorption current,  $i$ , and the fractional coverage of the adsorbate,  $\theta$ , to oscillate around quasi-steady-state values. The linear dependency of the response connected to the adsorption process is described by [253-256]:

$$\Delta i = \left( \frac{\delta i}{\delta E} \right) \Delta E + \left( \frac{\delta i}{\delta \theta} \right) \Delta \theta \quad 6-1$$

$\Delta$  corresponds to oscillating parameters during AC probing. Under the assumption that the adsorption currents and the current double layer charging are additive, equation 6-1 describes the interfacial impedance ( $Z$ ) as following:

$$Z(j\omega) = R_U + \left( (j\omega)^\varphi C'_{DL} + \frac{1}{R_{ads} + (j\omega C_{ads})^{-1}} \right)^{-1} \quad 6-2$$

where  $\omega$  is the angular frequency;  $R_{ads} = -1/(\partial i/\partial E)$  is the adsorption resistance;  $C_{ads} = -q_{ads}(\partial\theta/\partial E)$  is the adsorption capacitance;  $q_{ads}$  is the charge for the formation of an adsorbate layer, and  $j$  is the imaginary unit (see equivalent circuit in Figure 6-5A). At  $\omega \rightarrow 0$  the adsorption model derived from equation 6-2 does not show any continuous pathways for the direct current. This agrees with the circumstance that at the steady state the direct current of the surface limited adsorption (\*H or \*OH adsorption) becomes zero. The model however allows a direct current flow at non-steady state conditions in a potentiodynamic scan, enabling the adsorption capacitance to charge. For classical impedance experiments,  $R_{ads}$  determines the ability to distinguish between contributions of the double layer and the adsorption capacitance  $C_{ads}$ . Very fast adsorption causes small  $R_{ads}$ ; and  $C_{ads}$  is basically incorporated into the double layer response (Figure 6-5B).

If two adsorption processes with significantly different time constants occur, this allows to distinguish them with the interfacial impedance given below:

$$Z(j\omega) = R_U + \left( (j\omega)^\varphi C'_{DL} + \frac{1}{R_{ads,1} + (j\omega C_{ads,1})^{-1}} + \frac{1}{R_{ads,2} + (j\omega C_{ads,2})^{-1}} \right)^{-1} \quad 6-3$$

with  $R_{ads,1}$  and  $C_{ads,1}$  and  $R_{ads,2}$  and  $C_{ads,2}$  describing two adsorption processes (equivalent circuit is shown in Figure 6-5C).

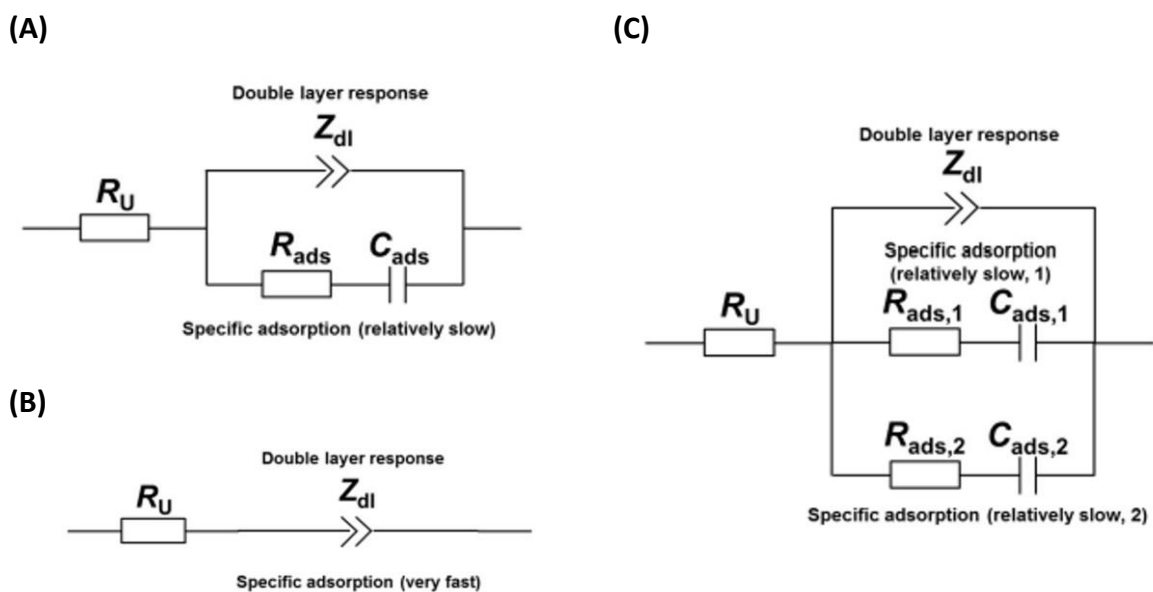


Figure 6-5: Revealed physical models of the electrode/electrolyte interface for Pt(331) electrodes in contact with 0.1M perchloric acid electrolyte.  $R_U$  – electrolyte resistance,  $Z_{dl}$  – impedance of the double layer,  $C_{ads,i}$  – adsorption capacitances,  $R_{ads,i}$  – adsorption resistances.

### 6.3.3 Assessment of the uncompensated resistance

The uncompensated resistance for each measurement was determined by measuring the EIS spectra at high frequencies. The measurements were conducted in the high frequency range and a 10 mV amplitude of the probing signals. The method is described by Colic et al. in detail elsewhere [257].

## 6.4 List of equipment, materials and chemicals

A list of all the equipment materials, and chemicals used in this work is given below.

### 6.4.1 Equipment

<b>Device</b>	<b>Specifications</b>	<b>Supplier</b>
<b>Potentiostat</b>	VSP-300	Bio-logic, France
<b>Rotating disc electrode</b>	Pine RDE 710 RDE with self-made electrode holder	Pine Research Instruments, USA
<b>Reference electrode</b>	Mercury – Mercury Sulphate	SI Analytics, Germany
<b>Water purification systems</b>	Evoqua Ultra Clear 10 TWF 30 UV	Evoqua, Germany

### 6.4.2 Materials

<b>Electrodes</b>	<b>Purity (%)</b>	<b>Parameter</b>	<b>Supplier</b>
<b>Pt(pc)</b>	99.99	diameter: 5mm roughness: 30nm	Mateck, Jülich, Germany
<b>Pt(111)</b>	99.99	diameter: 5mm oriented better than 0.1° roughness: 30nm	Mateck, Jülich, Germany
<b>Pt(110)</b>	99.99	diameter: 5mm oriented better than 0.1° roughness: 30nm	Mateck, Jülich, Germany
<b>Pt(331)</b>	99.99	diameter: 2.5mm oriented better than 0.5° roughness: 50nm	icryst, Jülich, Germany
<b>Pt(221)</b>	99.99	diameter: 2.5mm oriented better than 0.05° roughness: 50nm	Prof. Feliu, Alicante, Spain
<b>Pt(775)</b>	99.99	diameter: 2.5mm oriented better than 0.05° roughness: 50nm	Prof. Feliu, Alicante, Spain
<b>Pt<sub>5</sub>Pr(pc)</b>		diameter: 5mm roughness: 50nm	Mateck, Jülich, Germany
<b>Pt-wire (pc)</b>	99.99	diameter: 0.3mm	GoodFellow, Germany

<b>Gas</b>	<b>Purity</b>	<b>Supplier</b>
Argon	5.0	Air Liquide, Germany
Argon/CO-mixture (1000 ppm CO in Argon)	Ar: 5.0 / CO: 4.7	Air Liquide, Germany
Oxygen	4.5	Air Liquide, Germany

### 6.4.3 Chemicals

<b>Chemical</b>	<b>Purity</b>	<b>Supplier</b>
CuO	99.99%	Sigma Aldrich, Germany
HClO <sub>4</sub> (70%)	Suprapur	Merck, Germany
H <sub>2</sub> O <sub>2</sub> (30%)	Suprapur	Merck, Germany
H <sub>2</sub> SO <sub>4</sub> (96%)	Suprapur	Merck, Germany
LiOH*H <sub>2</sub> O	99.998%, trace select	Sigma Aldrich, Germany
NaOH*	99.99%, semiconductor grade	Sigma Aldrich, Germany
KOH*	99.99%, trace metal basis	Sigma Aldrich, Germany
RbOH (50%wt solution)	99.9%	Sigma Aldrich, Germany
CsOH (50%wt solution)	99.9%	Sigma Aldrich, Germany
NaOH <sup>#</sup>	analytic reagent grade	Fisher chemical, USA
KOH <sup>#</sup>	Reag. Ph. Eur.	VWR Prolabo Chemicals, USA

\* Chemicals were used for single crystal measurements.

# Chemicals were used for measurement of the Pt<sub>5</sub>Pr alloy activity.

### 6.4.4 Software

<b>Software</b>	<b>Area of application</b>
EC-LAB V 10.44	control and data acquisition from the potentiostats
EIS Data Analysis 1.0	fitting of electrochemical impedance spectra
GetData	digitalization of graphs from the literature
OriginPro 2015G - 2017G	data analysis, graphing, and processing

## 7 Results and discussion

The activity of state-of-the-art catalysts is limited by their, in general not optimal, adsorption properties of the intermediates for reactions of this study, namely the carbon monoxide oxidation, oxygen reduction and hydrogen evolution reaction. To enhance their activity, the density and quality of active sites need to be increased and improved, respectively. For this, realizing the optimal adsorption properties on surfaces is necessary by the following methods:

- the formation of random or periodical defects on pure surfaces
- the change of adsorbate structure at distinct sites by long-lived surface adsorbates in their vicinity
- the introduction of strains at the surface, which significantly changes the adsorption properties of the catalytic centers
- the electrolyte composition, which can be designed in order to tune the adsorption of the intermediates, since even spectator species interact either directly with the surface or with the first water-layer

In the following sections, these alternatives will be discussed in more detail.

## 7.1 The generalized coordination number as an activity descriptor

The assessment of trends in the adsorption energies is a fundamental aspect in heterogeneous catalysis. Nowadays, they are determined by rather time-consuming density functional theory-calculations with a significant error-margin of  $\pm 0.2$  eV in comparison to adsorption energies of only up to 1 eV [258]. A first model based on such calculations, which is still used today, is the d-band model, as discussed above. Nevertheless, because those calculations demand a high amount of computational power and time, their application in high-throughput screening is limited. Additionally, the predictive power of the d-band model is restricted since sites of completely different nature and structure on the surface show similar adsorption trends (see table in Figure 7-1). Additionally, the pDOS, cornerstone of the d-band model, is not able to differentiate key sites at the nanoscale [59, 259-261]. An alternative rather simple approach are coordination numbers used in chemistry, as discussed above [85]. Although the coordination numbers perform relatively well for extended surfaces they do not explain the activity of small nanoparticles adequately due to the finite size effect. A major problem for both descriptors is that they do not take into account the geometry of the surface sites.

The so-called generalized coordination number is an extension of the coordination number. It is a quick and mathematically straightforward method to estimate the activity of a specific surface site. In contrast to the coordination number, the generalized coordination takes not only the direct neighbors of the central atoms into account but also their neighbors. Therefore, the geometry of a potential active sites is considered. Nevertheless, it requires basic density functional theory-calculations for a single crystal model surfaces as reference point to determine its optimal adsorption properties [53].

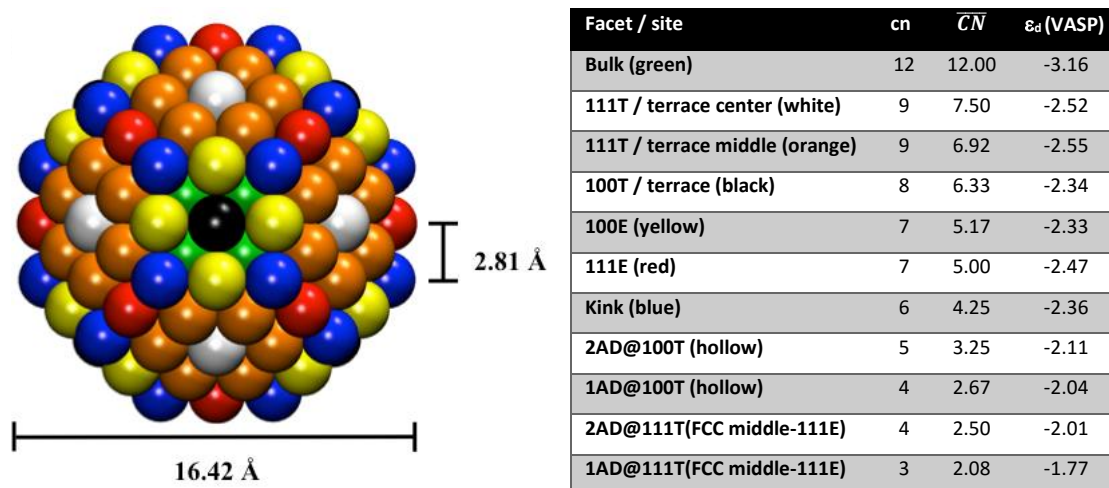


Figure 7-1: Generalized coordination number ( $\overline{CN}$ ), coordination number (cn) and d-band center ( $\epsilon_d$  (VASP)) for several surface sites on platinum nanoparticle ( $Pt_{201}$  / right). Taken from supplementary data in [53].

However, for the calculations the detailed knowledge of the crystal structure is essential to prevent miscounting. Especially in case of more complex surfaces, the counting can become challenging and in any case double counting of the neighbors needs to be prevented. Figure 7-1 shows the three mentioned descriptors relative to each other. While the d-band model and coordination number give similar values for different surface sites, the generalized coordination number takes all geometric characteristics into consideration [53].

Consequently, to determine the actual active sites the generalized coordination is the most suitable alternative. Based on its simple assessment, it will be used in the following discussion as sole descriptor to evaluate the contribution of specific sites to the overall activity of a catalyst.

## 7.2 The Hydrogen evolution reaction on model stepped platinum surfaces

Highly efficient catalysts for the hydrogen evolution reaction are an essential part for the economically feasible implementation of hydrogen for future energy storage. Nowadays state-of-the-art catalysts consist of high amount of expensive precious metals to compensate for their moderate activity [49]. Hence, the optimization of the catalyst must aim at increasing the quantity and activity of the active sites to allow a decrease of the catalytic materials.

For the analysis, it was assumed that solely the hydrogen intermediates adsorbed on the surface are important for the activity assessment. Additionally, no predominant reaction mechanism was considered, following to the approach by Norskov et al. [262, 263]; and the binding energy of the H-intermediate is considered as the activity descriptor. Surface diffusion of adsorbed hydrogen is also neglected, which is, however, important for the Tafel step. Following these concepts, the volcano plot in Figure 7-2 gives the first approximation on the optimal binding properties [263]. It links the activity trends of pure metals for the hydrogen evolution reaction with the binding energy of hydrogen to the surface. The binding energy is derived from density functional theory calculations. While the exact value for the binding energy also depends on the surface coverage of hydrogen [264], active sites should have an optimum electronic structure, binding hydrogen slightly weaker ( $\sim 0.1$  eV) than Pt(111) [50]. Unfortunately, this volcano plot does not provide any further design principles.

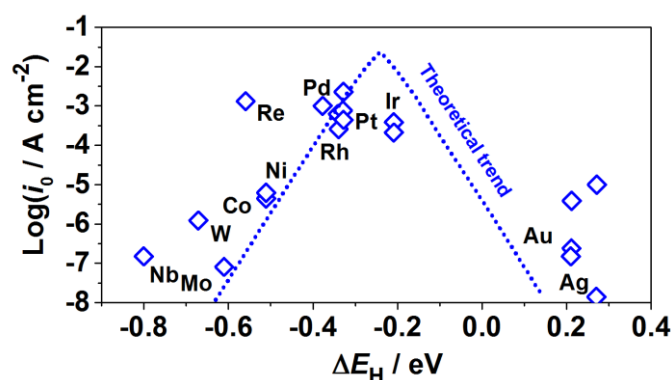


Figure 7-2: Theoretical volcano plot showing the relation between the experimentally measured HER-activities and calculated binding energies of the H-reaction intermediates. Taken from [263].

Figure 7-3 shows the coordination-activity plot for this reaction. Following its geometric considerations, one can reveal that the optimal active sites for the hydrogen evolution

reaction should have higher coordination with a value of the generalized coordination number of  $\sim 7.7$ . Based on the density functional theory calculations, it can be assumed that at low or moderate coverages hydrogen does not occupy “on-top” adsorption sites [264]. Therefore, only the bridge and hollow sites are taken into consideration as active sites for the electrochemical evolution of hydrogen.

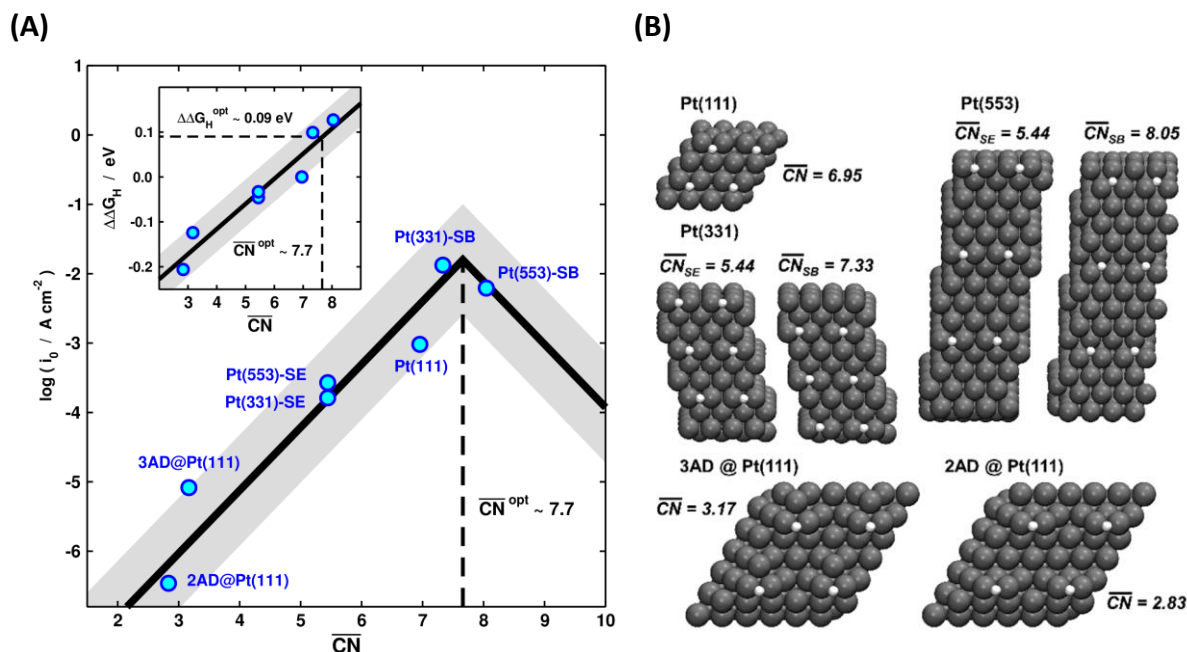
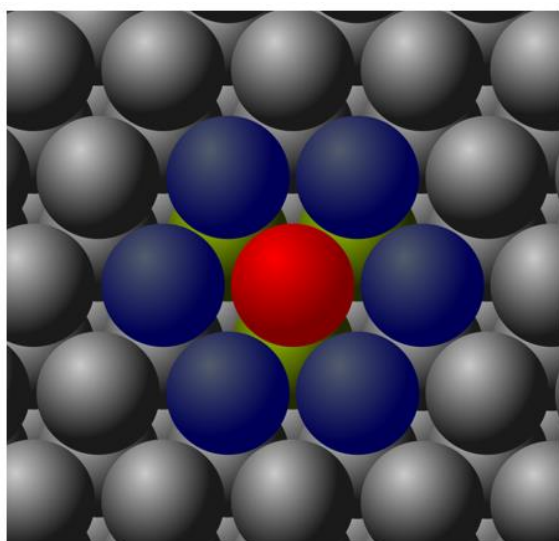


Figure 7-3: (A) Coordination-activity-plot for the hydrogen evolution reaction linking the activity of specific surface sites and their geometry (SE: step edge / SB: step bottom / AD: adatom on Pt(111)). In the Inset, the correlation between differential adsorption energies in respect to Pt(111) and the generalized coordination numbers is given. The optimal value of the generalized coordination number for the hydrogen evolution reaction on platinum is  $\sim 7.7$ . (B) Designated sites from the coordination-activity plot on single crystals.

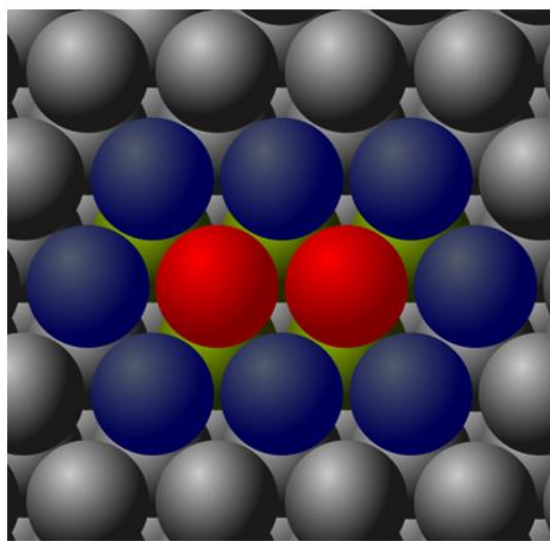
Figure 7-4 shows the generalized coordination number of these sites on a Pt(111) surface with the top site for comparison. While at the bridge sites adsorption of hydrogen is close to the optimum ( $\overline{CN} = 7.33$ ), the threefold hollow sites deviate strongly from the optimum ( $\overline{CN} = 6.95$ ). Optimization is possible by the introduction of foreign metals, which however potentially decrease the stability of the catalyst. On the other hand, the introduction of platinum adatoms on the surface has no beneficial effect on the activity of the catalyst. At these sites, the adsorbates are bond too strongly as illustrated by the generalized coordination number of these sites with 2.83 and 3.17 for two and three atomic adatoms, respectively. Alternatively, the activity can be increased by the introduction of periodical highly coordinated sites without the need of alloying. While such defects are only sporadically found on pristine Pt(111), they can be formed periodically by the introduction of

steps into the surface. These beneficial so-called concave defects are found below the step edges and increase the coordination of the adjacent terrace sites. An example for such surfaces are Pt(331), Pt(221) and Pt(775) consisting of three-, four- and seven-atomic (111)-terraces with (111)-steps. In comparison to Pt(111)  $\overline{CN} = 6.95$ , their concave sites get closer to the optimum with  $\overline{CN} = 7.33$  for Pt(331). However, the introduction of these defects also causes the formation of significantly less coordinated three-fold hollow sites at the step edges with  $\overline{CN} = 5.44$ . These sites bind hydrogen too strongly and are not further considered as potential active sites. Beyond a terrace length of four atoms, the extension does not influence the generalized coordination number further with the maximum being  $\overline{CN} = 8.05$  for the concave and  $\overline{CN} = 5.44$  for the convex sites. Therefore, Pt(553) was chosen to represent Pt(221) and Pt(775). However, the concave bridge sites on these surfaces are closer to the optimal value, giving higher activities. Pt(110), also denoted as Pt[2(111)x(111)], was not considered due to its reconstruction under reaction conditions and the resulting formation of longer terraces [265-267].

**(A) Top site**

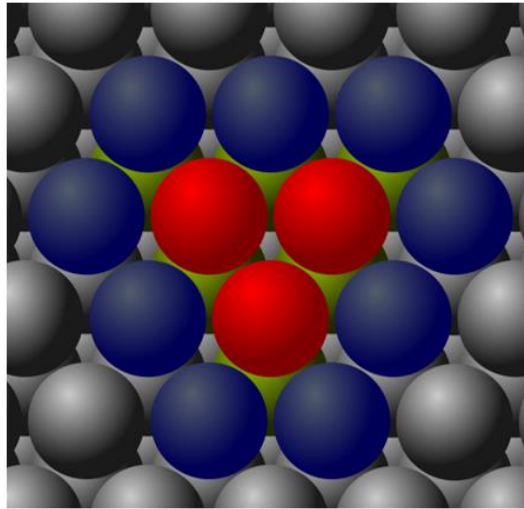


**(B) Bridge site**



$$\overline{CN} = \frac{6 * 9 + 3 * 12}{12} = 7.5 \quad \overline{CN} = \frac{8 * 9 + 5 * 12}{18} = 7.33$$

### (C) Threefold hollow site (fcc)



$$\overline{CN} = \frac{9 * 9 + 6 * 12}{22} = 6.95$$

Figure 7-4: Generalized coordination number of the typical adsorption sites on Pt(111) surfaces: (A) top, (B) bridge, and (C) threefold hollow site for the fcc crystal structure.

Figure 7-5A shows the cyclic voltammograms of the surfaces in argon-saturated 0.1 M perchloric acid within their area of electrochemical stability. In the relevant potential range of the cathodic scan from 0.4 to 0.1 V the underpotential deposition of hydrogen on the terraces is observed. The introduction of steps manifests itself in the additional adsorption features at ~0.13 V which are attributed to the adsorption/desorption of hydroxide and replacement of underpotential deposited hydrogen on the step edges. Above 0.5 V, the hydroxide adsorption on terraces is also observed. The characteristic features of cyclic voltammograms were taken as a criterion to ensure the quality of the surface [242].

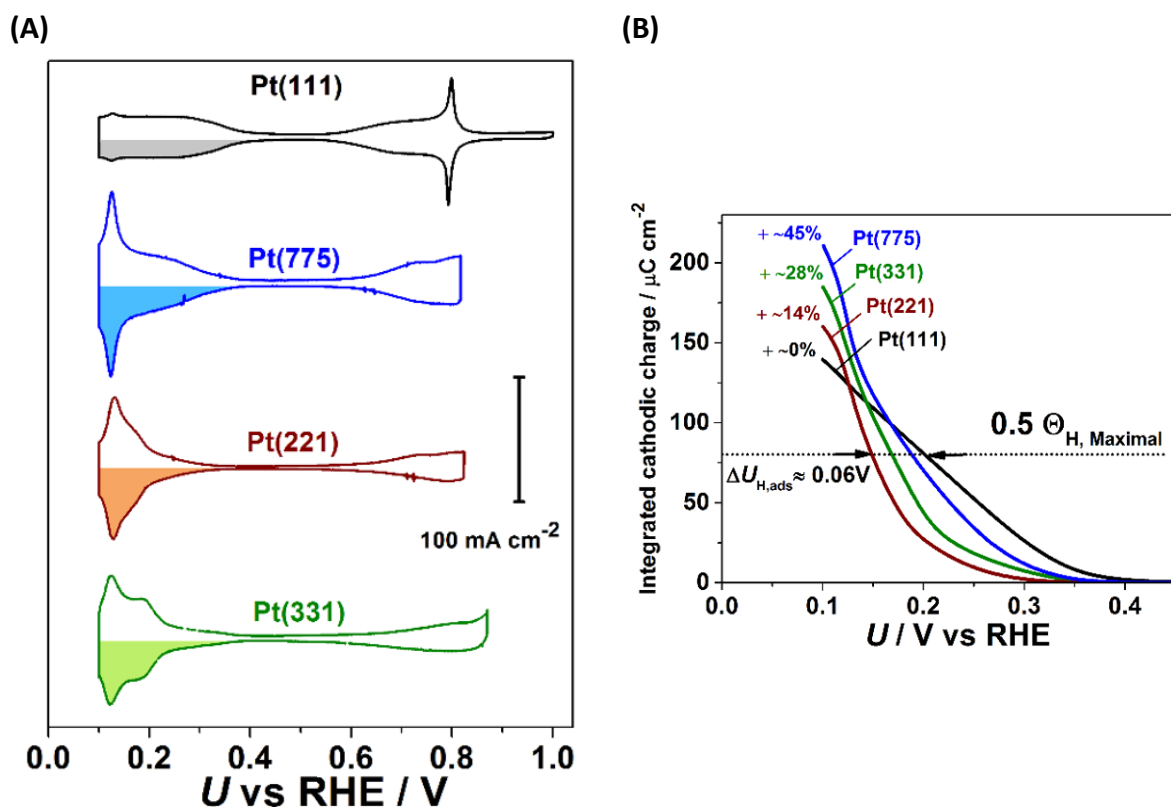
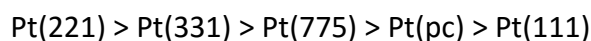


Figure 7-5: (A) Cyclic voltammograms of Pt(111) and the measured stepped surfaces. (B) Integrated cathodic charge of the cyclic voltammograms in the UPD-region.

The activity measurements were performed in argon-saturated perchloric acid in hanging meniscus configuration to ensure minimal influence of undesired experimental factors [257]. This allows to compare the results to literature values which are performed in hydrogen free electrolytes [119, 137, 268]. Moreover, the results are not corrected for the IR-drop to avoid introduction of additional errors and compare the model surfaces under the same conditions [257]. Because of the difficult assessment of the real exchange current densities, the experiments were performed under the same conditions and in the same cell geometry [137]. Figure 7-6A shows the activity for the hydrogen evolution reaction of Pt(111) and the stepped platinum surfaces. Indeed, as theoretically discussed, the introduction of steps increases the activity for the hydrogen evolution reaction. It even allows to achieve similar activities as the benchmark copper-based near surface alloy catalyst. Figure 7-6B shows a bar chart associating the activity at a potential of  $-0.036 \text{ V}$  normalized to the surface area of the electrode. As can be seen the activity, for those stepped surfaces the activity increases twofold relative to Pt(111) with Pt(775) showing the highest activity. However, the increase in potential adsorption sites for hydrogen demands a corresponding correction.

The indicated cathodic charge retrieved by integration (Figure 7-5B) shows a rise in the available H-adsorption sites for the stepped surfaces compared to Pt(111) in the H-UPD region. The increase is caused by the different adsorption sites resulting from the steps and increases for Pt(221) by ~14%, for Pt(331) by ~28% and for Pt(775) by ~45% relative to Pt(111). Additionally, their isotherms are shifted towards more negative potentials. At the reference point, at half of the maximal of the adsorbate coverage for Pt(111), the shifts represent the average differences in the adsorbate binding energies [54, 61, 269]. The shift is maximal for Pt(221) with ~0.06 V for Pt(221) followed by Pt(331) with ~0.04 V and Pt(775) with ~0.02V. Taking these results into account the corrected increase in activity is shown in Figure 7-6C. With the activity ranking as follows:



The assumption that concave sites offer superior adsorption properties compared to plane Pt(111) agrees well with the observed activity trend. On Pt(221) a high ratio of preferential sites with  $\overline{CN} = 7.33$  are found, with increasing terrace length more sites with a lower generalized coordination number are formed. Consequently, Pt(775) shows a lower activity than Pt(221). In case of Pt(331) the high activity is caused by the threefold hollow sites at the step bottoms which are closer to the optimum with an increase of towards  $\overline{CN} = 7.33$ . Here, Pt(221) shows an 1.8-fold and 1.5-fold increase in activity relative to Pt(111) and polycrystalline platinum, respectively.

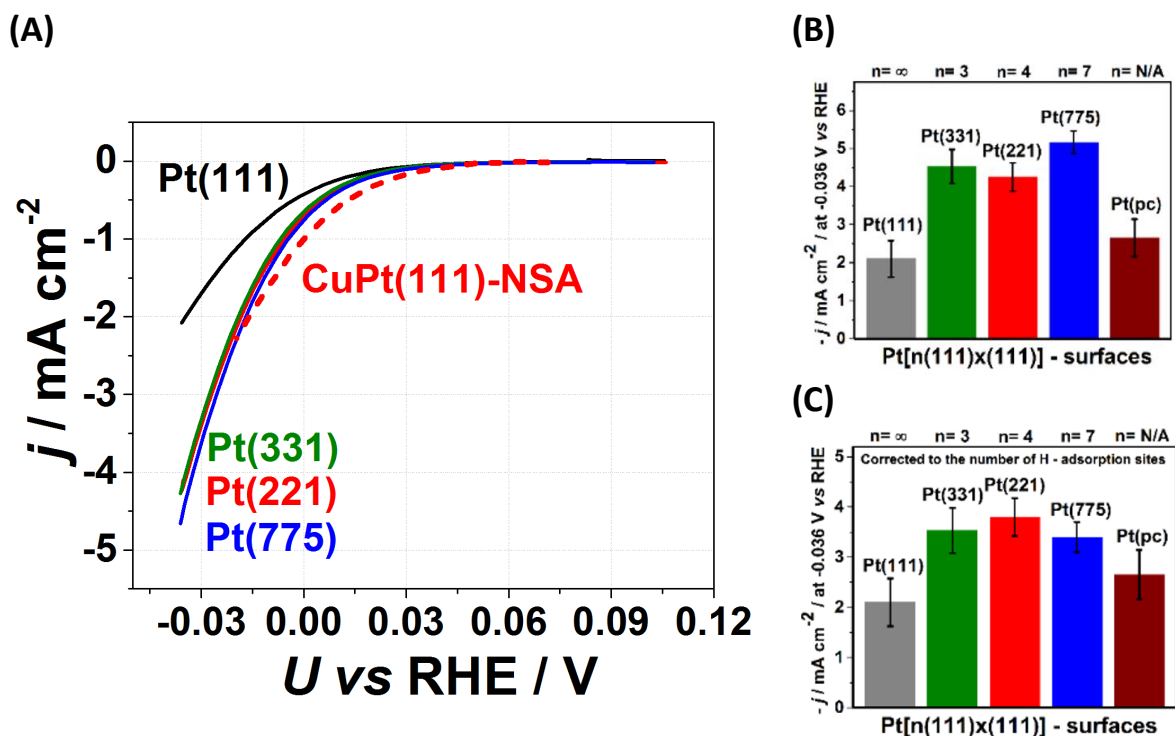


Figure 7-6: (A) Activity comparison of the hydrogen evolution reaction for all measured electrodes in argon-saturated 0.1 M perchloric acid in comparison to Pt(111) and a copper based platinum near surface alloy. (B) The activity of the surfaces in comparison to pristine Pt(111) and polycrystalline platinum at -0.036 V. (C) Activity of the surfaces corrected for the number of hydrogen adsorption sites. The reference data for the near surface alloy was taken from [269].

In contrast to the statements elsewhere [270], these results indicate that the hydrogen evolution reaction is indeed structure sensitive. Interestingly, on Pt[n(111)x(100)] only a twenty percent improvement is observed which only differs from the investigated surface by (100)-steps instead of (111) (compare Figure 7-7) [270]. While surface coordination is a primary factor to enhance the activity, also step symmetry is important to define water solvation [87, 271].

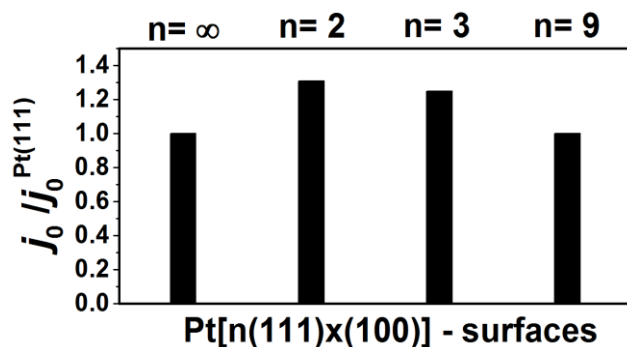


Figure 7-7: Relative "apparent" exchange current densities for Pt[n(111)x(100)] surfaces. Data taken from [269].

To conclude the introduction of steps causes an increase in the activity for the hydrogen evolution. This indicates that this reaction is indeed structure sensitive. The most active sites are the bridge and hollow sites with the generalized coordination number  $\sim 7.7$ . From the experimental results one can conclude that the activity increase is limited towards concave defects with (111)-terraces and (111)-steps. The optimal step density is achieved by Pt(221) also denoted as Pt[4(111)x(111)]; the latter demonstrate the highest hydrogen evolution activity for the pure Pt surfaces ever reported in the literature.

### 7.3 Oxygen reduction reaction at Pt surfaces elucidation of the nature of active sites

The electrochemical reduction of oxygen is an additional integral part of the hydrogen economy [272]. The reaction occurs in the fuel cells and limits their efficiency due to its sluggish kinetics [75, 273-277]. Nowadays, electrocatalysts for fuel cells mostly consist of expensive precious metals. The metal of choice is Pt and its alloys due to their nearly optimal binding energy, (as illustrated by the volcano plot in Figure 7-8) and stability in strongly alkaline and acidic environment [52, 278-280].

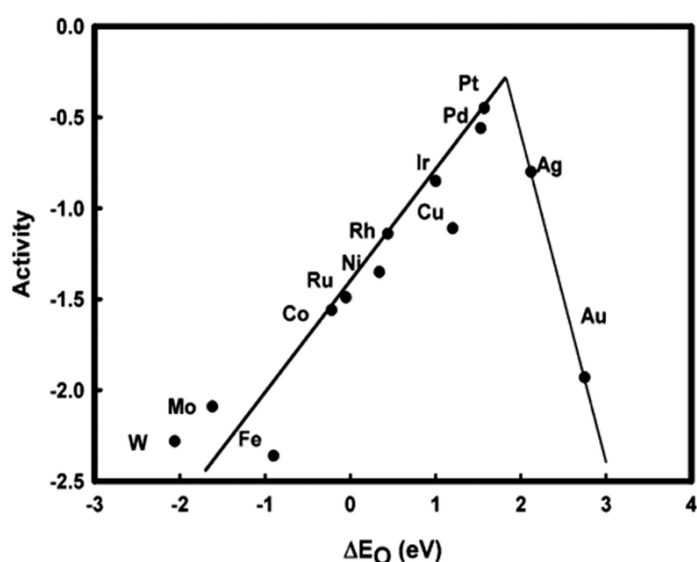


Figure 7-8: Oxygen reduction reaction activity volcano plot for different transition metals with (111)-surface arrangement. The theoretically assessed activity is plotted versus the oxygen binding energy. Taken from reference [281].

The identification and the subsequent optimization of active sites for this reaction would help to decrease the overpotential [90]. Nowadays, the moderate activity of most state-of-the-art catalysts is compensated by uneconomic amounts of catalytic material which limits the prevalence of fuel cells in the transportation and energy sector [282-285]. Therefore, identifying the active sites for these reactions is an important task.

### 7.3.1 Oxygen reduction reaction on Pt(111)

While pristine Pt(111) offers beneficial adsorption energy of hydroxide, its adsorption properties are still not optimal.

The active sites for the oxygen reduction reaction are found on “top” sites [286]. The bond strength toward the adsorbate is proportional to the coordination of the surface atoms resulting into a weaker bonding at higher coordinated sites [53, 59, 287-290].

In Figure 7-9A, the coordination-activity plot for the electrochemical reduction on oxygen is shown. It correlates the geometry of a surface site, through  $\overline{CN}$  as a descriptor, with the activity of the site. While adsorption energies derive with optimal adsorption properties [52, 174, 291], structural parameters (like  $\overline{CN}$ ) identify the optimal geometry of an active site. If  $\overline{CN}$  is used as descriptor, the intersection between both potential determining steps gives the optimal value for the generalized coordination number for the active site. In case of the oxygen reduction reaction this value is 8.3, agreeing with energetic volcano plots, indicating that the optimal catalyst requires a  $\sim 0.13$ - $0.15$  eV weaker binding of the adsorbate relative to pristine Pt(111) with  $\overline{CN} = 7.5$  [51, 52].

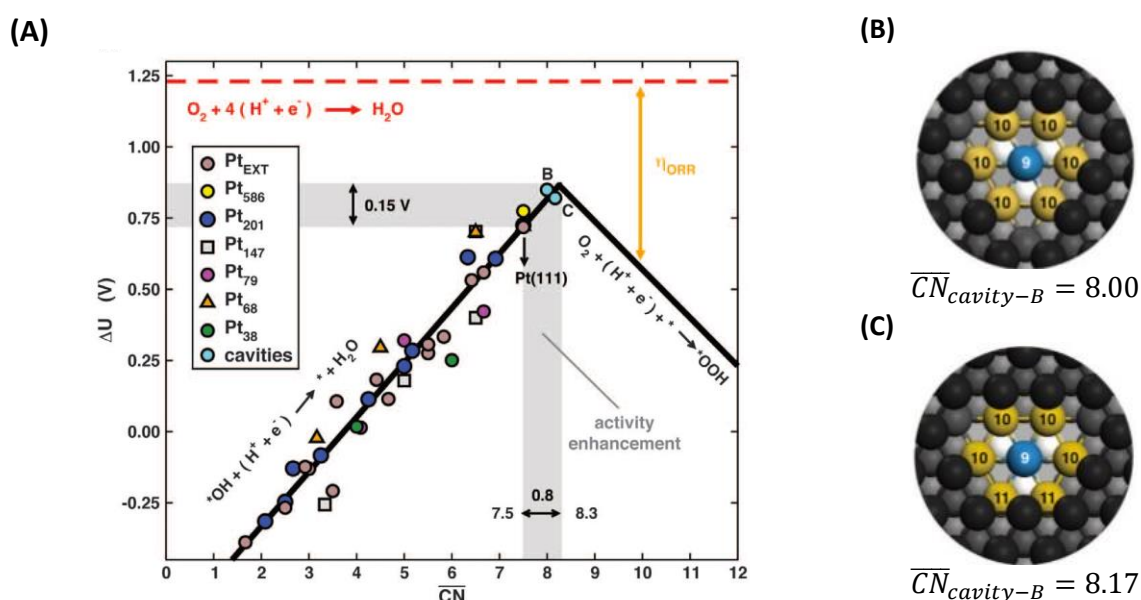


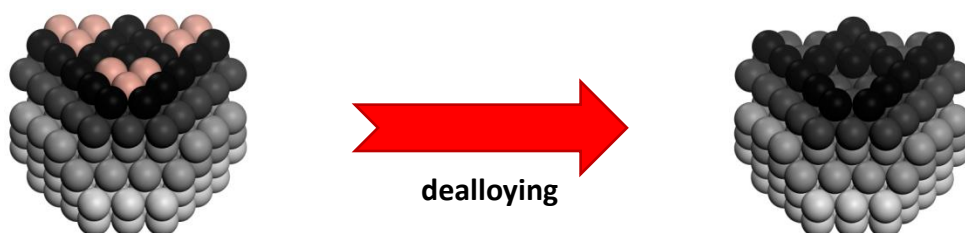
Figure 7-9: (A) Coordination-activity plot correlating the activity for the electrochemical reduction of oxygen with the geometry of sites on pristine Pt(111), defective Pt(111) with cavities and nanoparticles. The potential determining steps are indicated on the too strong (left) and weak (right) binding side of the volcano. Resulting (B) six and (C) five atomic cavities after treatment of the pristine Pt(111) with different methods with indicated coordination numbers. The resulting generalized coordination number is indicated below each picture. Taken from reference [59].

On pristine Pt(111), such higher coordinated sites are only randomly encountered at defects like steps or cavities. Therefore, the intermediates for the oxygen reduction reaction are generally bound too strongly to the surface. However, based on these theoretical assumptions highly active catalyst can be prepared without alloying. Hence, the optimal material should possess sites with an increased coordination of the surface atoms. Therefore, the controlled introduction of higher coordinated cavities into the surface should increase the activity of Pt(111) for the oxygen reduction reaction. Figure 7-9B and C show these “optimal” surface defects as six- and five-atomic cavities with  $\overline{CN} = 8.00$  and  $\overline{CN} = 8.17$  at the center, respectively. These sites are closer to the optimal value of  $\overline{CN} = 8.3$  for the electrochemical reduction of oxygen on platinum and should increase the activity of the surface. Such highly active catalysts can be engineered by treating Pt(111) with different methods (illustrated in Figure 7-10):

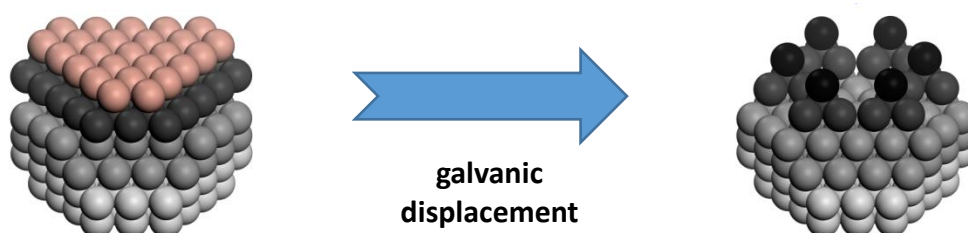
- (A) The selective electrochemical stripping of copper atoms from a Cu/Pt (111) top layer [227].
- (B) The ionic exchange of copper atoms from an electrochemically generated overlayer [292].
- (C) The reduction of subsurface generated platinum oxide by a cathodic potential sweep causing the desorption of platinum from the surface [293, 294].

These surface treatments form desired six-atomic and undesired five-atomic cavities increasing the activity of pristine Pt(111).

(A)



(B)



(C)

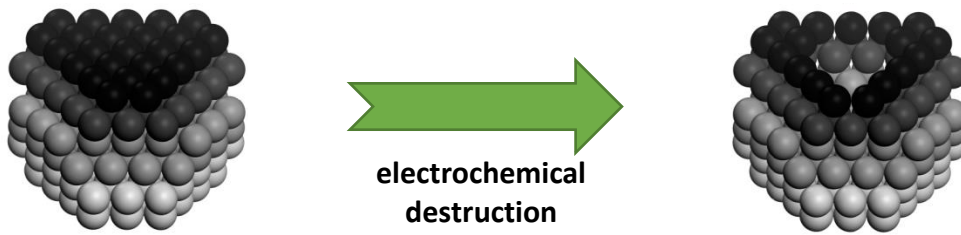


Figure 7-10: Schematic representation of the surface treatment to introduce defects into pristine Pt(111) by (A) dealloying, (B) galvanic displacement and (C) electrochemical destruction. Adapted from reference [59].

After the surface treatment, the samples showed increased activity for the electrochemical reduction of oxygen by up to 3.5 times at the reference potential 0.9V (see Figure 7-11).

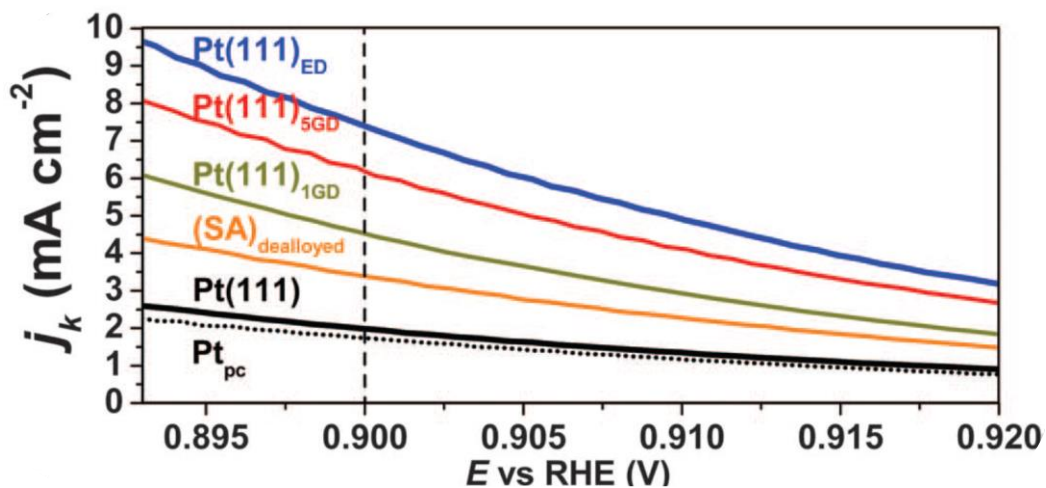
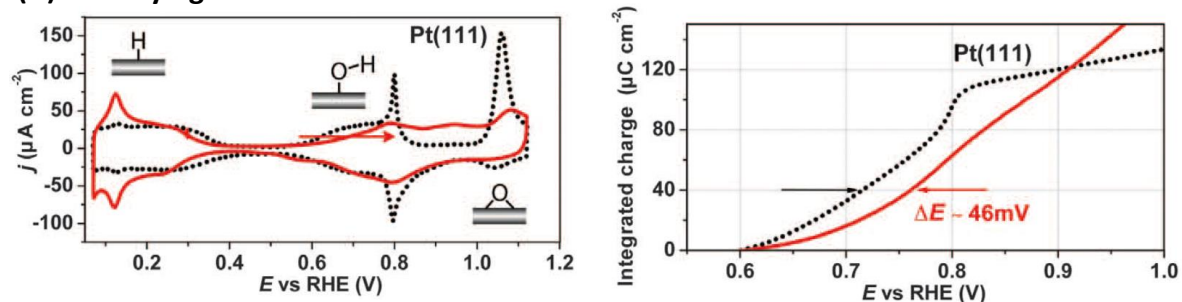


Figure 7-11: Kinetic current of the treated surfaces in comparison to pristine Pt(111) (black) and polycrystalline platinum (dotted). ED and SA stand for the electrochemically destroyed surface and the treated surface alloy. 1GD and 5GD indicated the one- and five-time galvanic displaced sample, respectively. Taken from reference [59].

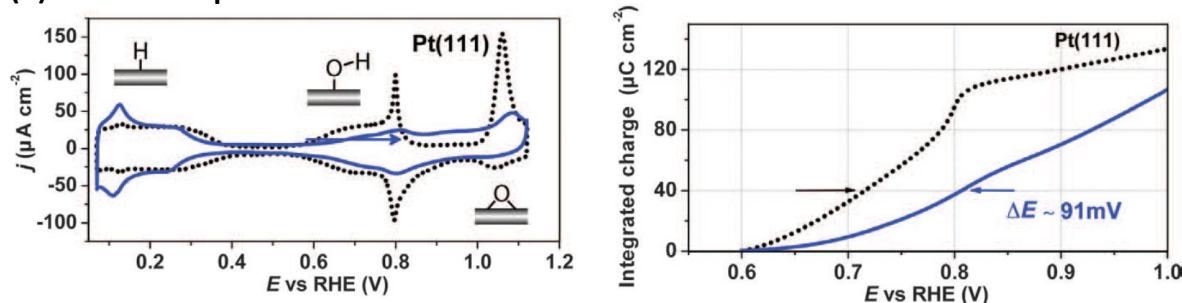
The surface treatment, as shown in Figure 7-12, influences the adsorption properties of pristine Pt(111) significantly by the formation of new sites. On pristine Pt(111) in the region from 0.06 up to 0.4 V solely the reversible adsorption of hydrogen is observed. After the surface treatments, a peak at the potential of  $\sim 0.06$  V is formed. This feature is also observed on stepped platinum surfaces and attributed to the replacement of underpotentially deposited hydrogen by hydroxide at step edges. Accordingly, the formation of cavities on the surface results into similar low coordinated sites on Pt(111); these so-called convex defects are found at the border of the cavities and are responsible for the

adsorption feature. The convex defects, as their coordination is decreased in respect to pristine Pt(111), bind oxygen too strongly and are not responsible for the high activity of the surfaces.

### (A) Dealloying



### (B) Galvanic displacement



### (C) Electrochemical destruction

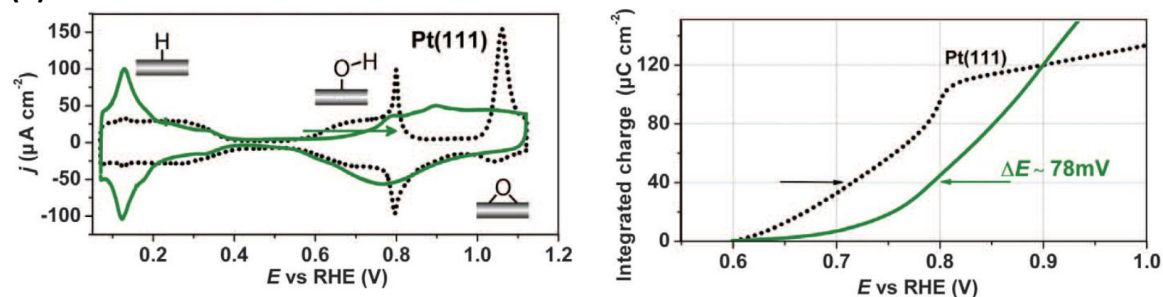


Figure 7-12: Cyclic voltammograms (left) of pristine (dotted line) and treated (solid line) Pt(111) measured in argon-saturated 0.1 M perchloric acid with a scan rate of 50 mV/s. Their integrated anodic charges is shown on the right. The different treatments results in the formation of new adsorption sites on the electrodes with a weaker binding of  $^*\text{H}$  and  $^*\text{OH}$ . Taken from reference [59].

Between the potential of 0.4 and 0.6 V, the contribution of the double layer charge is observed for treated and untreated Pt(111). Above a potential of 0.6 V the adsorption of hydroxide on the (111)-terraces is observed with the so-called “butterfly”-peak at 0.8 V on pristine Pt(111). The latter is attributed to the order and disorder phase-transition in the hydroxide adsorbate-layer [295]. The  $^*\text{OH}$  adsorption potentials theoretically derived from volcano plots are in good agreement with their experimental onset potentials [52, 60]. On the treated surfaces, the hydroxide adsorption on the terraces is moved to more positive

potentials. This emphasizes a weaker interaction between the hydroxide and the surface. The peak caused by the order/disorder phase transition is significantly diminished in magnitude for all samples. Therefore, it can be assumed that the treatment introduces a broad variety of new sites into the surface.

In the following, the introduced defects were characterized by different methods separated by their method of preparation. Figure 7-13A shows a typical AFM picture of the Pt(111)-surface after galvanic displacement. The surface is covered by platinum islands with an uniform defect density of roughly 25 defects per  $\mu\text{m}^2$ . Due to the tip geometry, the defects appear quasi rhombic, emphasizing, that the defects are too small for this imaging method. From Figure 7-13B and C the height and area distribution can be estimated. The islands show the most frequent height of 1.1 nm with the mean value of  $1.3 \pm 0.4$  nm and exceptional values like 2.5 nm. In lateral dimension, the values are highly uniform with  $34.9 \pm 5.6$  nm with the median at 35.1 nm.

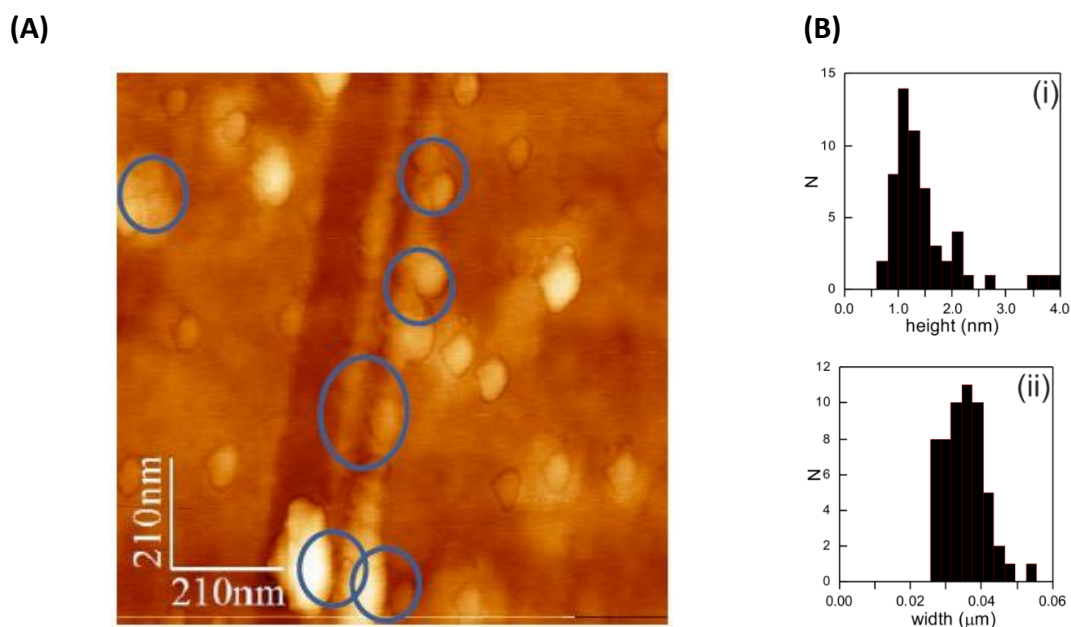


Figure 7-13: (A) Typical AFM image of the Pt(111) surface treated by one galvanic displacement procedure and (B) distributions of the defect dimensions. Taken from reference [59].

The desired highly coordinated defects with a decreased bonding towards hydroxide are found in between the protruding islands. The islands increase the coordination of the neighboring atoms and a weaker binding towards adsorbates is achieved. Figure 7-14 shows the positive shift of the integrated anodic parts of the voltammogram for pristine Pt(111),

after one and five cycles of galvanic displacement. As can be seen, one cycle only introduces a limited amount of new adsorption sites. The amount can be significantly increased with additional cycles. The resulting increase in activity by 3.5 times (compare Figure 7-11) cannot be explained by the 15% more adsorption sites on the surface derived from the volumetric data. Accordingly, the concave defects introduced by this method decrease the surface bonding compared to untreated Pt(111).

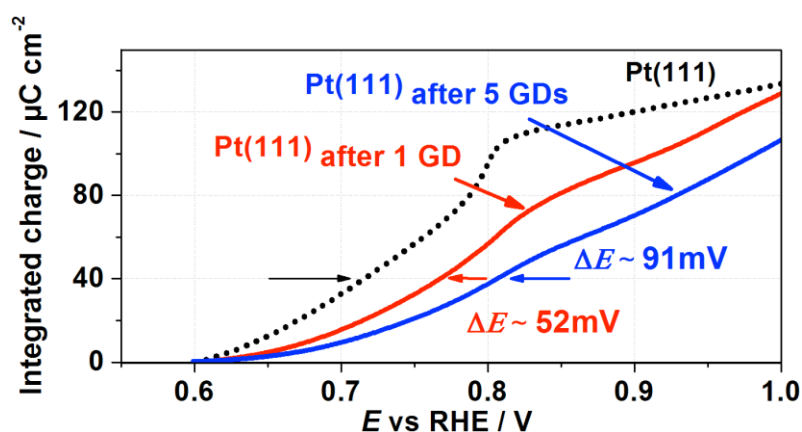


Figure 7-14: Positive shift of the integrated anodic parts of the voltammogram resulting from the galvanic displacement after one and five cycles. Taken from reference [59].

In comparison, the electrochemical destruction of the surface results into the formation of large concave defects on the surface. Hereby the number of cycles determines their dimensions. Hence, especially after ten cycles to a vertex potential of 1.72 V, the surface is covered by relatively big cavities with a broad distribution of cavity sizes.

In contrast to the former methods, the electrochemical destruction introduces a broad variety of cavities. Figure 7-15A shows a typical AFM image of the electrochemically modified surface. The surface is covered by a significantly lower number of defects with 0.08 per  $\mu\text{m}^2$  in comparison to the galvanic treatment. Nonetheless, the bigger diameter of the defects allows determining their exact dimension by AFM measurements. The formed cavities are round and elliptical, and an order of magnitude deeper, in the range from 10 to 70 nm, in comparison to the galvanic displaced surfaces (compare Figure 7-15B). The  $1.06 \pm 0.41 \mu\text{m}$  wide cavities are separated by 20 nm and coalesce with other defects.

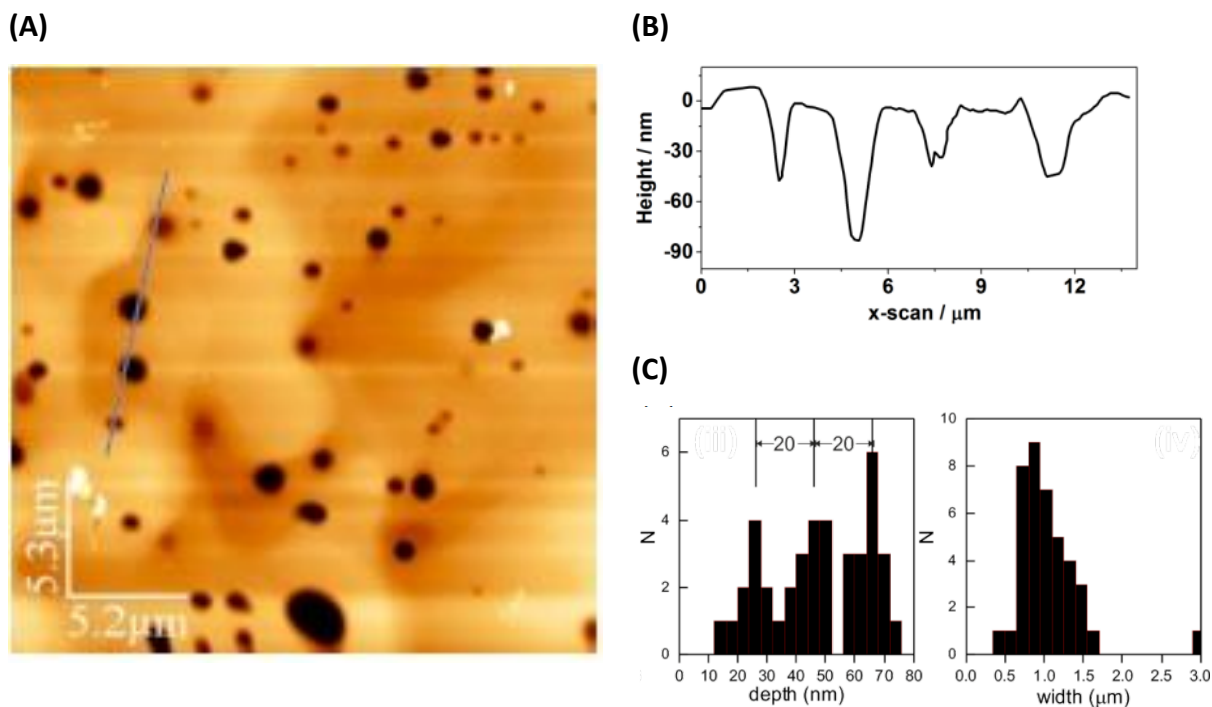
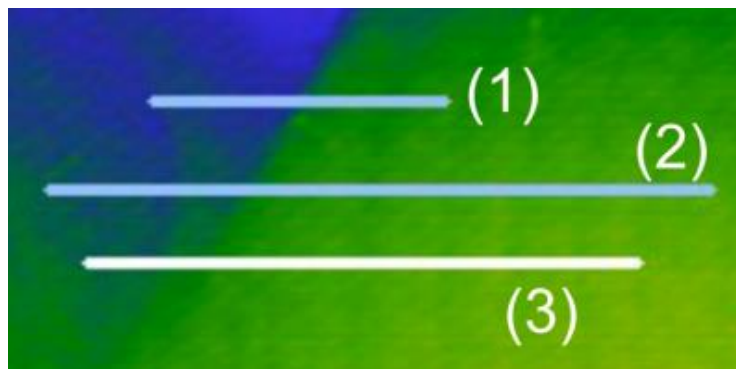


Figure 7-15: (A) Typical AFM picture of the electrochemically destroyed Pt(111) surface. The surface was cycled ten times up to 1.72 V. (B) Line scan of the specific path shown in (A). (C) Corresponding AFM-statistics of the magnitudes of the introduced defects. Taken from reference [59].

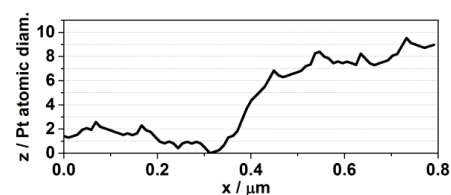
Of primary interest are the small cavities most likely found on the terraces resulting in the increase in activity. Figure 7-16A shows a fragment of the treated surface with a large and shallow cavity and a terrace with three line-scans (compare Figure 7-16B). The scan gives an overview over the cavities relative to the untreated terraces. The differences indicate that the amount and depth of defects are larger for both surfaces with the desired adsorption sites found below the step edges.

(A)

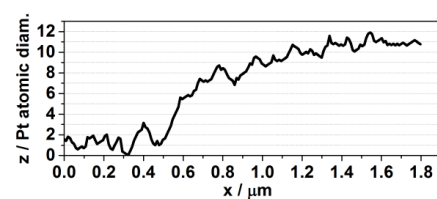


(B)

(1)



(2)



(3)

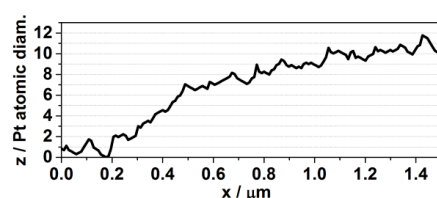
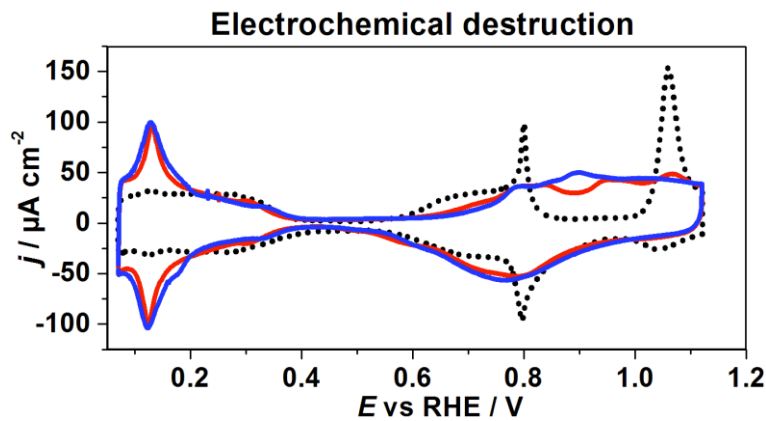


Figure 7-16: Fragment of the electrochemically destroyed Pt(111) surface after ten cycles (A) and the corresponding line scans (B). Taken from reference [59].

Figure 7-17A shows the cyclic voltammogram of the treated Pt(111) after one and ten cycles to the vertex potential of 1.72 V. As can be seen after ten cycles the peak at 0.12 V attributed to the hydroxide adsorption increases. Hence, it can be assumed that the longer cycling introduces a higher number of adsorption sites with increased coordination. Additionally, the peak resulting from the adsorption of hydroxide on the terraces is moved to more positive potentials indicating a weaker binding towards the adsorbates after ten cycles. This is further supported, by the movement of the integrated anodic charge towards more cathodic potentials by  $\sim 35$  mV. This indicates, in agreement with the atomic force microscopy data, a significant degree of site heterogeneity on the surface which additionally hinders the completion of the  $\text{OH}^*-\text{H}_2\text{O}^*$  adlayer.

(A)



(B)

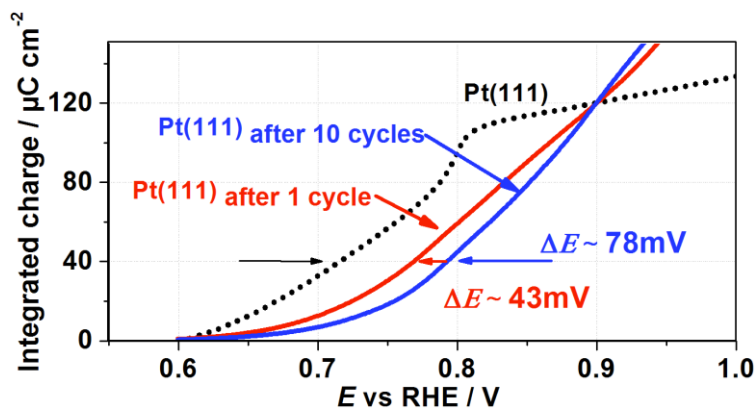


Figure 7-17: (A) Cyclic voltammograms of the electrochemically destroyed Pt(111) surface after one (red) and ten (blue) cycles. (B) Integration of the anodic parts of the voltammograms in the electrode potential range of  $^*\text{OH}$  adsorption measured with a scan rate = 50 mV/s in argon-saturated 0.1 M perchloric acid. Taken from reference [59].

To shed further light on the quantifiable effect of the electrochemical destruction, the measurements were performed in 0.1 M perchloric and 0.05 M sulfuric acid. Although, the inertia of perchlorate anions in the electrolyte was questioned recently [267, 296], perchloric acid is still used in these kind of measurements as a standard medium due to its assumed minimal anion adsorption on the electrode or influence on the surface adsorbates [297]. In comparison, sulfuric acid is used to simulate similar conditions as in PEM fuel cells. Anyhow, sulfate ions influence activity of the surface more than the sulfonate groups usually found in the NAFION polymer [298, 299].

Figure 7-18 shows the effect of the electrochemical destruction in dependence of different vertex potentials in the above-mentioned electrolytes. As descriptor for the activity the halfwave potential is plotted against the number of cycles. In both electrolytes, the highest activity is achieved after several cycles to the vertex potential of 1.72 V. Interestingly, the

half-wave potential is increased three times in sulfuric acid with 89 mV in comparison to perchloric acid with 30 mV. This enhancement is attributed to the effect of the surface structure on the bi(sulfate)-layer. For once the higher coordinated sites show a significantly weaker binding towards the sulfate. On the other hand, a stable bi(sulfate)-layer is formed on the plane electrode which competes with oxygen for the adsorption sites on the surface [300]. It seems the introduced defects and cavities hinder the formation of such a layer. Consequently, the concave sites responsible for the high activity of the surface become available for the adsorption of oxygen from the electrolyte.

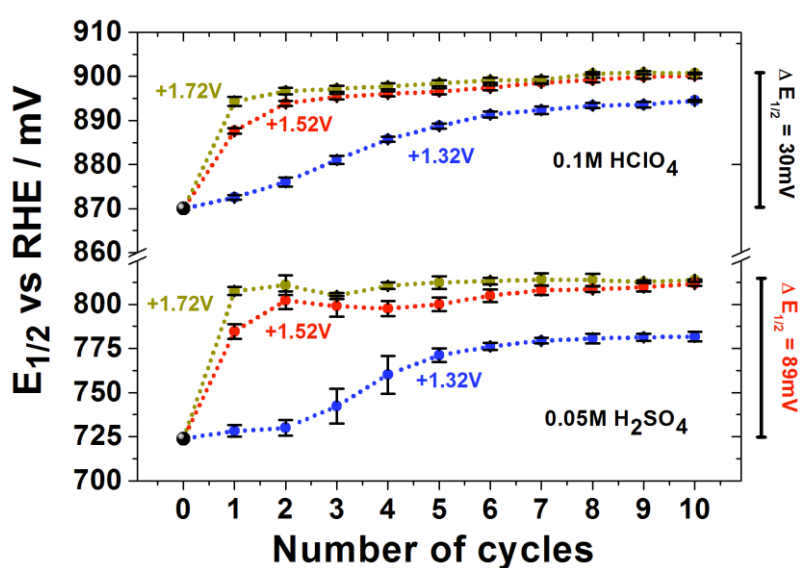


Figure 7-18: Effect of the electrochemical modification with respect to different vertex anodic potentials which were 1.32 V (blue), 1.52 V (red) and 1.72 V (olive) in oxygen-saturated 0.1 M perchloric and 0.05 M sulfuric acid as an electrolyte on the activity (dotted lines are a guide to the eye). As a suitable descriptor, the change in the half-wave potential ( $\Delta E_{1/2}$ ) is plotted against the number of cycles. The measurement was performed with a scan rate = 50 mV/s at 1600 rpm. Taken from reference [59].

To ensure that the increase in activity is caused by the coordination of the new sites and not by the increase in surface area, polycrystalline platinum was cycled in 0.1 M perchloric acid under the same conditions. Figure 7-19 shows the half-wave potential of the electrochemical reduction of oxygen on this electrochemically destroyed surfaces. The activity increase on the polycrystalline platinum is negligible with 5 mV in comparison to Pt(111). This increase can be attributed to the different corrosion mechanisms on both surfaces. Accordingly, it can be assumed that the increase of activity for Pt(111) is not caused by the increased amount of adsorption sites but the improved adsorption properties of the targeted defects.

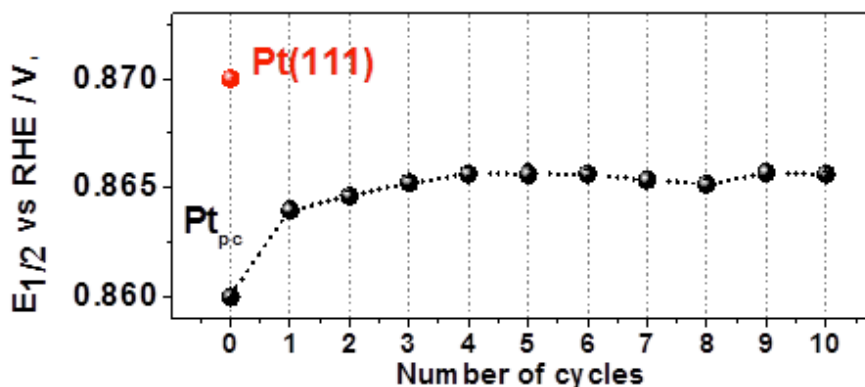


Figure 7-19: Half-wave potential of the oxygen reduction reaction in the pre-treated electrolyte as function of the oxidizing cycles up to a vertex potential of 1.72 V with the scan rate = 50 mV/s. The dotted line is a guide to the eye. Taken from reference [59].

As structure-sensitive reaction the analysis of the electro-oxidation of carbon monoxide can shed further light on the surface structure after the electrochemical oxidation [301]. Due to the adsorption of carbon monoxide on platinum prior to the experiment, the potential-determining step for this reaction is the formation of hydroxide species on the surface. Hydroxide adsorbs early at undercoordinated sites on platinum [302]. Accordingly, it can be assumed that convex defects, adatoms and kinks are the active sites and starting point for the oxidation. This topic will be discussed in detail later. The hydroxide formed reacts readily with carbon monoxide close to the undercoordinated sites to form carbon dioxide.

Figure 7-20 shows the stripping voltammogram for the stepped surface Pt(331), pristine Pt(111) and electrochemically destroyed Pt(111) (1 and 10 cycles). The peaks for the oxidation are in the following order:



This agrees with the formation of hydroxide in the different surface structures. On a stepped surface, like Pt(331), it is known that the oxidation of carbon monoxide is observed at low potentials, between 0.55 and 0.75 V, due to the early adsorption of hydroxide [302]. Both species readily react on the same short three-atomic terrace. In comparison, on pristine Pt(111) such defects are only randomly found. Accordingly, the reaction on this surface starts at more positive potentials, between 0.7 and 0.78 V, with the formation of hydroxide on the terraces. On the treated surfaces, the oxidation of carbon monoxide should occur in two steps. The first step should start at similar potentials as for pristine Pt(111) with the formation of hydroxide on the terraces at 0.7 V. Followed by the hydroxide formation in the

highly-coordinated cavities and the subsequent reaction with the adsorbed carbon monoxide. As the diffusion of hydroxide from one terrace to another is kinetically hindered, it can be assumed that the reaction in the cavities starts at significantly higher potentials. This can be seen as strong shoulder at 0.76 V resulting from the oxidation of carbon monoxide on the remaining terraces. This shoulder peak becomes even smaller after ten destructive cycles indicating the destruction of further terraces. Additionally, the long tail of the shoulder peak for both treated surfaces demonstrates a wide variety of new sites. Hence, it can be assumed, that the electrochemical cycling introduces a broad diversity of cavities.

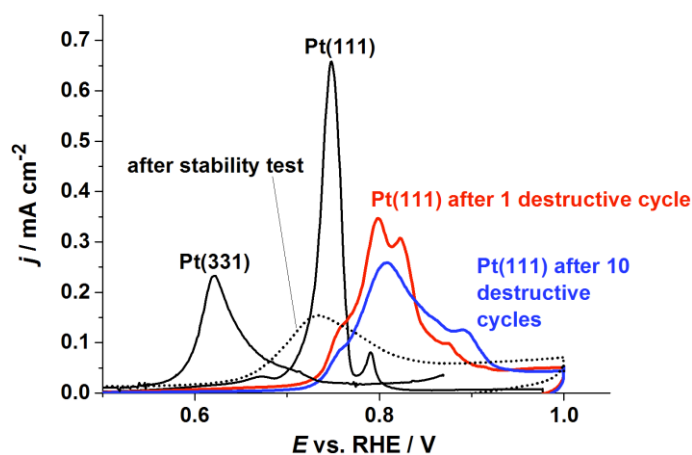


Figure 7-20: Carbon monoxide stripping voltammograms of the differently treated Pt(111) surfaces. Taken from reference [59].

To conclude this chapter all three methods increase the activity of Pt(111) by introducing highly coordinated defects into the surface. The galvanic displacement results into the formation of protruding adatoms with the active sites in-between these islands. In contrast, the selective stripping of copper atoms from the surface alloy results into the formation of highly coordinated cavities on the surface. The electrochemical destruction introduces similar cavities with a broad variety of adsorption sites.

### 7.3.2 Adsorbate surface coverage of stepped single crystals

The binding properties of active sites are strongly influenced by the adsorbate structure on a platinum surface. While the influence of short-lived or highly mobile species such as hydroxide can be neglected as they are part of the first water-layer, permanently bound species like bi(sulfate) must be taken into consideration [65, 297, 303, 304]. Such adsorbates bind towards the surface at energetically different sites and potentially limit the adsorption of a specific reactant from the electrolyte or change the adsorption properties of the adjacent surface sites. At 0.9 V, the working potential of fuel cells, it is assumed that the steps are most likely irreversibly covered by adsorbed oxygen [54, 305]. Already at early potentials this blockage is observed, after the desorption of underpotential deposited hydrogen in argon-saturated acidic electrolytes [52, 54, 305]. This hypothesis and additional experimental data can explain the observed trends in activities of Pt[n(111) x (111)] and Pt[n(111) x (100)] within the existing theoretical framework [54]. They are further supported by the assumption that the active sites for the electrochemical reduction of oxygen are found on the terraces with optimal binding properties for short terraces [54, 306]. Anyhow, the differences between Pt(111) and stepped surfaces remain unclear. Especially the *in situ* assessment of the adsorbate structure remains challenging as the intermediates such as hydroxide are highly mobile and are most likely part of the first water-layer [297, 303, 304, 307-309]. Nevertheless, the adsorbate structure and its effect on the electrocatalysis of the oxygen reduction reaction may be assessed based on reference points from quantum chemistry calculations and experimental results. A simplified model at various potentials can be proposed based on voltammetric and potentiodynamic electrochemical impedance spectroscopy in oxygen-saturated and oxygen-free electrolyte.

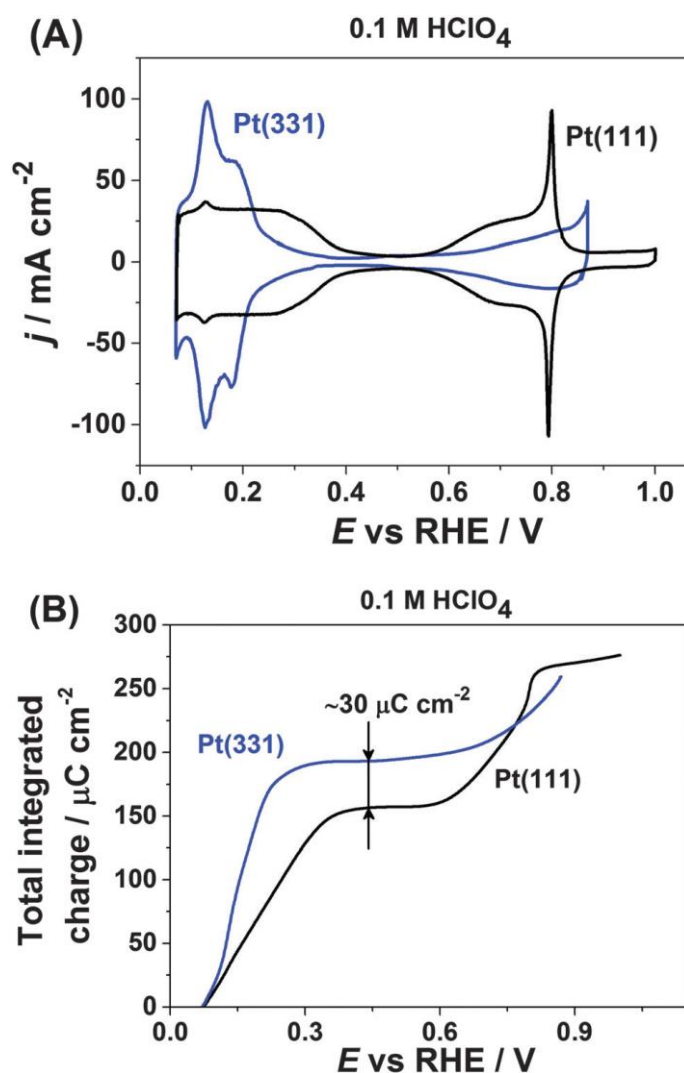


Figure 7-21: (A) Cyclic voltammogram of Pt(331) and Pt(111) in 0.1 M perchloric acid measured with a scan rate of 50 mV/s. (B) Total integrated charge of the voltammogram (corrected for the double layer capacitive current / scan rate: 50 mV/s). The difference of  $\sim 30 \mu\text{C}/\text{cm}^2$  results from the adsorption of OH on the steps on Pt(331). Each point can be correlated to a specific surface coverage.

The adsorbate coverage of an electrode is amongst other things determined by the working potential, the ions in the electrolyte, the surface structure and the electrode material [51, 54, 67]. For a well-defined platinum electrode in highly clean (Suprapur®) 0.1 M perchloric acid the influence of the last two parameter is negligible. In such a pure electrolyte only hydroxonium- and perchlorate-ions are present. A direct influence of the latter can be neglected as it is assumed that perchlorate does not adsorb onto the surface [297]. A simple characterization method of the potential influence on the surface coverage is the cyclic voltammogram. Figure 7-21A shows this characteristic measurement of Pt(111) and Pt(331) in 0.1 M perchloric acid. Both electrodes show specific adsorption features resulting from their unique surface structures. For instance, on Pt(111) in the potential range from 0.05

towards 0.4 V the measured current is attributed to the reversible hydrogen adsorption/desorption. At 0.13 V a small peak caused by the OH adsorption at defects on the extended Pt(111)-surface is visible [310]. These surface structures are sporadic on the total surface and contribute only marginally. In the potential range from 0.4 to 0.55 V contribution of the double layer is observed and followed by the hydroxide-adsorption on terraces between 0.55 and 0.9 V, with the so-called “butterfly-peak” at 0.8 V due to the order/disorder-transition of the OH-surface layer on the (111)-terraces [310]. On Pt(331) the intensity of the peak at ~0.13 V increases which is commonly attributed to the reversible adsorption of hydrogen on the steps [311, 312]. Integration of the anodic currents reveals a significant difference in the total integrated charge. It originates from the different surface coverage of both investigated surfaces as function of the applied potentials. In case of Pt(331) the charge is increased by a value of ~30  $\mu\text{C}/\text{cm}^2$  in the region of the anodic processes (Pt(111) = ~160  $\mu\text{C}/\text{cm}^2$  / Pt(331) = ~190  $\mu\text{C}/\text{cm}^2$ ). At the working potential of ~0.9 V the integrated charge for both surfaces are close to ~280  $\mu\text{C}/\text{cm}^2$ .

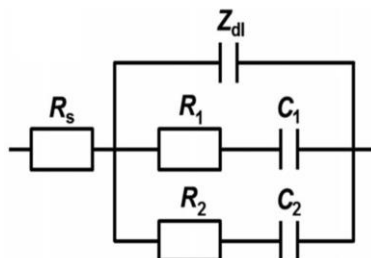
To determine the origin of this difference, potentiodynamic electrochemical impedance spectroscopy can be used on platinum model surfaces. While on Pt(111) the differentiation of the Faradaic processes from the double layer capacitance charge in the potential region from 0.05 to 0.4 V is not possible, on Pt(331) several Faradaic processes in this region are identifiable based on the equivalent electric circuit (EEC) for the reversible surface limited adsorption as illustrated in Figure 7-22A. See experimental section and reference [313] for discussion of the applied model. Hereby,  $R_s$  accounts for the uncompensated resistance of the system. The first branch represents the impedance of the so-called constant phase element (CPE) with

$$Z_{dl} = \frac{1}{C'_{dl}} (j\omega)^{-\phi}$$

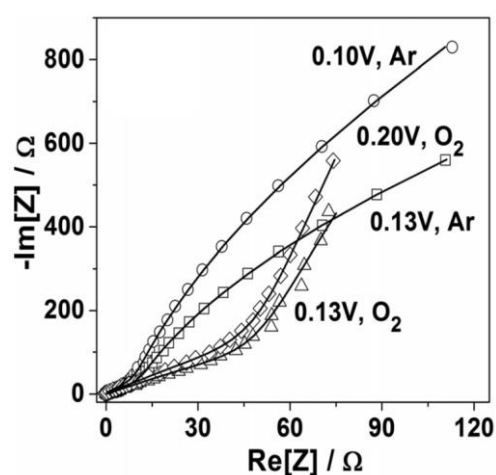
where  $C'_{dl}$  is proportional to the double layer capacitance ( $C_{dl}$ ), and  $\phi$  is the exponent accounting for the frequency dispersion of the double layer (detailed information related to this parameter are found in reference [297]). The remaining two branches consist of the resistance ( $R_1$  and  $R_2$ ) and capacitance ( $C_1$  and  $C_2$ ) of faradaic adsorption processes with slower time constants. In the oxygen-saturated electrolytes an additional resistance in parallel to the double layer impedance was added (not shown in the Figure 7-22A) to account for the electrochemical reduction of oxygen. As shown in Figure 7-22 B and C, the

EEC fit agrees well with the potentiodynamic impedance spectra shown for oxygen- and argon-saturated perchloric acid.

(A)



(B)



(C)

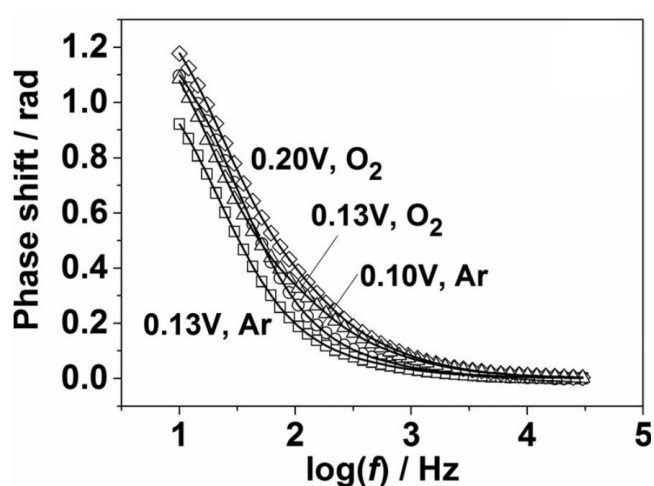


Figure 7-22: (A) Equivalent electric circuit (EEC) describing the adsorption processes at the surface of Pt(331). To account for the electrochemical reduction of oxygen, a charge transfer resistance is added in oxygen saturated electrolytes. (B and C) Exemplary impedance spectra of the electrolyte in contact with the differently saturated electrolyte (symbols / spectra corrected for uncompensated resistance) and the corresponding fits (line).

The effect of the potential on the adsorption capacitance ( $C_1$  and  $C_2$ ) and the double layer capacitance ( $C'_{dl} \approx C_{dl}$ ; based on the assumption that  $\varphi \approx 1$ ) is illustrated in Figure 7-23 for Pt(331) in oxygen- and argon-saturated perchloric acid. Based on the direct correlation between resistance and capacitance the focus will be limited to the latter. Integration of the investigated parameters in the potential region from 0.07 to 0.4 V gives a charge  $60 \mu\text{C}/\text{cm}^2$  for  $C_1$ ,  $30 \mu\text{C}/\text{cm}^2$  for  $C_2$  and  $110 \mu\text{C}/\text{cm}^2$  for  $C_{dl}$ . The unusually high value of the latter results from the fast hydrogen adsorption which cannot be differentiated from the double layer capacitance. Summing up the results gives a value of  $200 \mu\text{C}/\text{cm}^2$  which is relative close to the integrated charge of the cyclic voltammogram. The small deviations can be attributed to the necessary background corrections. While it is well known that the maximal charge associated with adsorption of hydrogen atoms for Pt(111) terraces is  $160 \mu\text{C}/\text{cm}^2$ , a 30

$\mu\text{C}/\text{cm}^2$  higher value is observed on the stepped surface. To determine the origin of this difference, the impedance measurements were repeated in oxygen-saturated perchloric acid (compare Figure 7-23 D-F). While all spectra are depressed, for  $C_2$  an additional shift to more negative potentials is observed. This influence on the capacitance agrees with the fact that hydroxide-adsorption is sensitive to dissolved oxygen in the electrolyte as it is an intermediate of the electrochemical reduction of oxygen [297, 314, 315]. Accordingly,  $C_2$  can be attributed to the adsorption capacitance of hydroxide on the electrode surface and explains the higher surface charge of Pt(331). Additionally, this agrees with hydroxide adsorption being observed already at 0.01 V for stepped surfaces due to their different geometric structure and the resultant electronic configuration. The additional adsorption capacitance,  $C_1$ , can be assigned to the slow adsorption of hydrogen as it is unaffected by the molecular oxygen and based on the limited availability of other species. A contribution of the adsorption of chlorine onto steps can be ruled out as its content in the solution is negligible.

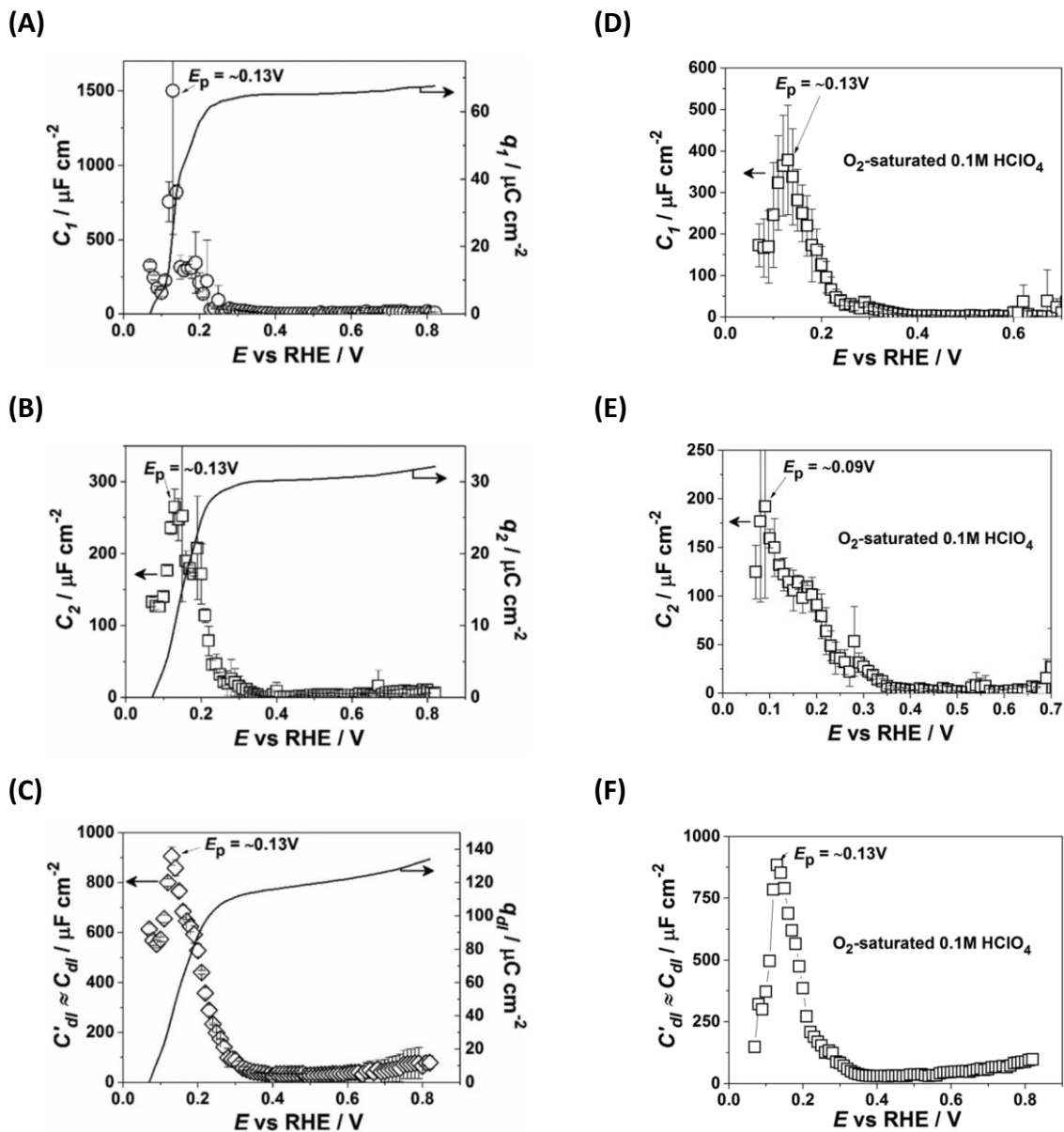
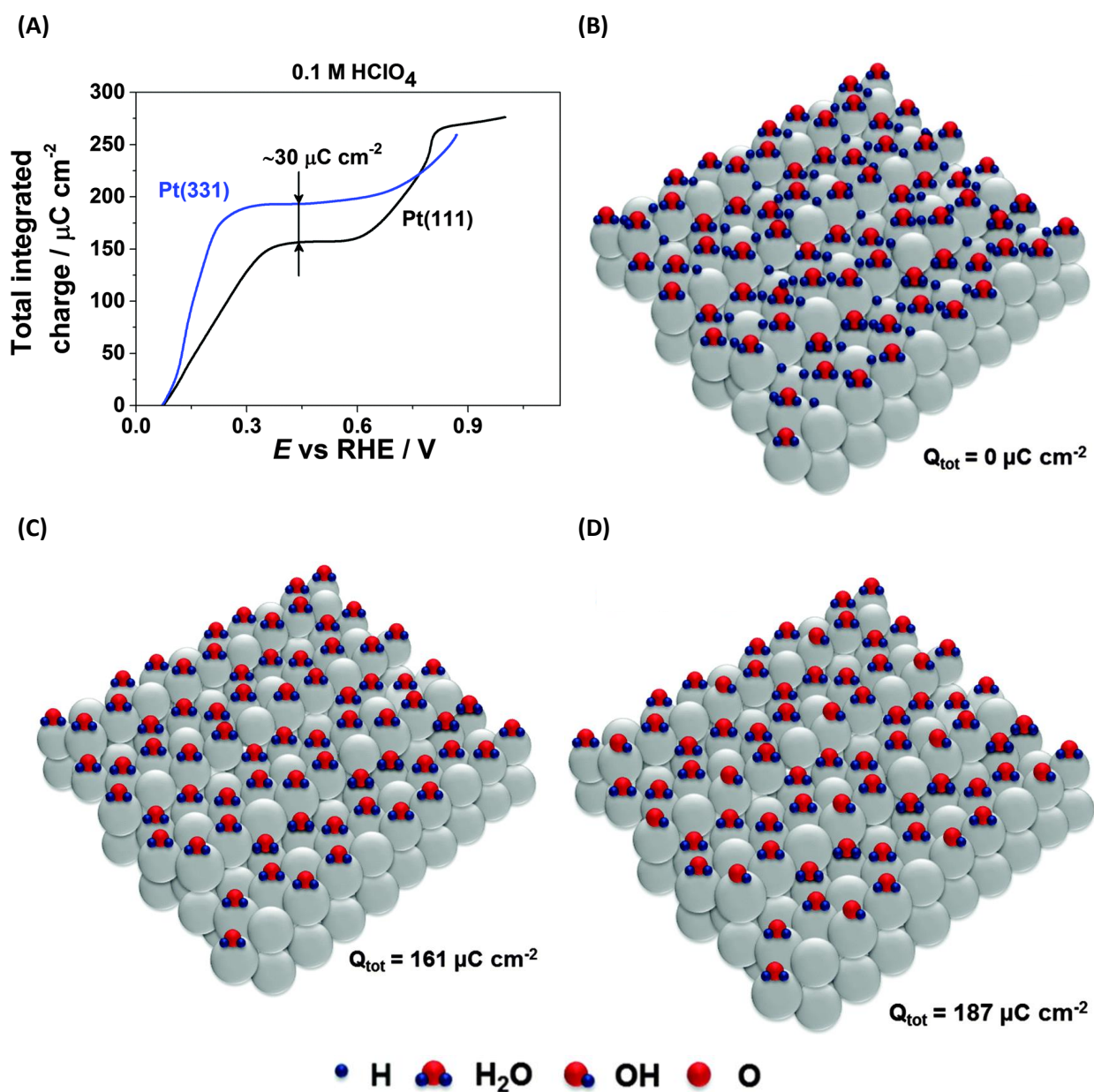


Figure 7-23: Different adsorption processes on Pt(331) in contact with 0.1 M perchloric acid as derived from the EEC-analysis (A-C) Adsorption capacitances  $C_1$  &  $C_2$  in argon- and (D-F) oxygen-saturated electrolyte. With the addition of oxygen,  $C_2$  shifts to a more negative potential. (C and F)) Approximated double layer capacitance with the inseparable contribution of fast hydrogen adsorption. The solid lines correspond to the integrated charges of the capacitance.

Based on the impedance and voltammetry data, the possible surface adsorbate coverage can be elucidated. For the pure electrolyte on the electrode, only  $H^*$ ,  $OH^*$ ,  $H_2O^*$  and  $O^*$  are assumed as surface species (\* denotes the species is adsorbed to the surface) [52, 54, 278]. As starting point, a density functional theory-supported superstructure for Pt(111) of  $H^*$  and  $H_2O^*$  is considered [264]. Although, Pt(331) shows different adsorption sites this structure is suitable as first approximation (see Figure 7-24B). With increasing potential, it can be assumed that the surface hydrogen is oxidized to water. This corresponds to the total

surface charge of  $161 \mu\text{C}/\text{cm}^2$  with water molecules distributed on the surface (compare Figure 7-24C). At a potential of 0.4 V the surface charge of  $\sim 190 \mu\text{C}/\text{cm}^2$  is derived from the integration of the voltammogram. This agrees with the oxidation of adsorbed water on the steps towards hydroxide resulting in a surface charge of  $187 \mu\text{C}/\text{cm}^2$  (see Figure 7-24D) and is equivalent to the adsorption of hydroxide from the electrolyte. The adsorbed water at step sites is most likely to undergo this oxidation.



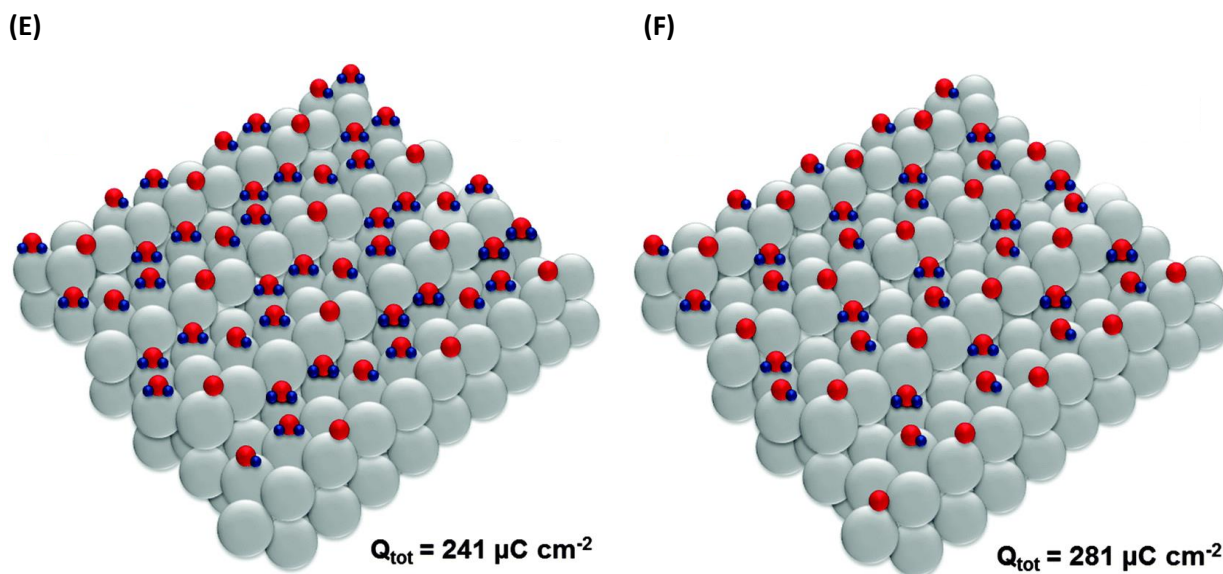


Figure 7-24: (A) Total integrated charge of Pt(331). (B-F) Different proposed adsorbate structures on the surface of Pt(331) at different potentials based on the oxidative sweep: (B and C) in the potential region from 0.05 to 0.4 V without a concurrent  $\text{OH}^*$  adsorption. The oxidation of hydrogen corresponds to an anodic charge of  $\sim 161 \mu\text{C/cm}^2$ . (D) In the potential region from 0.05 to 0.4 V with a concurrent  $\text{OH}^*$  adsorption. The oxidation of the adsorbed hydrogen and  $\text{OH}^*$ -adsorption should correspond to an anodic charge of  $\sim 187 \mu\text{C/cm}^2$  (E and F) in the potential region from 0.8 to 0.9 V.

Further oxidation at higher potentials would include the second-row hydroxide on the platinum atoms and at every third platinum step atom. Accordingly,  $\text{OH}^*$  is oxidized towards  $\text{O}^*$  and an  $\text{OH}^*$ -layer is formed on the one atomic terrace. This agrees with a surface charge of  $241 \mu\text{C/cm}^2$  at the potential of 0.8 V derived from the voltammogram (compare Figure 7-24E). At the working potential of 0.9 V a surface charge of  $281 \mu\text{C/cm}^2$  is reached. At this potential, the additional oxidation of surface species can be assumed and results in the increased coverage of the terraces by  $\text{OH}^*$  and steps by  $\text{O}^*$  like illustrated in Figure 7-24F.

While these structures are largely hypothetical, they explain the measured data with high accuracy. Unfortunately, the visualization of the adsorbate structure *in situ* is not possible nowadays for Pt-surfaces.

To conclude, the most important finding of these investigations is that hydroxide adsorption on stepped surfaces starts as early as 0.1 V and that the steps at the working potential are covered by long-lived oxygen species blocking these sites. Especially the latter has a strong influence on the electronic structure of the neighboring surface atoms and their binding strength towards intermediates.

### 7.3.3 The role of Introduction of steps in the electrochemical reduction of oxygen

Alternatively, to the targeted introduction of defects by electrochemical methods, the adsorption strength can be decreased by  $\sim 0.1$  eV with the introduction of quasi-periodic surface structures. According to Bandarenka et al., the electrochemical reduction should show a higher activity on stepped platinum surfaces [54]. Figure 7-25A illustrates the increased activity for structurally different single crystals with (111)-terraces and (100)/(111)-steps. Hereby, the introduced steps form additional adsorption sites for the intermediate species in relation to Pt(111). According to the volcano plot, the optimal platinum based catalyst should have a terrace length of three atoms. Introducing steps into platinum surfaces result in the formation of low coordinated convex and highly coordinated concave defects as illustrated in Figure 7-25B and discussed before.

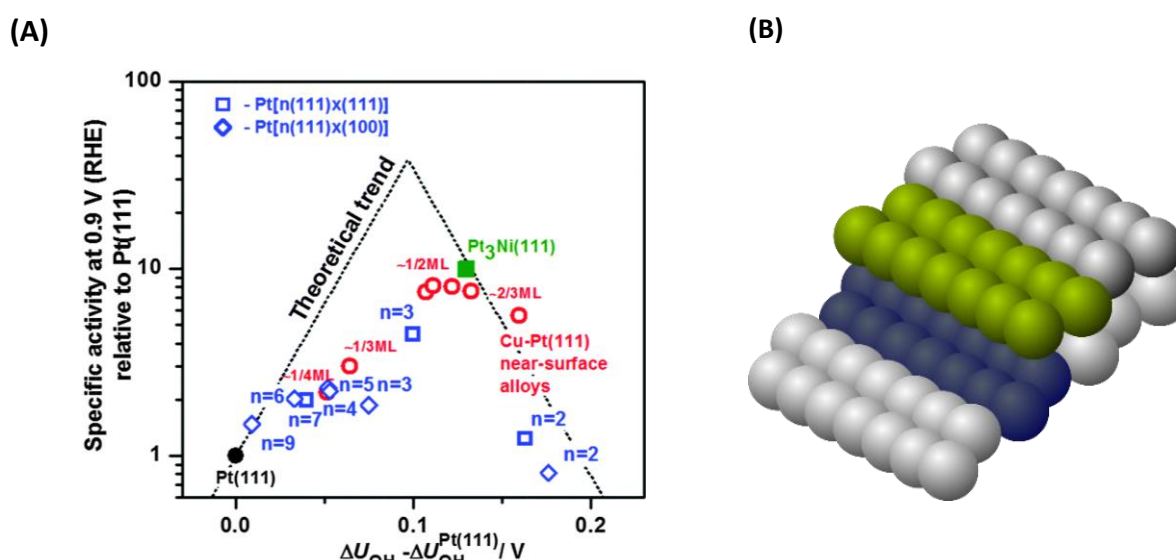


Figure 7-25: Activity “volcano” plot for pristine Pt(111) (circle), stepped Pt[n(111) x (111)] (square), Pt[n(111) x (100)] (diamond) and alloy surfaces (empty circle). Taken from reference [54] and references for surfaces found therein. The atomic length of the 111-terraces ( $n$ ) is provided in each case.

According to the generalized coordination number, the concave sites show values above 7.5 and should increase the activity. Figure 7-26 shows the different adsorption sites on the stepped surfaces Pt(331), Pt(221) and Pt(775) with three-, four- and seven-atomic terraces and their generalized coordination number.

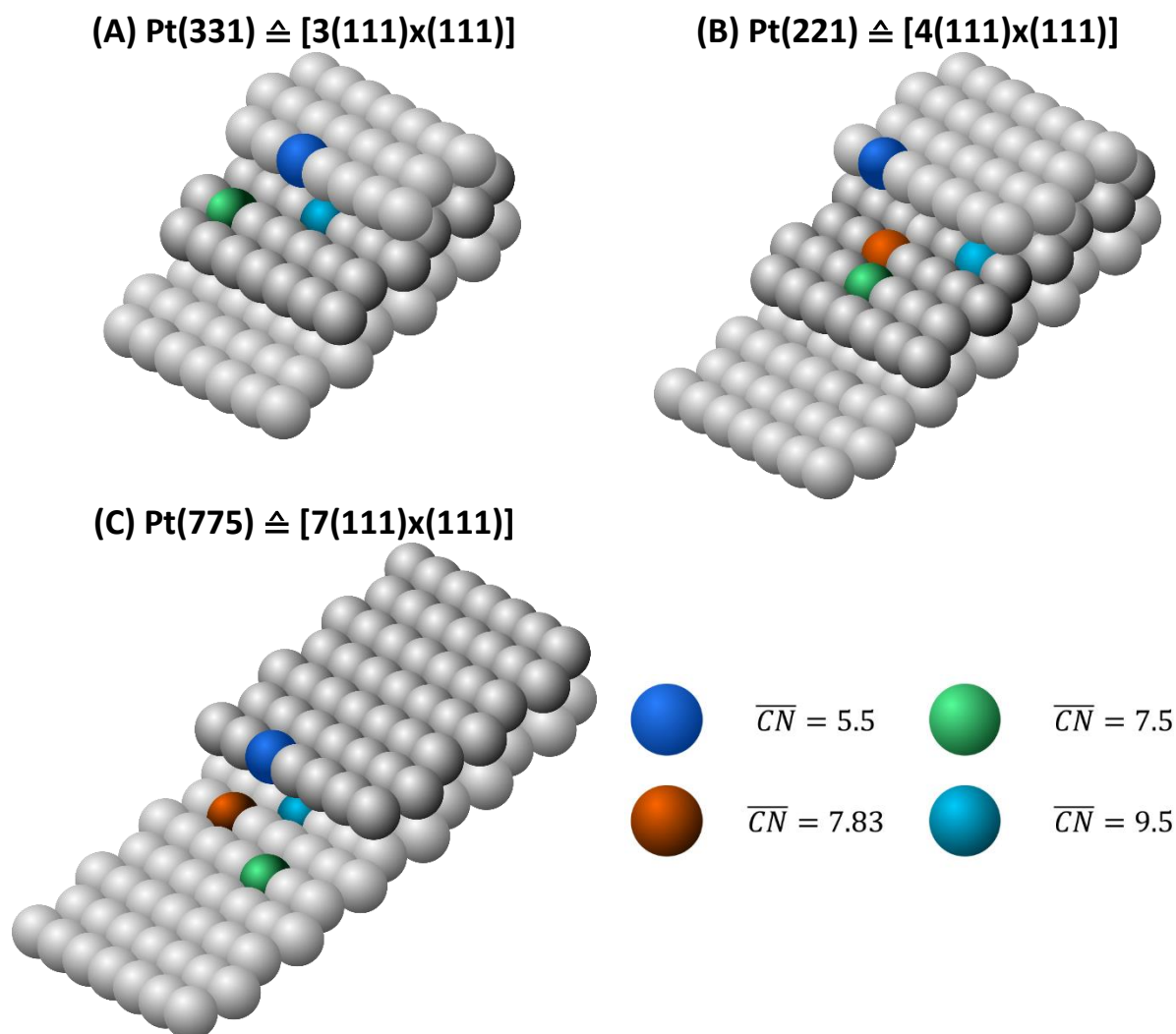


Figure 7-26: Generalized coordination number for the different top adsorption sites of the investigated surfaces. The different surfaces are based on the (111)-facet and only differ in terrace length. The different atoms layer are slightly different colored as a guide for the eye.

While Pt(111) has only one type of adsorption site with  $\overline{CN} = 7.5$ , Pt(331) has three additional adsorption sites. As active sites for the electrochemical reduction only “on-top” sites are considered [286, 316]. At the step edge a low coordinated site with  $\overline{CN} = 5.5$  is formed. Based on its lower coordination with seven direct neighbours in comparison to pristine Pt(111) with nine, these convex defect with  $\overline{CN} = 5.5$  compensate their lack of coordination by a too strong bonding towards adsorbates and consequent deactivation of the reactant. An additional “on-top” site is below the step edge with  $\overline{CN} = 9.5$ . This site has higher amount of direct neighbours (eleven) similar to the bulk material. Accordingly, this site binds weaker towards adsorbates. Anyhow, the steric hindrance by the step edge shields this site from the reactant. The third “on-top” site is found on the terraces with  $\overline{CN} = 7.5$ , due to its short three-atomic terraces the coordination at this site is similar to Pt(111). The

highly coordinated neighbours at the step edge are countered by the lower coordinated step edge. Increasing the terrace length by already one atom, towards Pt(221) with four-atomic terraces, changes the coordination of these atoms significantly. The additional atom increases the generalized coordination number for this concave defect towards  $\overline{CN} = 7.83$ . The same increase is observed for Pt(775). Controversially, following the theoretical assumptions the activity of Pt(331) should not be increased relative to Pt(111).

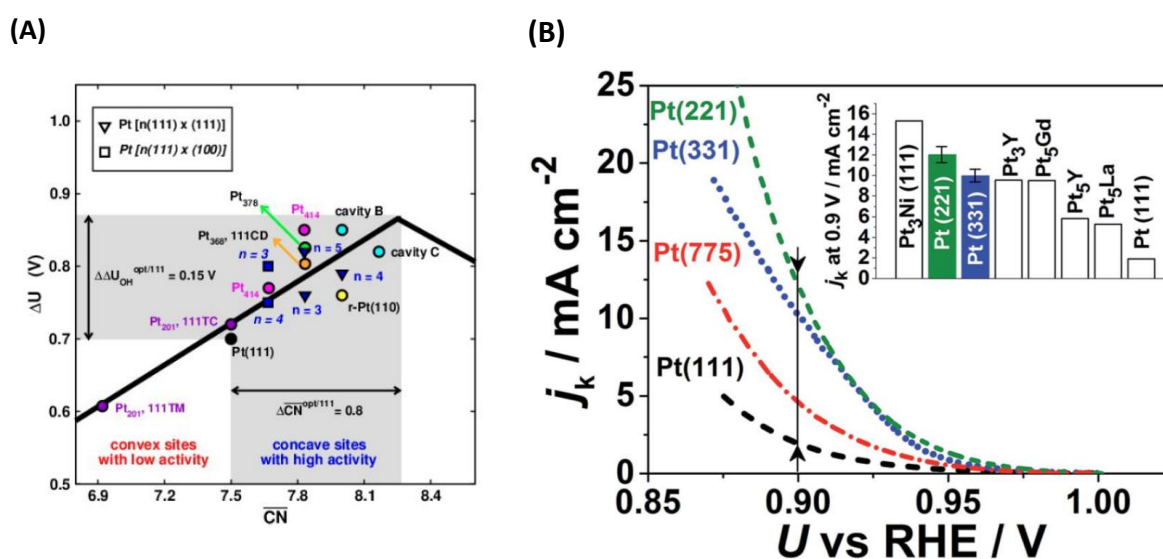


Figure 7-27: (A) Coordination-activity plot for the electrochemical reduction on platinum. The optimal active site would have a generalized coordination number of 8.3. (B) Activity measurement of the surfaces in oxygen-saturated 0.1 M perchloric acid measured with a scan rate of 50 mV/s and a rotation of 1600 rpm. The inset shows the activity of the stepped surfaces relative to several state-of-the-art platinum based alloyed catalysts from literature.

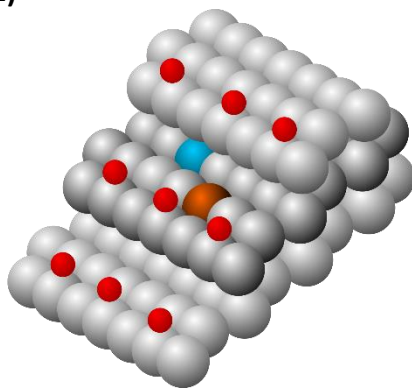
However, the coordination-plot shown in Figure 7-27A predicts that the activity of this surface should be significantly increased. This is further supported by the experimental results shown in Figure 7-27B with a significant increase of the activity for Pt(331) even surpassing several alloys. To explain this discrepancy, the surface adsorbates on the stepped surfaces must be taken into consideration. As discussed in the previous chapter, oxygen is bound towards the step edges at the working potential of the fuel cell [317]. The oxygen adsorbs at a three-fold hollow sites formed by two edge- and a terrace-atom (compare Figure 7-26) [318, 319]. Its negligible mobility originates from the substantial adsorption energies and its high diffusion barrier [320]. Based on its long-lived character, its effect on the adsorption properties of the adjacent terrace sites needs to be considered for the assessment of the generalized coordination number.

As a first approximation for the generalized coordination number it can be assumed that the oxygen is accounted for by adding the factor “ $k$ ” to the coordination number resulting into the following equation for one atom:

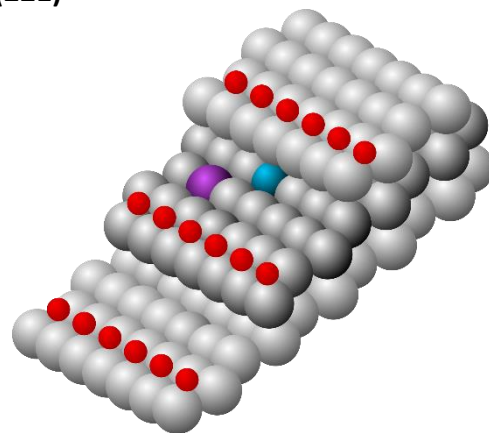
$$cn(j) = cn_s + k \quad 7-1$$

where  $cn_s$  represents the coordination number of the uncovered surface atom and  $k$  is a factor considering the ratio between the energetics of the metal-metal bonds or the adsorbate-metal bonds. Momentarily, the exact impact of an adsorbate needs to be evaluated for every surface species. As reference point the irreversible adsorbed oxygen on platinum is accounted for as an additional surface atom with  $k = 1$ . Hence, depending on the degree of oxygen coverage, the coordination of a central atom can be, significantly increased. The effect for the Pt[n(111)x(111)]-surfaces is illustrated in Figure 7-28 for all sites.

**Pt(331)**



**Pt(221)**



**Pt(775)**

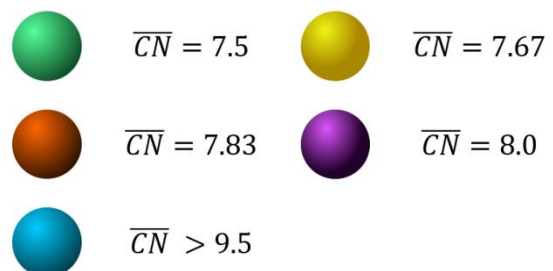
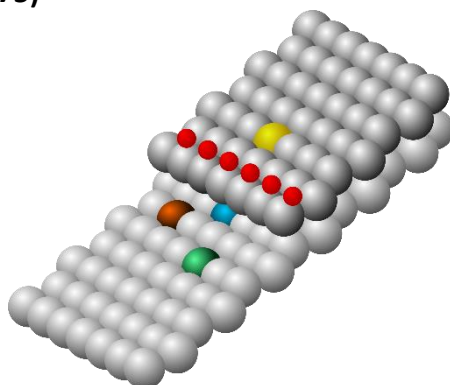


Figure 7-28: Effect on the generalized coordination number on all surfaces investigated for the electrochemical reduction of oxygen with surface oxygen above a potential of 0.9 V.

On Pt(331), the oxygen increases the generalized coordination number towards of the “on-top” active sites to 7.83 at the potential of 0.9V. However, at lower potentials, the oxygen

becomes less stable and is removed from the surface and decreases  $\overline{CN}$  from 7.83 to 7.5 [174]. Hence, it can be assumed, that the activity of Pt(331) is strongly dependent on the applied potential, as shown in Figure 7-27. In contrast to Pt(221) and Pt(775) with longer terraces, Pt(331) deviates from their nearly exponential growth. On Pt(221) the oxygen coverage increases the generalized coordination number further from 7.83 towards 8.0. Hence, making it theoretically the most active site on the investigated stepped surfaces. This agrees with the experimental results for Pt(221) with the highest measured activity. On Pt(775), the adsorbed oxygen has no influence on the concave sites and only increases the coordination of an adjacent terrace site with  $\overline{CN} = 7.5$  towards 7.67 and making it marginally more active for the electrochemical reduction of oxygen.

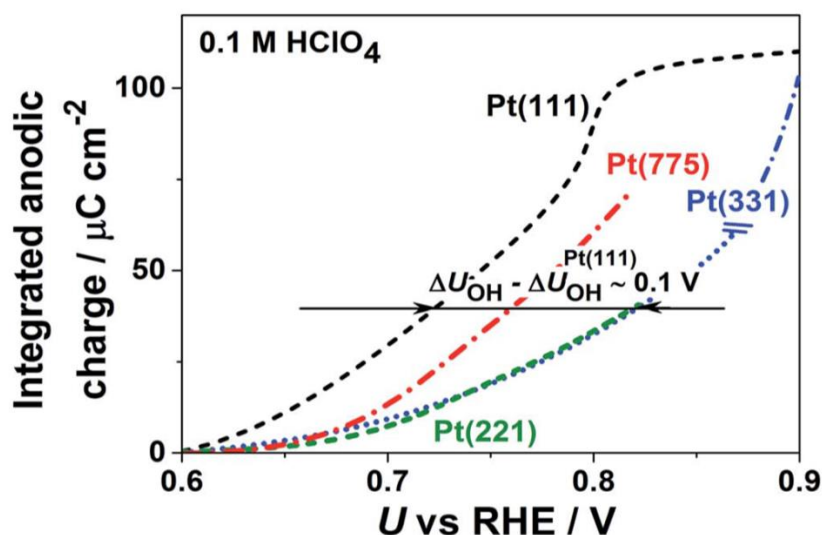


Figure 7-29: Integrated anodic parts of the voltammograms showing of the investigated stepped surfaces relative to Pt(111).

This weakening in binding towards hydroxide species is also observed by the integration of the anodic charges as displayed in Figure 7-29. While on Pt(111) the intermediates are bound too strongly, the binding decreases with the terrace length and reaches its lowest value for four-atomic terraces at the working potential. Based on the similar integrated anodic charge for Pt(331) and Pt(221), it can be assumed that the surface coverage for both surfaces is similar. In case of Pt(775), the shift is less pronounced which can be attributed to the significantly longer seven-atomic terraces.

According to the coordination-activity plot, pristine Pt(110) (p-Pt(110)), or Pt[2(111)x(111)], should not be active towards the electrochemical reduction of oxygen. Anyhow, under

electrochemical working conditions the surface reconstructs into the so-called missing row configuration (r-Pt(110)) as illustrated by Figure 7-30A and B [265-267, 321].

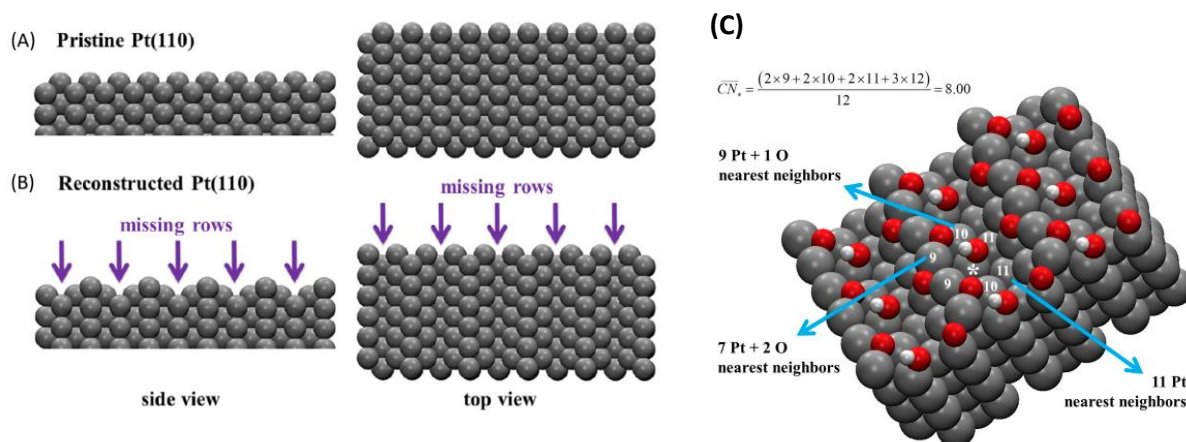
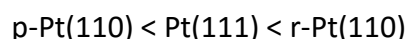


Figure 7-30: Schematic illustration of (A) pristine and (B) reconstructed Pt(110). (C) Visualization of Pt(110) with co-adsorbed \*O and \*OH in the missing-row reconstruction. For the adsorption site of hydroxide (marked with \*) the generalized coordination number is provided. Taken from reference [189].

The reconstructed Pt(110) possess wider terraces with  $\overline{CN} = 8.0$  which are responsible for the 20% increase of activity in respect to pristine Pt(111). This agrees with the measurements by Attard and Brew with the activity ranking [322]:



To conclude, the introduction of steps results in the formation of convex and concave defects. While the convex defects bind hydroxide too strongly for the reaction to proceed, the concave defects decrease the binding energy closer to the optimal value. Anyhow, the effect of the steps alone is not strong enough to explain the activity increase of the surface. Hence, the potential dependent adsorbate coverage needs to be considered. The oxygen formed at the step edges increases the generalized coordination number of the adjacent sites closer towards the optimum. Hence, the highest activity is measured on Pt(221) with highly coordinated sites followed by Pt(331) and Pt(775) with less coordinated sites.

### 7.3.4 Nanoparticles and complex structures for the electrochemical reduction of oxygen

Most state-of-the-art catalysts in heterogeneous electrocatalysis are nanoparticle based on their optimal surface-volume-ratio. Nanoparticles allow to decrease the quantity of material while enabling high surface area [323]. Anyhow, convex nanoparticle for the electrochemical reduction of oxygen are significantly less active (in terms of the specific activity) than the bulk material with well-defined surfaces like Pt(111) [324, 325]. Nevertheless, the size of the particle plays a key role on the activity of the particles.

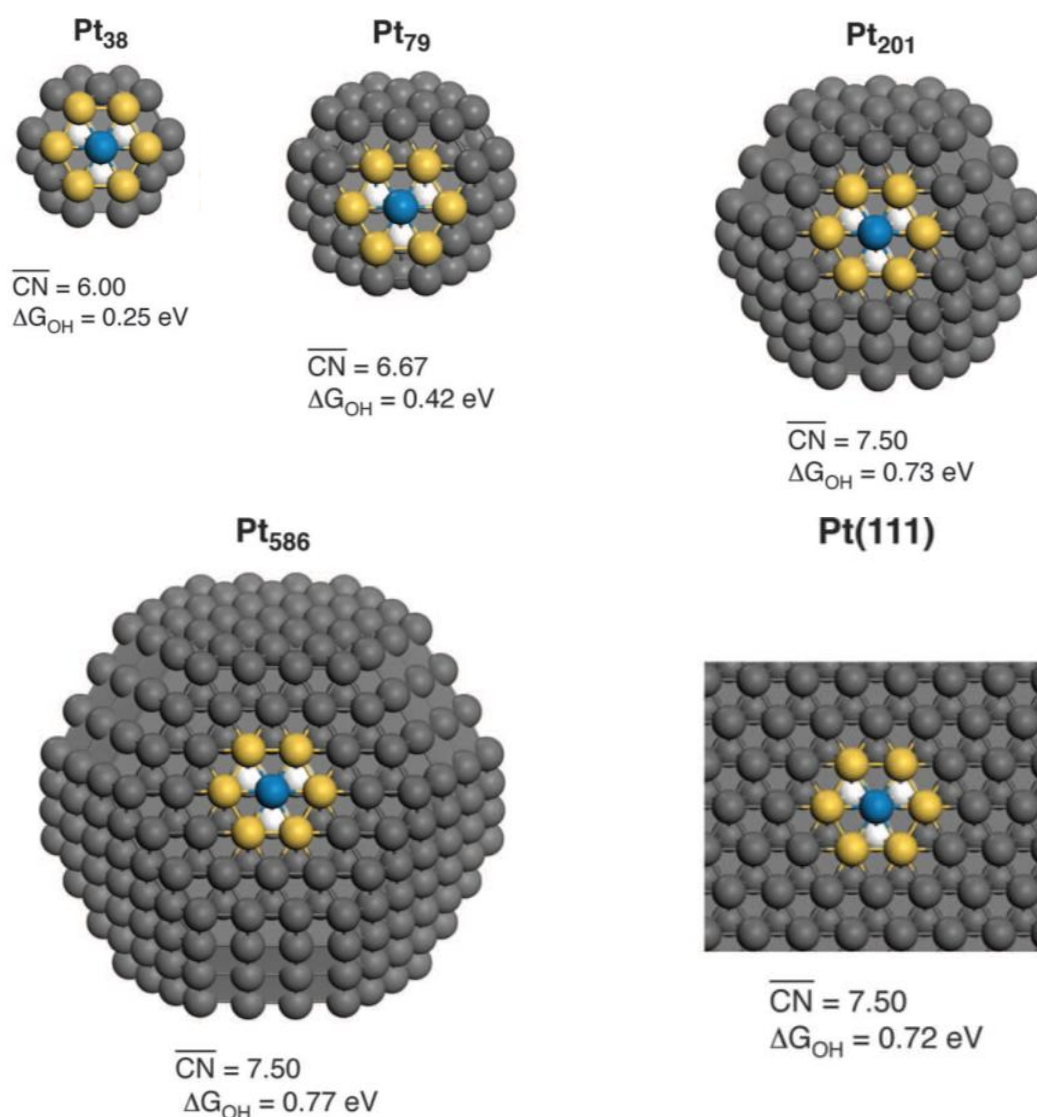
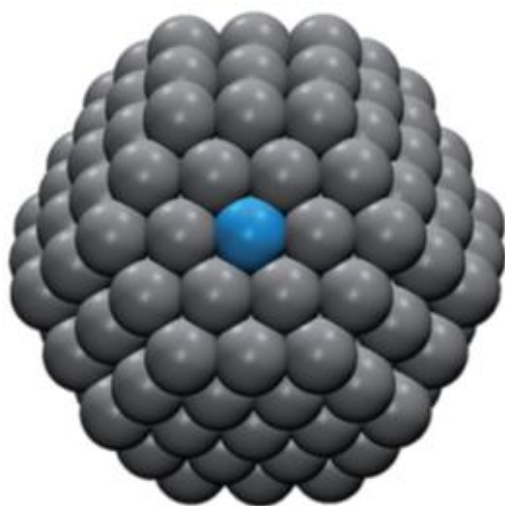


Figure 7-31: Size effect of convex nanoparticles on the generalized coordination. With increasing particle size the activity approach the one of a plane (111)-surface with the maximum of  $\overline{CN} = 7.5$ . Taken from reference [59].

For convex nanoparticles, the activity is solely determined by the size of the (111)-facet as the additionally (100)-facet is significantly less active [326, 327]. On small nanoparticles, the

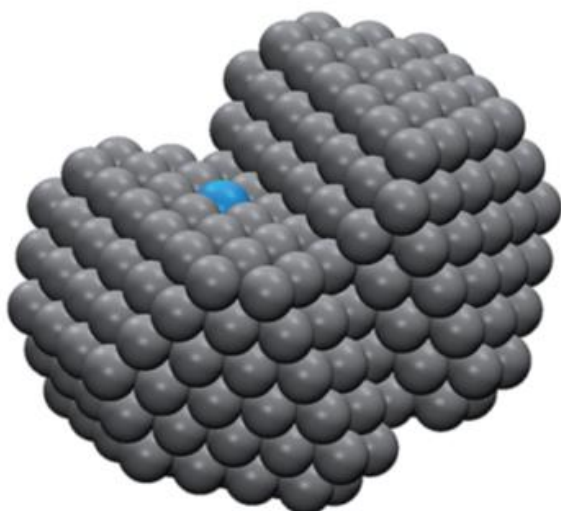
intermediates would adsorb too strong to the surface at the undercoordinated surface sites. At the minimum size of 201 platinum atoms for the nanoparticle, the adsorption properties become similar to a pristine (111)-surface with  $\overline{CN} = 7.5$ , as illustrated in Figure 7-31. With the growth of the facet, the activity of the nanoparticle increases with the maximum being close to pristine Pt(111).

(A) Convex nanoparticle (Pt<sub>201</sub>)



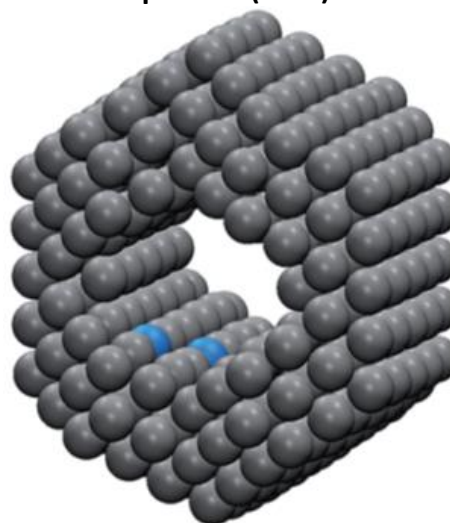
$$\overline{CN}_{max} = 7.5$$

(C) Coalescent nanoparticle (Pt<sub>368</sub>)



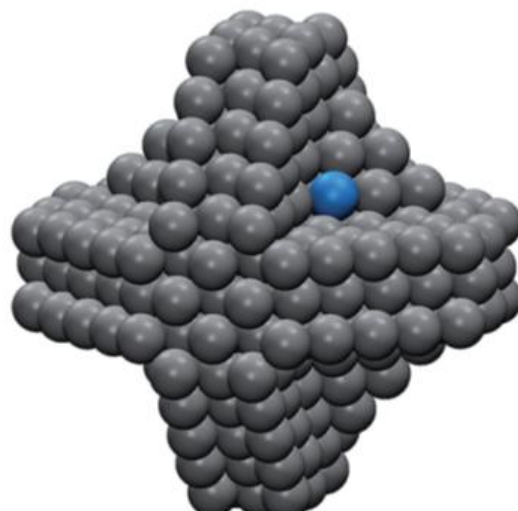
$$\overline{CN}_{max} = 7.83$$

(B) Frame nanoparticle (Pt<sub>414</sub>)



$$\overline{CN}_{max} = 7.83$$

(D) Cross nanoparticle (Pt<sub>378</sub>)



$$\overline{CN}_{max} = 7.83$$

Figure 7-32: Generalized coordination number for the most active sites for the electrochemical reduction of oxygen on a convex nanoparticle (A), coalescent nanoparticle (B) and more complex structures (Frame and Cross nanoparticle / C and D). The geometry of the structures from B-D results into a higher coordination of the sites and increases  $\overline{CN}$  towards the optimum of 8.3. Taken from reference [189].

The reported high activity of some convex nanoparticles can be explained by particle coalescence, without aggregation of the particles. In this case even the overlap of their double layer is sufficient for an activity increase [328]. Nonetheless, it is important to prevent agglomeration, as it would decrease the available surface area. At such, high particle loadings, the nanoparticles connect to each other like shown in Figure 7-32B. At the area close to the contact region concave sites with higher coordinated surface atoms are formed with  $\overline{CN} > 7.5$ . This phenomenon is observed for highly loaded nanoparticulate electrocatalysts and in ordered arrays of nanoparticles in 1D and 2D [329].

Alternatively, highly active nanoparticles can be realized through sophisticated structures with an increased amount of concave sites like shown in Figure 7-32C and D as frame [330-332] and cross-shaped [333] nanoparticles with experimentally measured high activities. At the indicated sites concave sites with  $\overline{CN} > 7.5$  are observed which increase their activity. Naturally, the design of such particles is only limited by the applicable template methods.

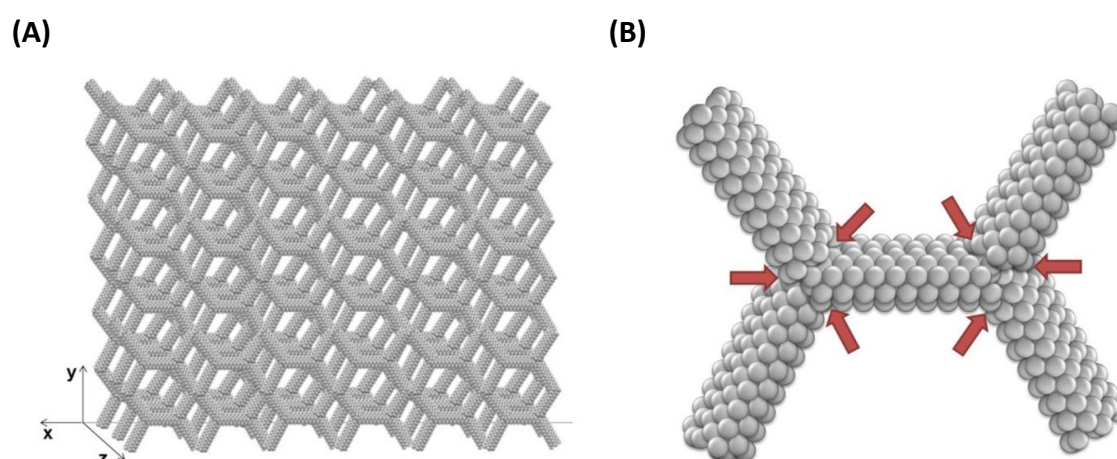


Figure 7-33: (A) Illustration of a porous platinum based electrocatalyst. (B) Magnification of some part of the structure with indicated (red arrow) higher coordinated sites causing the higher activity of the structure. Taken from reference [59].

An alternative class of highly active catalysts are mesoporous structures. Those structures are mostly prepared by template methods which allow the periodically introduction concave sites (red arrow) as shown in Figure 7-33 [334].

To conclude the activity of nanoparticles is increased by the formation of concave defects either by the coalescence of convex nanoparticles or more complex nanoparticulate or mesoporous structures.

## 7.4 Carbon monoxide oxidation on model stepped platinum surfaces: the nature of active catalytic centers

The oxidation of carbon monoxide is an important reaction for carbon-based fuel cells. It is a fundamental reaction step which can be found in all such fuel cells [335-337]. Based on the structure sensitivity of this reaction, it can be further used to evaluate the effect of surface treatments [226, 302, 338, 339]. Interestingly, again the activity increases with the introduction of steps into the surface [335-337]. The underlying energy-structure relationships can be explained by the generalized coordination number.

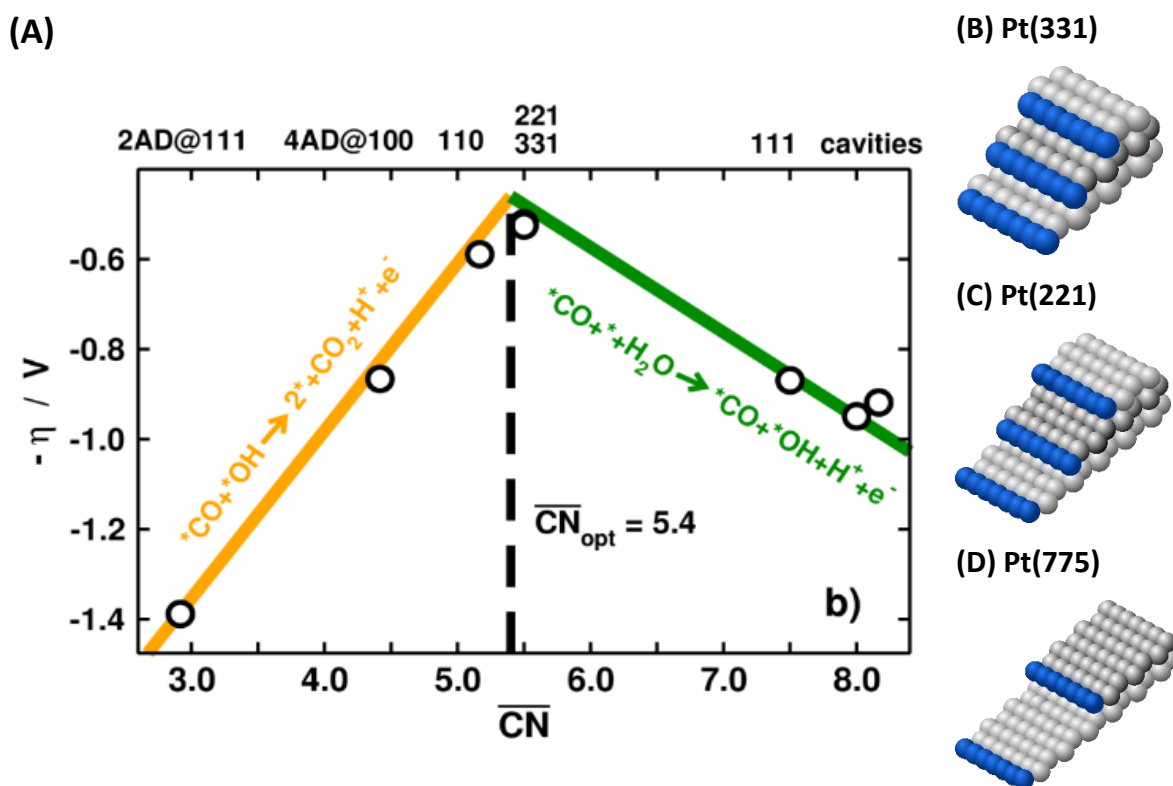
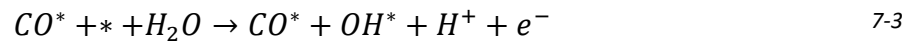
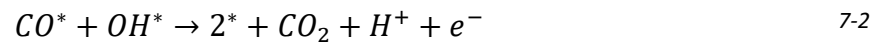


Figure 7-34: (A) Coordination-activity plot for platinum. At the step edges of Pt(331) (A), Pt(221) (B) and Pt(775) (C) sites are found with  $\overline{CN} = 5.5$  (indicated in blue) close to  $\overline{CN}_{opt} = 5.4$ . The overpotential is calculated as  $\eta = \max(\Delta G_2, \Delta G_3, \Delta G_4) - E^0$ .

Figure 7-34 shows the volcano-shaped coordination-activity plot in which the density functional theory-calculated overpotentials of the active sites for different reactions are linked to  $\overline{CN}$ . The limiting steps can be derived from the underlying reaction mechanism [226, 227]. On the too strong-binding side (left) of the volcano curve is the recombination of surface hydroxide and carbon monoxide as shown in Equation 7-2. The reaction on the weak-

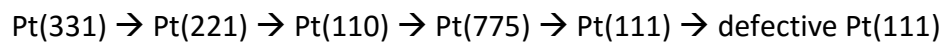
binding side (right) is the adsorption of water and subsequent oxidation towards hydroxide (Equation 7-3).



An optimal catalyst would show the adsorption energies of  $\Delta G_{CO}^{opt} = -1.1 \text{ eV}$  and  $\Delta G_{OH}^{opt} = -0.4 \text{ eV}$  for carbon monoxide and hydroxide, respectively.

Combining these findings in the coordination-activity plot shows that the optimal active sites would have  $\overline{CN}_{opt} = 5.4$ . Such low coordinated sites are found on the step edges of stepped surfaces like Pt(331), Pt(221) and Pt(775). At these sites the coordination is relatively low and a strong bonding towards the adsorbates is observed compared to Pt(111) as illustrated in Figure 7-34. Most importantly, at the convex defects the adsorption of hydroxide – which is an important intermediate for the carbon monoxide oxidation – is observed already at low potentials like described before.

As shown in Figure 7-35 the higher the step density, the “sooner” the oxidation occurs in terms of overpotential. Accordingly, the oxidation occurs in the following order for the measured surfaces:



Pt(110), pristine and defective Pt(111) are used as a reference point to further shed light on the influence of the defect type. Based on the bimolecular mechanism of the carbon monoxide oxidation normally the adsorption of two intermediates must be considered for the elucidation of active sites [226, 227]. Since the surfaces were saturated prior to the experiments with carbon monoxide, its adsorption is neglected for the following considerations. The remaining carbon monoxide in the solution was removed by flushing the electrolyte with argon. Accordingly, the activity of the surfaces solely depends on the potential dependent adsorption of hydroxides onto the surface as potential-determining step.

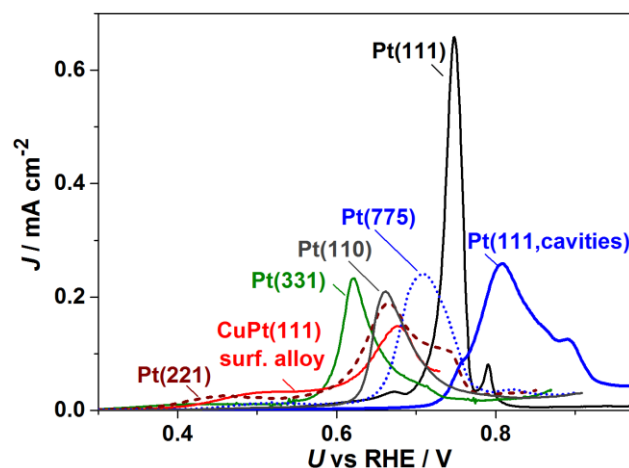


Figure 7-35: Anodic parts of the carbon monoxide stripping voltammogram in 0.1 M perchloric acid for Pt(111), Pt(775), Pt(331), Pt(221), Pt(110), and Pt(111) with concave surface defects [340] and CuPt(111) surface alloy [227] measured with a scan rate of 50 mV/s.

As mentioned the introduced convex defects allow the adsorption of hydroxide as early as 0.06 V. In argon-saturated solutions the CO adlayer changes, so that part of the adsorbed carbon monoxide is weaker adsorbed and reacts readily with the early adsorbed hydroxide on the surface [341]. Consequently, the reaction proceeds primarily in the proximity of the convex defects. This causes the oxidation current prior to the main peak. Consequently, the stepped surfaces can be ranked according to the terrace length and their number of preferential sites for hydroxide adsorption. Accordingly, the activity increases with the decreasing terrace length from Pt(331) to Pt(221) to Pt(110) to Pt(775). Thereby, the maximum is reached at a step length of three atoms. Based on the too strong adsorption of carbon monoxide on Pt(110), which can also be denoted as Pt[2(111)x(111)], it prevents the desorption of the formed carbon dioxide. Additionally, this surface undergoes permanent reconstruction under experimental conditions and thereby changes its adsorption properties as discussed before [265-267].

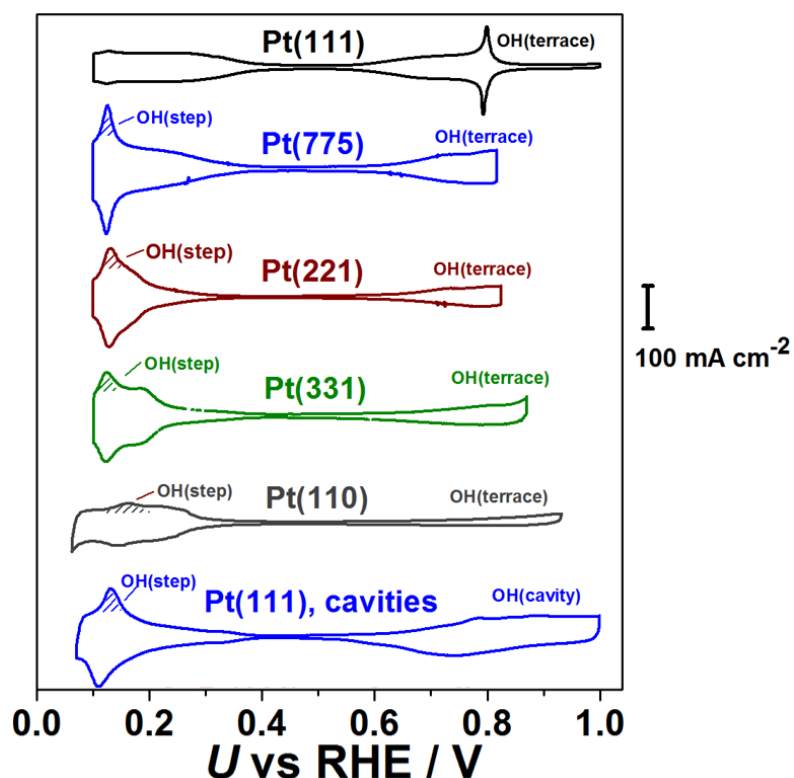


Figure 7-36: Cyclic voltammograms of Pt(111), Pt(775), (331), (221) and (110), Pt(111) with concave surface defects [340] and PtCu(111) surface alloy [227] in argon-saturated 0.1 M perchloric acid measured with a scan rate of 50 mV/s. To emphasize the importance of the hydroxide adsorption on the onset of the carbon monoxide oxidation its early adsorption on steps is indicated.

The most active not stepped surface is pristine Pt(111). In theory, the surface should be free of any kind of defects and thus offer no preferential sites for the adsorption. Hence, the reaction should start with the adsorption of hydroxide on the terraces. As mentioned before a completely defect-free Pt(111)-surface cannot be realized under experimental conditions. On all surfaces, a small number of defects is found which allows the adsorption of hydroxide already at low potentials. Accordingly, a low oxidation current prior to the main peak is observed at which hydroxide adsorbs to the defects and reacts with the surrounding carbon monoxide. At the start of the main peak of around 0.7 V the adsorption of hydroxide also on the (111)-facet is sufficient to allow the complete oxidation of the remaining CO - surface layer. The start of the carbon monoxide oxidation at potentials at which hydroxides are mostly adsorbed at steps or defects indicates that the active sites are at the low-coordinated step edges (compare Figure 7-35 and Figure 7-36).

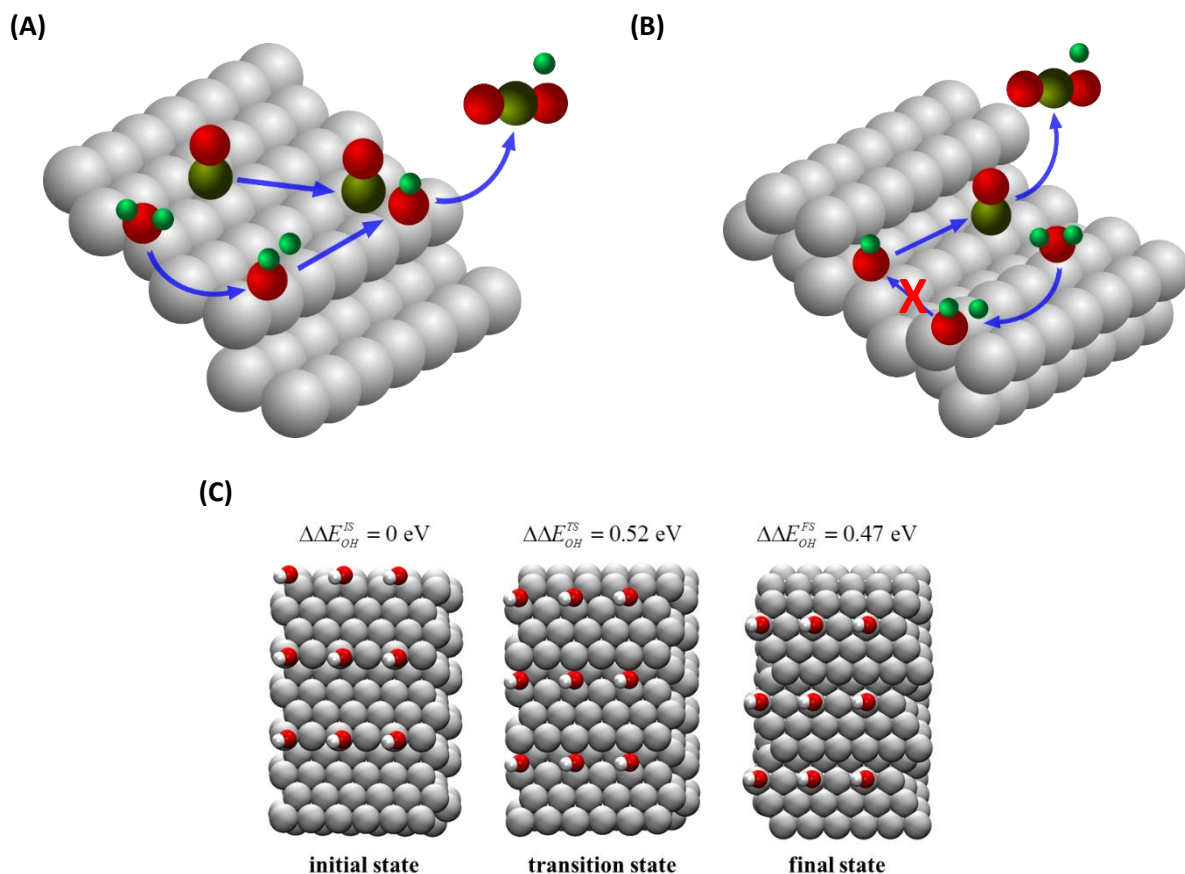


Figure 7-37: Schematic representation of the carbon monoxide oxidation at a) convex and b) concave sites on platinum (red = oxygen, light green = hydrogen, dark green = carbon & grey = platinum). On step edges surface hydroxide is formed and reacts with surface carbon monoxide. On the contrary, in cavities hydroxide formation proceeds at larger potentials. Additionally, the diffusion into the cavity is kinetically hindered by an energetic barrier for adsorbed hydroxide of roughly 0.52 eV on Pt(221) (c / red = oxygen, white = hydrogen & grey = platinum).

Although on defective Pt(111) hydroxide adsorbs readily at already low potentials the oxidation occurs at higher potentials than on Pt(111). The introduction of cavities coincides with the formation of beneficial convex defects like described earlier. Nevertheless, the adsorption of carbon monoxides occurs inside of the cavities while hydroxide is found on the edges outside of the defects [305]. This prevents the direct contact between carbon monoxide and hydroxide important for the reaction to proceed as the diffusion of hydroxide over the step edge to the lower terrace is kinetically hindered by 0.52 eV like illustrated for Pt(221) in Figure 7-37 according to DFT calculations. Consequently, the adsorption of hydroxides in the cavities is required. Hence, it can be assumed that reaction proceeds directly at and in the surrounding of the convex defects.

To conclude carbon monoxide oxidation occurs at the convex defects found on stepped surfaces and starts already at low potentials in their direct surrounding. With increasing

potential, the adsorption of hydroxide is sufficient to oxidize the complete carbon monoxide layer.

## 7.5 Oxygen reduction reaction on polycrystalline Pt-based alloys

An alternative to pure precious metals catalysts for the electrochemical reduction of oxygen are platinum alloys with transition metals or lanthanides of the type  $Pt_nX$  [51, 62, 274, 342-349]. The different diameter of the alloyed elements in respect to the host metal causes strain inside the material which influences the electronic structure of the surface and decrease its binding towards the intermediates. Colic et al. proposed a so-called double volcano plot to quantify the activity of such catalysts [61]. Therefore, the activity of polycrystalline and nanostructured platinum based alloys is plotted against the atomic radius of the alloyed element in 0.1 M perchloric acid as shown in Figure 7-38. This plot results into a volcano shaped curve with two maxima for the activity at small and big atomic diameter for copper and yttrium, respectively. While the alloyed elements in between the maxima would bind the intermediates too strong, the binding of the alloys on the outside is too weak.

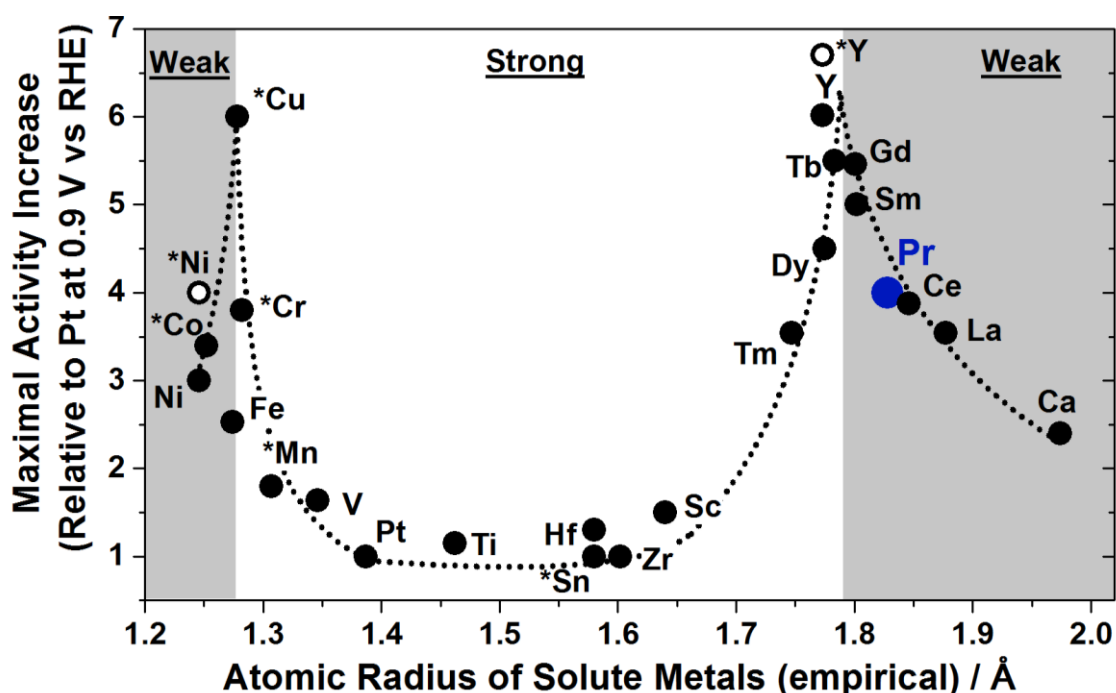
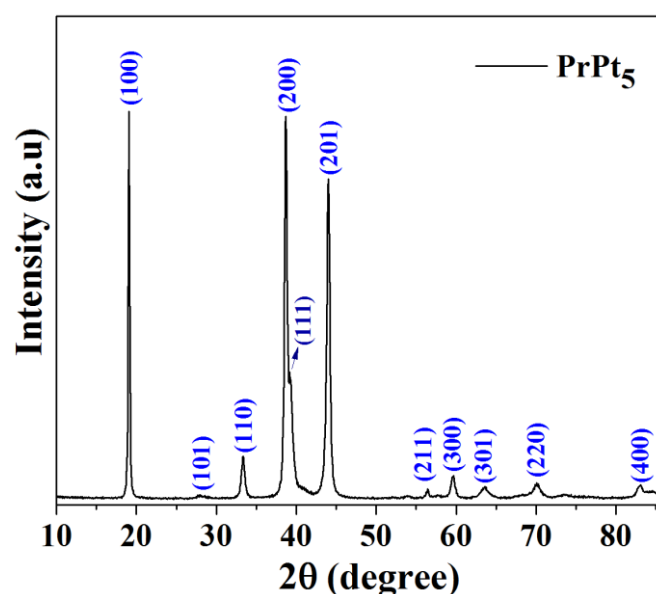


Figure 7-38: "Double volcano" plot of platinum based alloys for the electrochemical reduction of oxygen. The investigated alloy  $Pt_5Pr$  is indicated with a blue dot. Adapted from reference [61].

To experimentally prove the validity of the formulated volcano plot,  $Pt_5Pr$  alloy was chosen because of its stability and location in the weaker binding area of the double volcano plot. Based on its atomic diameter of  $\sim 1.85$  Å for praseodymium, its activity should be slightly

increased compared to polycrystalline platinum with decreased adsorption strength of the intermediates. This would allow to increase the binding of the intermediates by decreasing the particle size of nanoparticles [61]. Prior to the electrochemical measurements, to guarantee the quality of the alloy, X-ray diffractogram and AFM pictures were recorded. The X-ray diffraction peaks for the untreated  $\text{Pt}_5\text{Pr}$  alloy, as shown in Figure 7-39A, agree with the standard PDF-65-8059 with a hexagonal symmetry and space group  $P6/mmm$  (191). The lattice parameters were calculated to be  $a = b = 5.353$  and  $c = 4.386$  Å in agreement with the standard values. A typical AFM-image of the surface is shown in Figure 7-39B with a roughness around 50 nm.

(A)



(B)

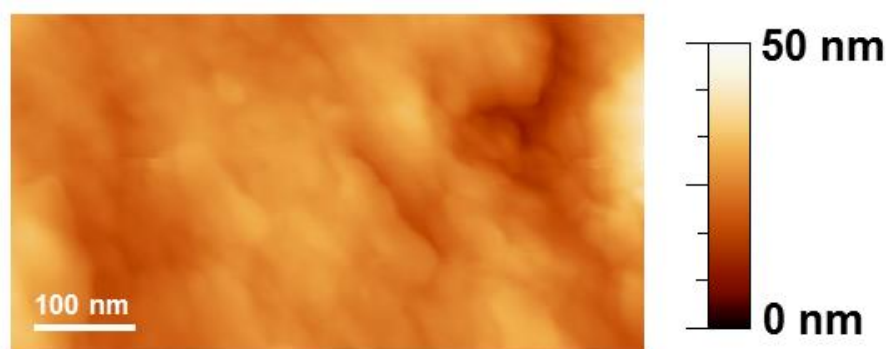


Figure 7-39: (A) X-ray diffractogram of the untreated electrode with the indicated peaks for polycrystalline  $\text{Pt}_5\text{Pr}$ . (B) Typical AFM image of its rough surface.

In contrast, to the so far investigated well-defined stepped surface with specific adsorption sites, the determination of active sites for this surface is extremely difficult. The polycrystalline surface and the introduced strain cause a broad variety of adsorption sites.

Additionally, polycrystalline alloys consisting of platinum and a less noble lanthanide are not stable under conditions for electrochemical cycling [52, 61, 62, 188]. The lesser noble metal is leached from the first three to five atomic layers of the alloy resulting into a stable platinum rich shell with an alloyed core. The formed platinum shell eliminates the influence of the ligand effect which is limited to only a few atomic layers. This leaching is most prominent at defective sites which are common on polycrystalline surface. Notably, the Pt-shells are not epitaxial grown around the alloy cores. The shell does not simply expand around the core, but forms a distinct structure with the atoms being closer to each other than in normal unstrained *fcc*-structures which increases the surface roughness further [350]. While this minimizes the resulting surface energy, it additionally causes compressive strain. The latter significantly changes the electronic structure of the surface, so that the resulting surface shell in this case binds the intermediates statistically weaker [52, 61, 62, 188].

Figure 7-40 shows the stable and reproducible cyclic voltammograms of polycrystalline platinum in comparison to the investigated Pt<sub>5</sub>Pr alloy after several cycles up to an upper vertex potential of 1.2 V. For polycrystalline platinum, which comprises of several different surface facets and structures to an unknown degree, the typical voltammogram consists of their define adsorption features superimposed onto each other [351]. Accordingly, the determination of contributing sites for this electrode requires the comparison of measured features with the characteristic adsorption features of well-defined single crystal surfaces.

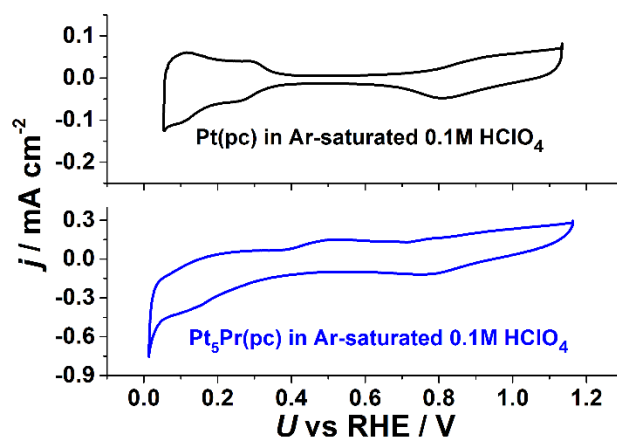


Figure 7-40: Cyclic voltammogram of polycrystalline platinum (black) and polycrystalline Pt<sub>5</sub>Pr-alloy measured in 0.1M perchloric acid with a scan rate of 50 mV/s.

For the Pt<sub>5</sub>Pr alloy in the potential region from 0.06 to 0.4 V, no characteristic peaks are observed. Seemingly the introduced strain results in several newly formed adsorption sites without preferential formation of one adsorption site over the whole potential region from 0.25 V to 1.0 V. Interestingly, above 0.4 V the adsorption to the surface becomes even stronger than for polycrystalline platinum. This agrees with the copper UPD-monolayer stripping which indicates *in situ* a broad variety of energetically different adsorption sites for both surfaces. The integrated charge gives a value of  $\sim 440 \mu\text{C cm}^{-2}$  for both crystals and confirms that no additional sites are generated by the de-alloying. This charge is typical for a smooth polycrystalline platinum surface and supports the assumed core/shell structure for the alloy.

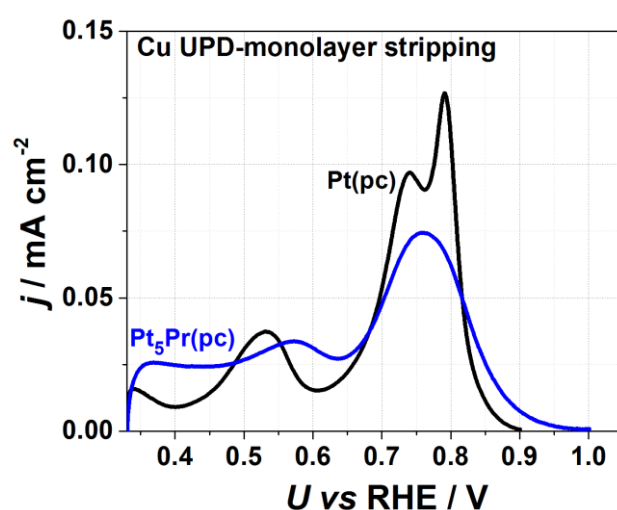


Figure 7-41: Copper UPD-monolayer stripping of polycrystalline platinum (black) and Pt<sub>5</sub>Pr alloy (blue) in 0.1 M perchloric acid with 0.001 M of Cu<sup>2+</sup>.

The nearly identical surface area of the both electrodes allows to directly compare the electrochemical results. The rotating disc measurements of the surfaces in Figure 7-42A demonstrates a significant increase of the activity for the alloy.

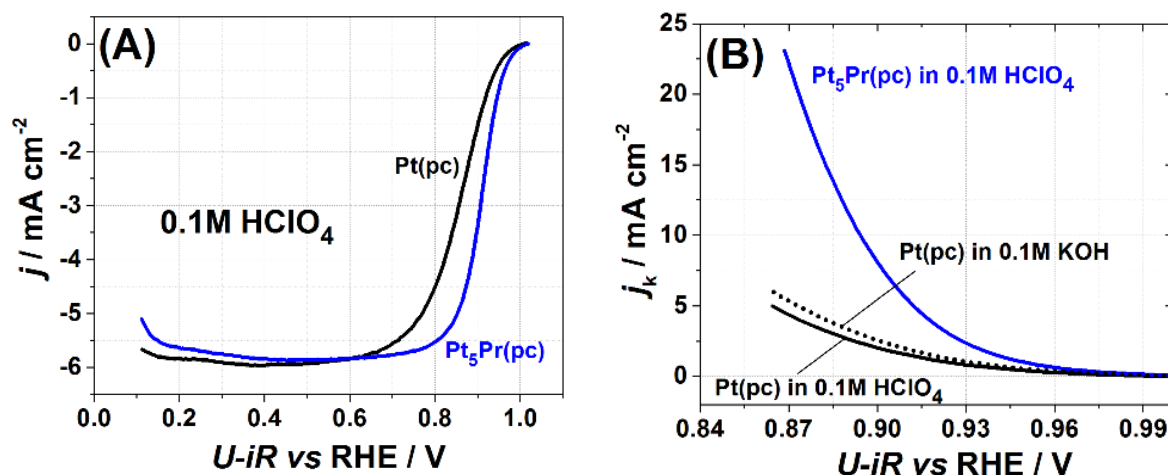


Figure 7-42: (A) Activity measurement of polycrystalline platinum (black) and Pt<sub>5</sub>Pr alloy (blue) in 0.1 M perchloric acid. (B) Kinetic current for polycrystalline platinum (black solid line) and Pt<sub>5</sub>Pr alloy (blue solid line) in 0.1 M perchloric acid. For comparison, polycrystalline platinum in 0.1 M potassium hydroxide solution (black dotted line) is added.

Figure 7-42B shows the kinetic current of the investigated alloy in 0.1 M potassium hydroxide solution and perchloric acid relative to polycrystalline platinum in perchloric media. Hereby, the nature of the present alkali metal ions significantly influences the activity in alkaline media. In general, it can be assumed that potassium ions destabilize the surface bound hydroxide to some degree [67, 68, 95]. As the investigated alloy binds the intermediates too weakly, the influence of the ions should additionally weaken the interaction between the surface and the intermediates and make Pt<sub>5</sub>Pr less active. Indeed, the activity of the alloy in potassium hydroxide is relative low, while the activity of polycrystalline platinum increases. This further supports the assumption that the resulting surface is too noble as catalyst for the electrochemical reduction of oxygen. The effect of the alkali metal cations will be discussed in more detail in the next chapter.

To conclude, the adsorption properties of the platinum surfaces can be changed through the introduction of strain by alloying with other metals and subsequent leaching of the element.

## 7.6 The role of the electrolyte composition on the performance of active sites

An additional degree of freedom is the influence of the electrolyte components (in many cases so-called spectator species, e.g. alkali metal cations) on the adsorption of the reaction intermediates. Hereby, these species can interact directly with either the intermediates or the sites at the metallic electrode [66-68, 95, 352]. For instance, in sulfuric acid a (di)sulfate layer is formed on the platinum surface, which moves the adsorption of reactants from the electrolyte to higher potentials [65, 66]. As mentioned before nowadays most electrochemical experiments are performed in perchloric acid. It is mostly assumed that perchlorates do not adsorb on the electrode surface and do not interact with the reactants [297]. Anyhow, recently this assumption was questioned by Huang et al [296]. They observed an one-to-one interaction between perchlorate-ions and adsorbed hydroxide. The possible decrease in mobility of the surface species could cause an increase in overpotential for the oxygen reduction reaction in perchloric acid. However, the total effect still requires some evaluation. Figure 7-43 shows the activity for Pt(221) in potassium hydroxide with and without added potassium perchlorate. As can be seen, the addition of the latter significantly decreases the activity relative to the potassium hydroxide. This agrees with Huang and indicates, that perchlorates may not be the optimal electrolyte for the investigation of electrochemical reactions in aqueous electrolytes [296].

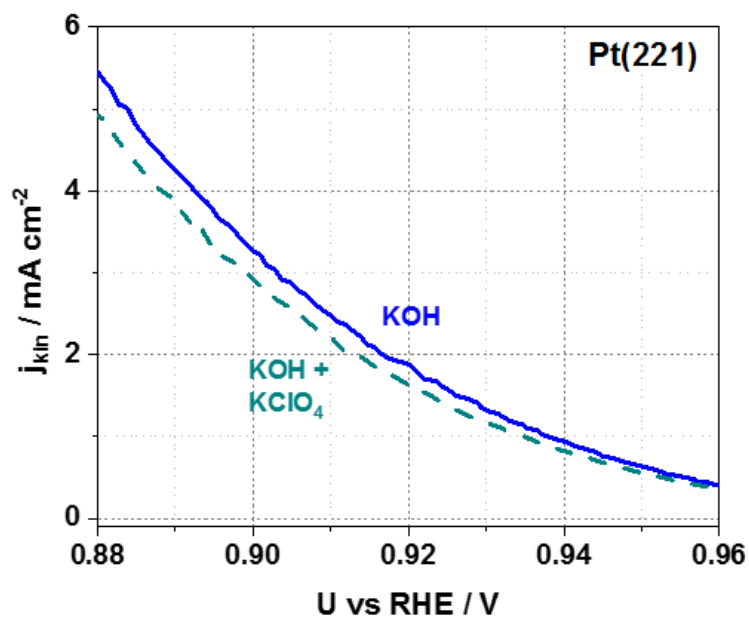


Figure 7-43: Activity for the electrochemical reduction of oxygen on Pt(221) in 0.1 M argon-saturated potassium hydroxide and the solution with added potassium perchlorate. The activity with perchlorates decreases significantly.

An alternative are the alkali metal solutions with mostly hydroxide adsorbed on the electrode surface like in perchloric acid in the relevant potential range [353]. This should indicate a similar activity for the electrochemical reduction of oxygen in alkaline media. Controversially, several investigations showed a significant decrease of the activity in these solutions. For instance, the stepped surface Pt(331) with high activities in perchloric acid, shows a lower activity than Pt(111) in sodium hydroxide [237]. While the electrochemical reduction of oxygen on platinum has been investigated extensively in acidic media, the studies in alkaline media are limited especially for the influence of the alkali metal cations on stepped platinum surfaces [286, 353, 354]. It is commonly accepted, that the alkali cations interact with the intermediates of the oxygen reduction reaction on Pt(111) [67, 68, 95]. Anyhow, based on their different surface geometry and different adsorption sites it cannot be assumed that the effect on the stepped surfaces is identical to pristine Pt(111).

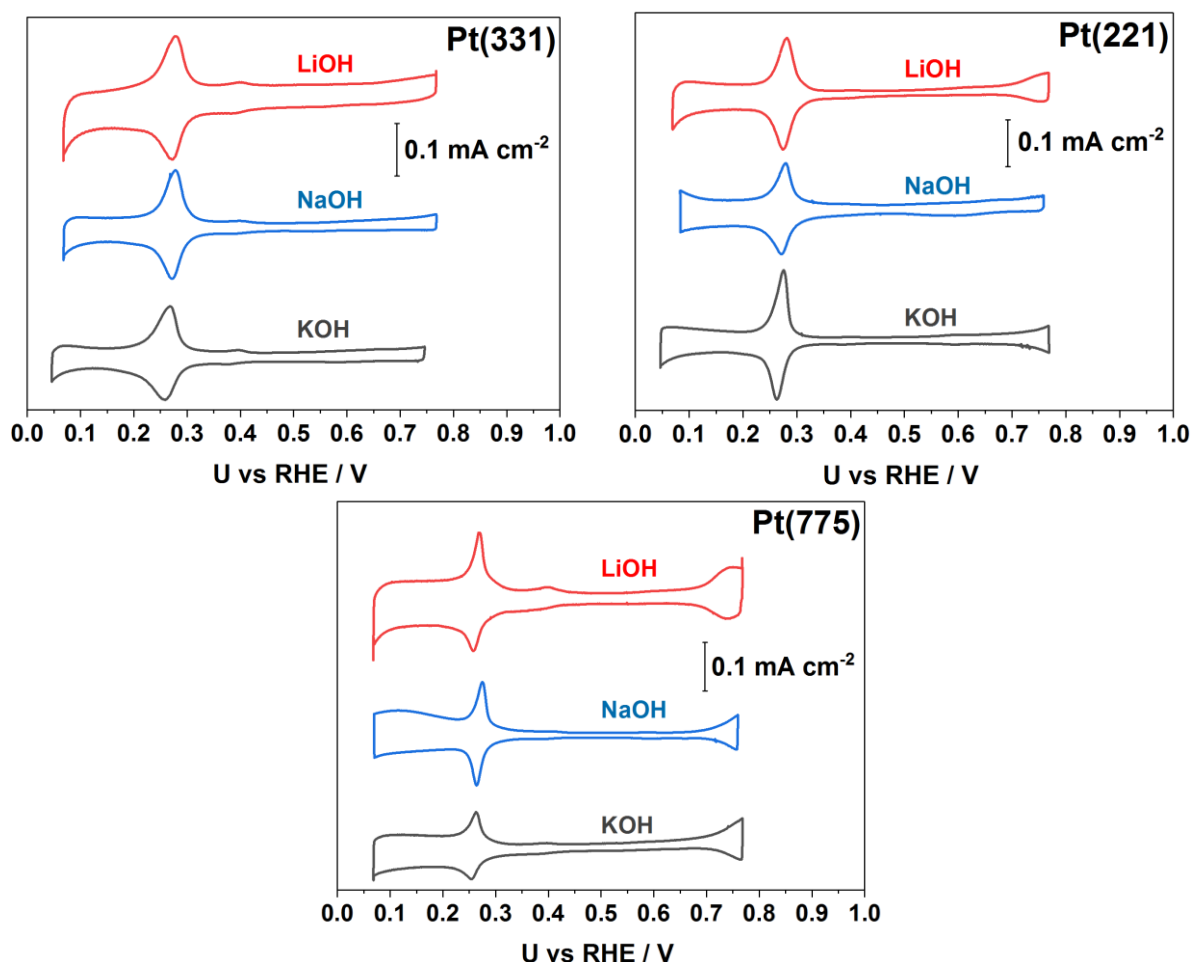


Figure 7-44: Cyclic voltammograms of the stepped surfaces Pt(331), Pt(221) and Pt(775) in the alkali-metal solutions (lithium, sodium and potassium).

Figure 7-44 shows the cyclic voltammograms of the stepped platinum surfaces for the oxygen reduction reaction in pure 0.1 M solutions of the alkali metal hydroxide solutions for lithium, sodium and potassium corrected for the pH. Based on experimental difficulties, the measurements in cesium and rubidium hydroxide are not included as no typical cyclic voltammograms were observed. Interestingly, the adsorption profile of the surfaces shows only a single strongly pronounced peak at a potential of  $\sim 0.26$  V for all surfaces. The origin of this adsorption feature is still under discussion. Rizo et al. proposed that this peak is caused by hydrogen adsorption/desorption or the competitive adsorption of hydroxide and oxygen from the electrolyte like in acidic media [237]. This is in agreement with the high purity of the electrolyte solutions which are mostly limited to their cations and hydroxides. In the potential range from  $\sim 0.35$  towards 0.7 V the contribution of the double layer capacitance is visible. Above a potential of 0.7 V the formation of hydroxide and oxygen surface is observed.

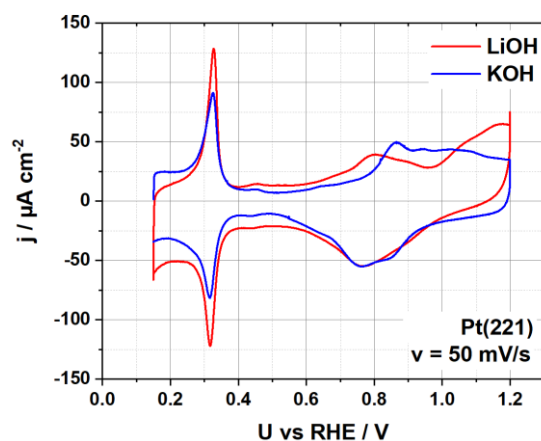


Figure 7-45: Cyclic voltammograms of the stepped surface Pt(221) in 0.1M potassium hydroxide compared to 0.1M lithium hydroxide. The adsorption of oxygen species is moved towards higher potentials in the weaker interacting potassium hydroxide relative to the lithium solution.

To determine the influence of the cations on the adsorption from the electrolyte the cyclic voltammogram of Pt(221) is shown up to a vertex potential of 1.2 V in 0.1 M lithium and potassium hydroxide in Figure 7-45. In the latter, the peak attributed to the adsorption and the formation of hydroxide and oxides on the surface are moved to more positive potentials in comparison to lithium hydroxide. Apparently, the stronger interaction by lithium hinders the formation of those species.

To further shed light on this influence, the activity for the electrochemical reduction of oxygen on stepped platinum surface in different alkali metal solution and in perchloric acid

were measured as shown in Figure 7-46. With the activity in the different alkali metal hydroxides ranking as follows:  $\text{Li}^+ > \text{Na}^+ > \text{K}^+ > \text{Cs}^+ > \text{Rb}^+$ . The deviations for the last two ions will be discussed later.

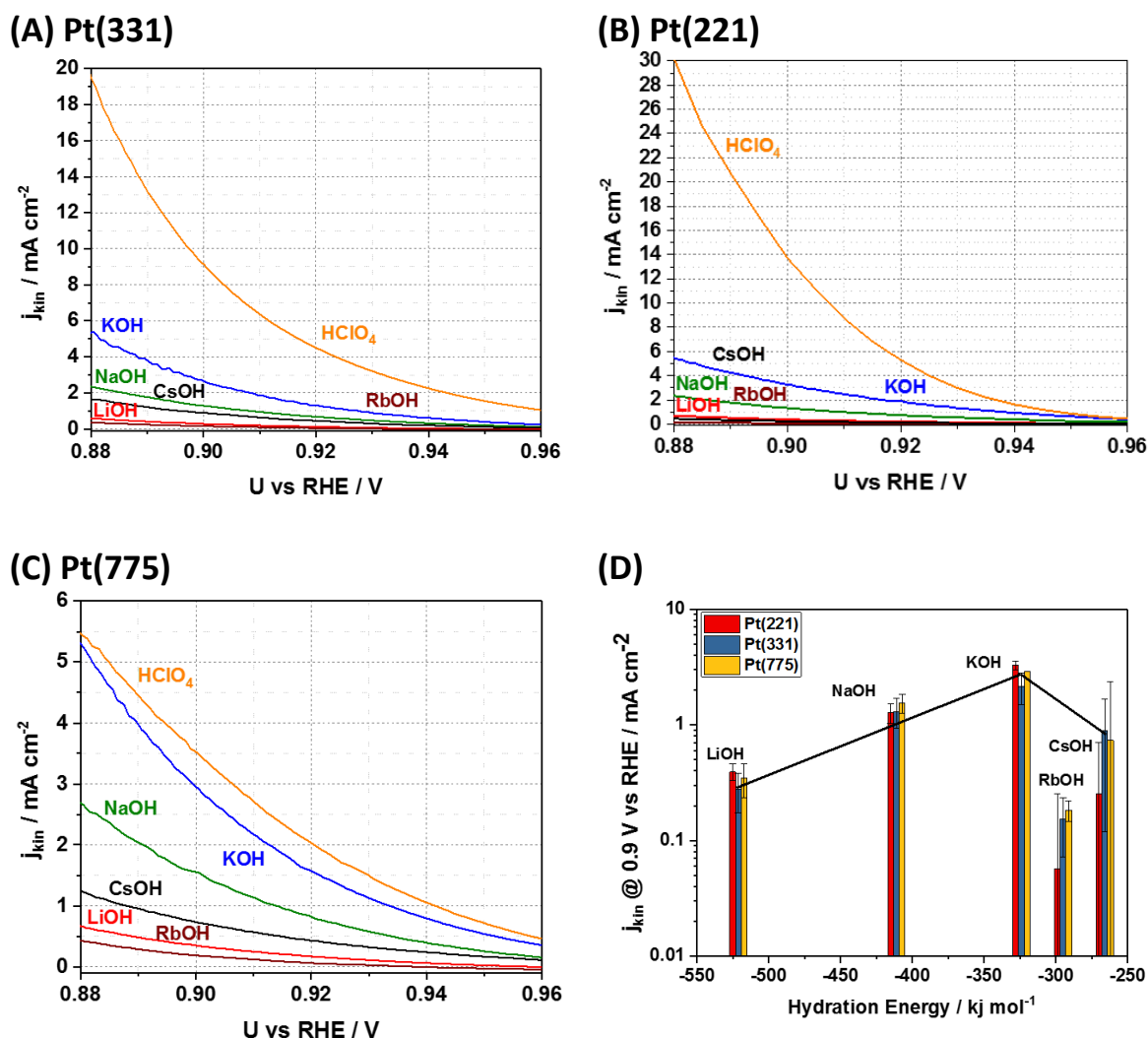


Figure 7-46: (A-C) Kinetic currents of the stepped surfaces in different alkali metal solutions and perchloric acid. (D) Kinetic current of the surfaces at the working potential of  $0.95 \text{ V}$  in  $0.1 \text{ M}$  alkali-metal solutions versus the hydration energy of their cations. The black line is added as a guide for the eye. The activity increases with the declining hydration energy for lithium to potassium and decreases afterwards. This agrees with the measurements done by Strmcnik for Pt(111) [67].

These observations are mostly in agreement with the model proposed by Strmcnik et al. which discusses the influence of the alkali cations on Pt(111) [67]. According to them, the solvated alkali metal cations interact with two hydroxide ions on the surface via hydrogen bonds and hold them on the surface. Accordingly, their mobility is significantly decreased and the on-set potential for the oxygen reduction reaction is moved to higher potentials.

This influence decreases with the hydration energy of the cations which gives the following ranking:  $\text{Li}^+ > \text{Na}^+ > \text{K}^+ > \text{Cs}^+$ . The same trend is observed for the stepped platinum surfaces with the highest activity for potassium. Interestingly, an exception is observed for cesium and rubidium which show a decrease in activity in comparison to Pt(111).

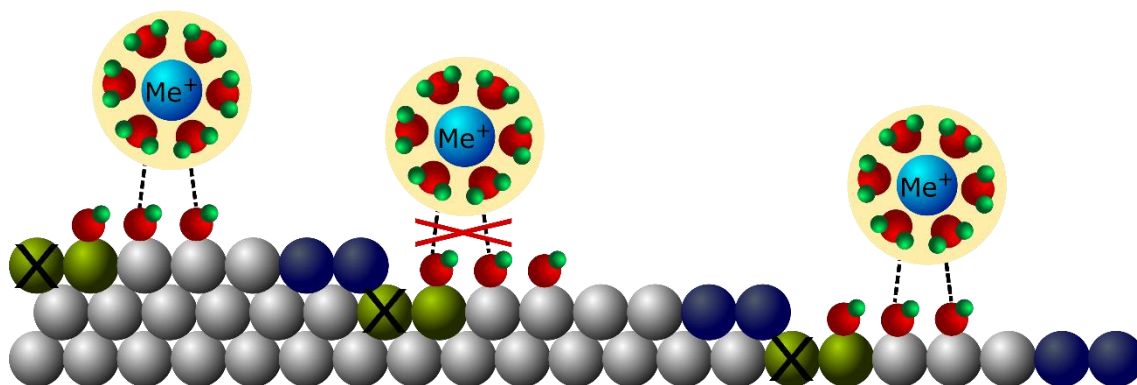


Figure 7-47: Schematic visualization of the stabilized first water-layer by the solvated alkali-metal cations over the terraces on Pt(775). The degree of stabilization is influenced by the type of ion. The introduction of steps causes the formation of concave (dark green) and convex (dark blue) defects with weaker and stronger adsorption of hydroxide to the surface, respectively. The atom directly below the step edge (black cross) cannot partake in the reaction due to steric hindrance by the step edge. Additionally, the step edge shields the concave sites from the voluminous cations. Adapted from the model of Strmcnik [67].

For these two ions, the structural features introduced with the steps seem to influence the ion. While on a plane Pt(111) surface the cation can interact with the whole first water-layer unhindered, on a stepped surface the step edges seem to shield the terrace from these voluminous cations as shown in Figure 7-47. The measurements indicate, that the interaction of the electrolyte is too weak for subsequent activation of the intermediates on the surface. Consequently, the weaker interaction results into insufficiently activated intermediates and an decrease in the activity.

Interestingly, in alkaline media an increase in terrace length does not influence the activity like in acidic media. This indicates that in alkaline media the electrochemical reduction of oxygen may not be structure sensitive. To further evaluate this observation and the effect of the cations, additional experiments would be required.

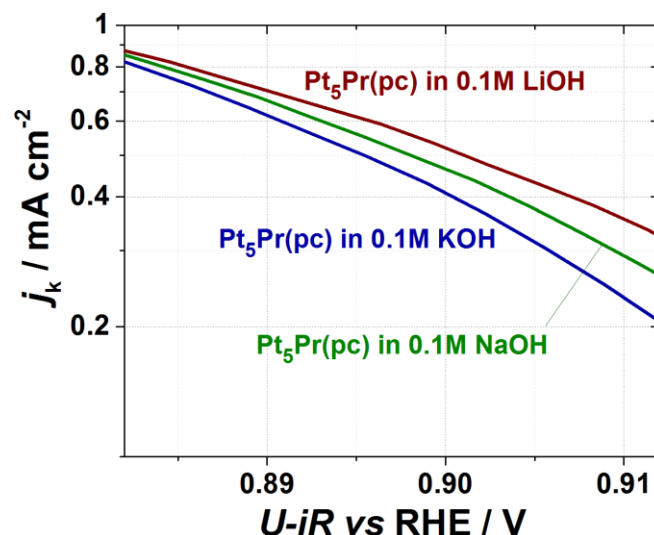


Figure 7-48: Kinetic currents of the alloy sample measured in oxygen-saturated 0.1 M lithium hydroxide, sodium hydroxide and potassium hydroxide. The samples were measured with a scan rate of 50 mV/s and a rotation rate of 1600 rpm.

The described effect can be utilized to tune the activity of platinum and its alloys. Figure 7-48 shows the kinetic currents for the oxygen reduction reaction on Pt<sub>5</sub>Pr. This alloy is too noble for the reaction intermediates and adsorbs them too weakly as discussed before. If the electrolyte “forces” the intermediates to be bound stronger to the surface, the conditions are moved closer to the optimum and higher activities should be achieved. Indeed, the highest activity is measured in lithium hydroxide and decreases towards potassium.

To conclude, the electrolyte composition has a major influence on the activity of surfaces. Especially, alkali metal cations can be utilized to change the adsorption and formation of intermediates for the oxygen reduction reaction. With the progress in experimental methods the important role of the cations needs to be further determined.

## 8 Conclusion and outlook

The focus of this thesis was the identification of active sites for energy relevant reactions such as the hydrogen evolution reaction, oxygen reduction reaction and the carbon monoxide oxidation on platinum model electrocatalysts. In this context, the effect of surface structure, adsorbate structure, alloying and electrolyte components on the adsorption properties of platinum model systems was investigated. The conducted experiments were theoretically explained using density functional theory calculations and the generalized coordination number approach, which considers the neighboring atoms of the direct neighbors.

It has been shown that the most active sites for the hydrogen evolution reaction on Pt in acidic media are the hollow sites with generalized coordination number being  $\sim 7.7$ . These kind of sites can be for instance found at quasi-periodic steps, where the sites with e.g. the generalized coordination number 7.33 for Pt(221) can be found. These sites are closer to the optimum and result into an increased measured activity for the hydrogen evolution reaction. The measurements indicate, that the hydrogen evolution reaction is structure sensitive on surfaces of the Pt[n(111)x(111)]-type. The highest reported in the literature for the pure platinum surfaces activity has been found for Pt(221), where the density of active sites with optimal coordination is maximal.

For the oxygen reduction reaction, it has been shown that for pure platinum surfaces the optimal generalized coordination number for the catalytically sites in acidic media is  $\sim 8.3$ . These sites can be found as the “on top” adsorption sites at step-like defects and concavities on pristine Pt(111) terraces. Based on this finding, for the first time the increased oxygen reduction activity of Pt[n(111)x(111)] surfaces, concave nanoparticles and arrays of nanoparticles was explained. Accordingly, design principles for the optimal platinum oxygen reduction electrocatalysts are formulated.

At defects strongly binding adsorbates, namely  $\ast\text{O}$ , significantly influence the adsorption of the reactants for the oxygen reduction reaction. Based on “in situ” potentiodynamic electrochemical impedance spectroscopy experiments, the increased activity for the electrochemical reduction of oxygen on Pt(331) has been explained and the nature of active

sites at its surface was elucidated. The optimal adsorption properties are found on high-index surfaces at the step bottom.

The nature of active sites for the carbon monoxide oxidation in acidic media has been revealed for various Pt surfaces. The coordination-activity plot for the carbon monoxide oxidation gives the optimal generalized coordination number being 5.4 for the most active “on-top” sites. These sites can also be found at surface defects like steps at the lower coordinated atoms at the step edges, according to the examples given in the thesis. Carbon monoxide oxidation activity trends for Pt[n(111)x(111)] samples and concave samples were explained based on experimental and theoretical data with the highest activity for the stepped surfaces.

The predictive power of the recently suggested “double volcano”-descriptor, the radii of the solute atoms in Pt-alloys, has been experimentally confirmed. Based on this approach the new highly active alloyed catalysts Pt<sub>5</sub>Pr for the oxygen electroreduction has been identified. Its activity in acidic media appeared to be ~4 times higher at 0.9 V compared to pure polycrystalline Pt. It is assumed that only strain effects affect the performance of active catalytic centers.

The influence of the non-covalent interactions on the performance of active catalytic centers has been revealed for a series of new platinum systems. The electrolyte components (spectator species, namely alkali metal cations) can influence the adsorption strength of the oxygen reduction reaction intermediates. The alkali metal cations interact with the first water-layer on stepped Pt surfaces and stabilize the adsorbate structures. The degree of stabilization decreases from lithium towards potassium. For rubidium and cesium, the steps seem to shield the ions resulting into a too weak adsorption of the intermediate species. Based on this model, the activity trends on Pt[n(111)x(111)] samples in different alkaline media have been explained. In the case of Pt<sub>5</sub>Pr, the oxygen reduction intermediates are adsorbed too weakly. Introduction of alkali metal cations can only decrease its activity towards oxygen electroreduction, which was confirmed experimentally in this work.

## **Outlook**

The generalized coordination number can be used to derive design principles for several reactions such as the oxygen reduction reaction, the hydrogen evolution reaction and the

carbon monoxide oxidation. However, it is at the moment used to elucidate the activity trends only for few reactions and few metals in acidic media. Additionally, preliminary STM results in alkaline media indicate that the concept cannot be directly applied to alkaline media due to poorly predictable non-covalent interactions. Hence, it is necessary to further experimentally and theoretically elaborate the effect of the different electrolytes. Another factor is the evaluation of different adsorbates and their influence on the adsorption strength. For instance, for the oxygen reduction reaction the influence of sulfates needs to be considered based on their similarity to sulfonic groups found in commercial polymer electrolyte membrane fuel cells with Nafion® as electrolyte. For the identification of active sites, the generalized coordination number needs to be further extended towards these species to become a more robust descriptor. It should be considered to extend this concept also to non-noble metals and oxide surfaces.

Finally, the effect of cation species is only basically understood and not sufficiently elaborated. Further experiments are required to evaluate their total effect on the first water-layer and reaction intermediates in alkaline and acidic media. In this respect, also their effect on different reactions such as the hydrogen evolution reaction or carbon monoxide oxidation in both electrolytes should be of importance.

## 9 References

1. Wigley, T.M. and Schimel, D.S., *The carbon cycle*. Vol. 6. 2005, Cambridge: Cambridge University Press. ISBN: 0521018625
2. Cloud, P. and Gibor, A., *The oxygen cycle*. *Sci Am* (1970), **223**: p. 111-23.
3. Canfield, D.E., Glazer, A.N., and Falkowski, P.G., *The evolution and future of Earth's nitrogen cycle*. *Science* (2010), **330**: p. 192-6.
4. Galloway, J.N., *The global nitrogen cycle: changes and consequences*. *Environmental pollution* (1998), **102**: p. 15-24.
5. Grace, J., *Understanding and managing the global carbon cycle*. *Journal of Ecology* (2004), **92**: p. 189-202.
6. Zhengfu, B., Inyang, H.I., Daniels, J.L., Frank, O., and Struthers, S., *Environmental issues from coal mining and their solutions*. *Mining Science and Technology (China)* (2010), **20**: p. 215-223.
7. Jackson, J.H., *Migration and Urbanization in the Ruhr Valley: 1821-1914*. Vol. 9. 1997, Amsterdam: Brill. ISBN: 0391040332
8. *BP Statistical Review of World Energy June 2017*. 2017, BP Global.
9. Cox, P.M., Betts, R.A., Jones, C.D., Spall, S.A., and Totterdell, I.J., *Acceleration of global warming due to carbon-cycle feedbacks in a coupled climate model*. *Nature* (2000), **408**: p. 184.
10. Solomon, S., Plattner, G.K., Knutti, R., and Friedlingstein, P., *Irreversible climate change due to carbon dioxide emissions*. *Proceedings of the National Academy of Sciences of the United States of America* (2009), **106**: p. 1704-1709.
11. Oreskes, N., *The scientific consensus on climate change: how do we know we're not wrong?* *Climate change: What it means for us, our children, and our grandchildren* (2007: p. 65-99.
12. *BP Statistical Review of World Energy June 2016*. 2016, BP Global.
13. *2017 Revision of World Population Prospects 2017*; Available from: [https://esa.un.org/unpd/wpp/Publications/Files/WPP2017\\_KeyFindings.pdf](https://esa.un.org/unpd/wpp/Publications/Files/WPP2017_KeyFindings.pdf).
14. *The World Factbook*. 2017 18.07.2017; Available from: <https://www.cia.gov/library/publications/the-world-factbook/>.
15. Erb, K.H., Gingrich, S., Krausmann, F., and Haberl, H., *Industrialization, Fossil Fuels, and the Transformation of Land Use*. *Journal of Industrial Ecology* (2008), **12**: p. 686-703.
16. *June 2017 Monthly Energy Review 2017* 18.07.2017]; Available from: [www.eia.gov/mer](http://www.eia.gov/mer).
17. Parson, E.A. and Keith, D.W., *Climate change - Fossil fuels without CO2 emissions*. *Science* (1998), **282**: p. 1053-1054.
18. Hawranek, D., Hesse, M., Jung, A., Pauly C., Sauga, M., Schulz, T., Traufetter, G. and Zand, B. *The New Age of Protectionism - Trump's Attack on Germany and the Global Economy*. 18.07.2017]; Available from: <http://www.spiegel.de/international/world/the-new-age-of-protectionism-trump-attacks-german-business-model-a-1132050.html>.
19. Katainen, J. and Bieńkowska, E. *Protectionism does not make Europe's industry stronger*. 2017 18.07.2017]; Available from: [https://ec.europa.eu/commission/commissioners/2014-2019/bienkowska/announcements/protectionism-does-not-make-europes-industry-stronger\\_en](https://ec.europa.eu/commission/commissioners/2014-2019/bienkowska/announcements/protectionism-does-not-make-europes-industry-stronger_en).

20. Tran, M. *EU trade reforms 'will hurt developing countries'*. 2012 18.07.2017]; Available from: <https://www.theguardian.com/global-development/2012/jul/27/eu-trade-reforms-developing-countries>.
21. Correlje, A. and van der Linde, C., *Energy supply security and geopolitics: A European perspective*. Energy Policy (2006), **34**: p. 532-543.
22. Asif, M. and Muneer, T., *Energy supply, its demand and security issues for developed and emerging economies*. Renewable & Sustainable Energy Reviews (2007), **11**: p. 1388-1413.
23. *Paris Agreement*. 18.07.2017]; Available from: [https://ec.europa.eu/clima/policies/international/negotiations/paris\\_en](https://ec.europa.eu/clima/policies/international/negotiations/paris_en).
24. Sorensen, P., Cutululis, N.A., Viguera-Rodriguez, A., Jensen, L.E., Hjerrild, J., Donovan, M.H., and Madsen, H., *Power fluctuations from large wind farms*. IEEE Transactions on Power Systems (2007), **22**: p. 958-965.
25. Luo, C.L., Banakar, H., Shen, B., and Ooi, B.T., *Strategies to smooth wind power fluctuations of wind turbine generator*. IEEE Transactions on Energy Conversion (2007), **22**: p. 341-349.
26. Marcos, J., Marroyo, L., Lorenzo, E., Alvira, D., and Izco, E., *Power output fluctuations in large scale PV plants: one year observations with one second resolution and a derived analytic model*. Progress in Photovoltaics (2011), **19**: p. 218-227.
27. Ahmed, N.A., Miyatake, M., and Al-Othman, A.K., *Power fluctuations suppression of stand-alone hybrid generation combining solar photovoltaic/wind turbine and fuel cell systems*. Energy Conversion and Management (2008), **49**: p. 2711-2719.
28. Züttel, A., Borgschulte, A., and Schlapbach, L., *Hydrogen as a future energy carrier*. 2011, Weinheim: John Wiley & Sons ISBN: 352762290X
29. *Nuclear explained - Nuclear power and the Environment*. 2017 18.07.2017]; Available from: [https://www.eia.gov/energyexplained/?page=nuclear\\_environment](https://www.eia.gov/energyexplained/?page=nuclear_environment).
30. Lenzen, M., *Life cycle energy and greenhouse gas emissions of nuclear energy: A review*. Energy Conversion and Management (2008), **49**: p. 2178-2199.
31. Sovacool, B.K., *Valuing the greenhouse gas emissions from nuclear power: A critical survey*. Energy Policy (2008), **36**: p. 2950-2963.
32. Cowley, S.C., *The quest for fusion power*. Nature Physics (2016), **12**: p. 384-386.
33. Verberck, B. and Bigot, B., *Building the way to fusion energy*. Nature Physics (2016), **12**: p. 395-397.
34. 2017 19.07.2017]; Available from: <https://www.agora-energiewende.de/en/topics/-agothem-/Produkt/produkt/76/Agorameter/>.
35. Borowy, B.S. and Salameh, Z.M., *Dynamic response of a stand-alone wind energy conversion system with battery energy storage to a wind gust*. IEEE Transactions on Energy Conversion (1997), **12**: p. 73-78.
36. Divya, K.C. and Ostergaard, J., *Battery energy storage technology for power systems- An overview*. Electric Power Systems Research (2009), **79**: p. 511-520.
37. Van Noorden, R., *The rechargeable revolution: A better battery*. Nature (2014), **507**: p. 26-8.
38. Rezvani, Z., Jansson, J., and Bodin, J., *Advances in consumer electric vehicle adoption research: A review and research agenda*. Transportation Research Part D-Transport and Environment (2015), **34**: p. 122-136.
39. Judd, R. and Pinchbeck, D., *Power to Gas Research Roadmap. Offering a solution to the energy storage problem*. Gas for energy (2013).

40. Yoshida, T. and Kojima, K., *Toyota MIRAI fuel cell vehicle and progress toward a future hydrogen society*. The Electrochemical Society Interface (2015), **24**: p. 45-49.
41. Bockris, J.O., *A hydrogen economy*. Science (1972), **176**: p. 1323.
42. Züttel, A., Remhof, A., Borgschulte, A., and Friedrichs, O., *Hydrogen: the future energy carrier*. Philos Trans A Math Phys Eng Sci (2010), **368**: p. 3329-42.
43. Bockris, J., *Energy: the solar-hydrogen alternative*. 1975, New York: Halsted Press, ISBN: 978-0470084298.
44. *H2 Mobility Wasserstoff tanken*. 2017 [18.07.2017]; Available from: <http://h2-mobility.de/>.
45. Dutta, S., *A review on production, storage of hydrogen and its utilization as an energy resource*. Journal of Industrial and Engineering Chemistry (2014), **20**: p. 1148-1156.
46. Ley, M.B., Jepsen, L.H., Lee, Y.S., Cho, Y.W., von Colbe, J.M.B., Dornheim, M., Rokni, M., Jensen, J.O., Sloth, M., Filinchuk, Y., Jorgensen, J.E., Besenbacher, F., and Jensen, T.R., *Complex hydrides for hydrogen storage - new perspectives*. Materials Today (2014), **17**: p. 122-128.
47. Bagotsky, V.S., *Fuel cells: problems and solutions*. Vol. 56. 2012, Hoboken: John Wiley & Sons. ISBN: 1118087569
48. Carrette, L., Friedrich, K.A., and Stimming, U., *Fuel Cells - Fundamentals and Applications*. Fuel Cells (2001), **1**: p. 5-39.
49. Vielstich, W., Lamm, A., Yokokawa, H., and Gasteiger, H.A., *Handbook of fuel cells: fundamentals technology and applications*. Vol. 2. 2009, Hoboken: John Wiley & Sons. ISBN: 0470723114
50. Sabatier, P., *Hydrogénations et déshydrogénations par catalyse*. Berichte der deutschen chemischen Gesellschaft (1911), **44**: p. 1984-2001.
51. Greeley, J., Stephens, I.E.L., Bondarenko, A.S., Johansson, T.P., Hansen, H.A., Jaramillo, T.F., Rossmeisl, J., Chorkendorff, I., and Norskov, J.K., *Alloys of platinum and early transition metals as oxygen reduction electrocatalysts*. Nature Chemistry (2009), **1**: p. 552-556.
52. Stephens, I.E.L., Bondarenko, A.S., Gronbjerg, U., Rossmeisl, J., and Chorkendorff, I., *Understanding the electrocatalysis of oxygen reduction on platinum and its alloys*. Energy & Environmental Science (2012), **5**: p. 6744-6762.
53. Calle-Vallejo, F., Martinez, J.I., Garcia-Lastra, J.M., Sautet, P., and Loffreda, D., *Fast prediction of adsorption properties for platinum nanocatalysts with generalized coordination numbers*. Angew Chem Int Ed Engl (2014), **53**: p. 8316-9.
54. Bandarenka, A.S., Hansen, H.A., Rossmeisl, J., and Stephens, I.E., *Elucidating the activity of stepped Pt single crystals for oxygen reduction*. Phys Chem Chem Phys (2014), **16**: p. 13625-9.
55. Arora, A. and Gambardella, A., *The Changing Technology of Technological-Change - General and Abstract Knowledge and the Division of Innovative Labor*. Research Policy (1994), **23**: p. 523-532.
56. Stamenkovic, V.R., Fowler, B., Mun, B.S., Wang, G., Ross, P.N., Lucas, C.A., and Markovic, N.M., *Improved oxygen reduction activity on Pt<sub>3</sub>Ni(111) via increased surface site availability*. Science (2007), **315**: p. 493-7.
57. Alkire, R.C., Bartlett, P.N., and Lipkowsky, J., *Nanopatterned and Nanoparticle-Modified Electrodes*. 2017, Hoboken: John Wiley & Sons. ISBN: 3527340920
58. Bandarenka, A.S., Ventosa, E., Maljusch, A., Masa, J., and Schuhmann, W., *Techniques and methodologies in modern electrocatalysis: evaluation of activity, selectivity and stability of catalytic materials*. Analyst (2014), **139**: p. 1274-91.

59. Calle-Vallejo, F., Tymoczko, J., Colic, V., Vu, Q.H., Pohl, M.D., Morgenstern, K., Loffreda, D., Sautet, P., Schuhmann, W., and Bandarenka, A.S., *Finding optimal surface sites on heterogeneous catalysts by counting nearest neighbors*. *Science* (2015), **350**: p. 185-9.
60. Stephens, I.E., Bondarenko, A.S., Perez-Alonso, F.J., Calle-Vallejo, F., Bech, L., Johansson, T.P., Jepsen, A.K., Frydendal, R., Knudsen, B.P., Rossmeisl, J., and Chorkendorff, I., *Tuning the activity of Pt(111) for oxygen electroreduction by subsurface alloying*. *J Am Chem Soc* (2011), **133**: p. 5485-91.
61. Čolić, V. and Bandarenka, A.S., *Pt Alloy Electrocatalysts for the Oxygen Reduction Reaction: From Model Surfaces to Nanostructured Systems*. *ACS Catalysis* (2016), **6**: p. 5378-5385.
62. Strasser, P., Koh, S., Anniyev, T., Greeley, J., More, K., Yu, C., Liu, Z., Kaya, S., Nordlund, D., Ogasawara, H., Toney, M.F., and Nilsson, A., *Lattice-strain control of the activity in dealloyed core-shell fuel cell catalysts*. *Nat Chem* (2010), **2**: p. 454-60.
63. Bligaard, T. and Norskov, J.K., *Ligand effects in heterogeneous catalysis and electrochemistry*. *Electrochimica Acta* (2007), **52**: p. 5512-5516.
64. Sachtler, W.M., *Ensemble and ligand effects in metal catalysis*. *Handbook of Heterogeneous Catalysis* (2008).
65. Gamboa-Aldeco, M.E., Herrero, E., Zelenay, P.S., and Wieckowski, A., *Adsorption of bisulfate anion on a Pt(100) electrode: A comparison with Pt(111) and Pt(poly)*. *Journal of Electroanalytical Chemistry* (1993), **348**: p. 451-457.
66. Kolics, A. and Wieckowski, A., *Adsorption of bisulfate and sulfate anions on a Pt(111) electrode*. *Journal of Physical Chemistry B* (2001), **105**: p. 2588-2595.
67. Strmcnik, D., Kodama, K., van der Vliet, D., Greeley, J., Stamenkovic, V.R., and Markovic, N.M., *The role of non-covalent interactions in electrocatalytic fuel-cell reactions on platinum*. *Nat Chem* (2009), **1**: p. 466-72.
68. Suntivich, J., Perry, E.E., Gasteiger, H.A., and Shao-Horn, Y., *The Influence of the Cation on the Oxygen Reduction and Evolution Activities of Oxide Surfaces in Alkaline Electrolyte*. *Electrocatalysis* (2013), **4**: p. 49-55.
69. Bond, G.C., *Heterogeneous catalysis*. 1987, New York: Oxford University Press. ISBN: 5847708 (OSTI)
70. Chorkendorff, I. and Niemantsverdriet, J., *Introduction to Catalysis. Concepts of Modern Catalysis and Kinetics*. 2003, Weinheim: Wiley-VCH. ISBN: 3527602658
71. Lindstrom, B. and Pettersson, L.J., *A brief history of catalysis*. *Cattech* (2003), **7**: p. 130-138.
72. Berzelius, J., *Quelques Idées sur une nouvelle Force agissant dans les Combinaisons des Corps Organiques*. *Ann. Chim* (1836), **61**: p. 146-151.
73. Ertl, G., Knözinger, H., and Weitkamp, J., *Handbook of heterogeneous catalysis*. 1997, Weinheim: Wiley-VCH. ISBN: 9783527610044
74. Erisman, J.W., Sutton, M.A., Galloway, J., Klimont, Z., and Winiwarter, W., *How a century of ammonia synthesis changed the world*. *Nature Geoscience* (2008), **1**: p. 636-639.
75. Debe, M.K., *Electrocatalyst approaches and challenges for automotive fuel cells*. *Nature* (2012), **486**: p. 43-51.
76. Appleby, A., *Electrocatalysis and fuel cells*. *Catalysis Reviews* (1971), **4**: p. 221-244.
77. Atkins, P.W. and De Paula, J., *Physikalische Chemie*. 2013, Weinheim: Wiley-VCH. ISBN: 3527332472
78. Sabatier, P. and Senderens, J., *Direct hydrogenation of oxides of carbon in presence of various finely divided metals*. *CR Acad Sci* (1902), **134**: p. 689-691.

79. Medford, A.J., Vojvodic, A., Hummelshoj, J.S., Voss, J., Abild-Pedersen, F., Studt, F., Bligaard, T., Nilsson, A., and Norskov, J.K., *From the Sabatier principle to a predictive theory of transition-metal heterogeneous catalysis*. *Journal of Catalysis* (2015), **328**: p. 36-42.
80. Abild-Pedersen, F., Greeley, J., Studt, F., Rossmeisl, J., Munter, T.R., Moses, P.G., Skulason, E., Bligaard, T., and Norskov, J.K., *Scaling properties of adsorption energies for hydrogen-containing molecules on transition-metal surfaces*. *Phys Rev Lett* (2007), **99**: p. 016105.
81. Calle-Vallejo, F., Martinez, J.I., Garcia-Lastra, J.M., Rossmeisl, J., and Koper, M.T.M., *Physical and Chemical Nature of the Scaling Relations between Adsorption Energies of Atoms on Metal Surfaces*. *Physical Review Letters* (2012), **108**: p. 116103.
82. Taylor, H.S., *A theory of the catalytic surface*. *Proceedings of the Royal Society of London. Series A, Containing Papers of a Mathematical and Physical Character* (1925), **108**: p. 105-111.
83. Hammer, B. and Norskov, J.K., *Why Gold Is the Noblest of All the Metals*. *Nature* (1995), **376**: p. 238-240.
84. Calle-Vallejo, F., Koper, M.T.M., and Bandarenka, A.S., *Tailoring the catalytic activity of electrodes with monolayer amounts of foreign metals*. *Chem Soc Rev* (2013), **42**: p. 5210-30.
85. Hoppe, R., *Die Koordinationszahl—ein „anorganisches Chamäleon“* □. *Angewandte Chemie* (1970), **82**: p. 7-16.
86. Burt, R., Birkett, G., and Zhao, X.S., *A review of molecular modelling of electric double layer capacitors*. *Phys Chem Chem Phys* (2014), **16**: p. 6519-38.
87. Kolb, M.J., Farber, R.G., Derouin, J., Badan, C., Calle-Vallejo, F., Juurlink, L.B., Killelea, D.R., and Koper, M.T., *Double-Stranded Water on Stepped Platinum Surfaces*. *Phys Rev Lett* (2016), **116**: p. 136101.
88. Stern, O., *Zur theorie der elektrolytischen doppelschicht*. *Berichte der Bunsengesellschaft für physikalische Chemie* (1924), **30**: p. 508-516.
89. Zhang, L.L. and Zhao, X.S., *Carbon-based materials as supercapacitor electrodes*. *Chemical Society Reviews* (2009), **38**: p. 2520-2531.
90. Bard, A.J., Faulkner, L.R., Leddy, J., and Zoski, C.G., *Electrochemical methods: fundamentals and applications*. Vol. 2. 1980, New York: Wiley ISBN: 9780471043720
91. Colic, V., Pohl, M.D., Scieszka, D., and Bandarenka, A.S., *Influence of the electrolyte composition on the activity and selectivity of electrocatalytic centers*. *Catalysis Today* (2016), **262**: p. 24-35.
92. Bicakova, O. and Straka, P., *Production of hydrogen from renewable resources and its effectiveness*. *International Journal of Hydrogen Energy* (2012), **37**: p. 11563-11578.
93. P. Herasymenko, I.S., *Z. Phys. Chem. A* (1930), **149**.
94. Lamoureux, G. and Roux, B., *Absolute hydration free energy scale for alkali and halide ions established from simulations with a polarizable force field*. *J Phys Chem B* (2006), **110**: p. 3308-22.
95. Stoffelsma, C., Rodriguez, P., Garcia, G., Garcia-Araez, N., Strmcnik, D., Markovic, N.M., and Koper, M.T.M., *Promotion of the Oxidation of Carbon Monoxide at Stepped Platinum Single-Crystal Electrodes in Alkaline Media by Lithium and Beryllium Cations*. *Journal of the American Chemical Society* (2010), **132**: p. 16127-16133.
96. Nakamura, M., Sato, N., Hoshi, N., and Sakata, O., *Outer Helmholtz Plane of the Electrical Double Layer Formed at the Solid Electrode-Liquid Interface*. *Chemphyschem* (2011), **12**: p. 1430-1434.

97. Katsounaros, I. and Mayrhofer, K.J., *The influence of non-covalent interactions on the hydrogen peroxide electrochemistry on platinum in alkaline electrolytes*. Chem Commun (Camb) (2012), **48**: p. 6660-2.
98. Tymoczko, J., Colic, V., Ganassin, A., Schuhmann, W., and Bandarenka, A.S., *Influence of the alkali metal cations on the activity of Pt(111) towards model electrocatalytic reactions in acidic sulfuric media*. Catalysis Today (2015), **244**: p. 96-102.
99. Pillay, D., Johannes, M.D., Garsany, Y., and Swider-Lyons, K.E., *Poisoning of Pt<sub>3</sub>Co Electrodes: A Combined Experimental and DFT Study*. Journal of Physical Chemistry C (2010), **114**: p. 7822-7830.
100. Omole, M.A., Okello, V.A., Lee, V., Zhou, L.S., Sadik, O.A., Umbach, C., and Sammakia, B., *Catalytic Reduction of Hexavalent Chromium Using Flexible Nanostructured Poly(amic acids)*. ACS Catalysis (2011), **1**: p. 139-146.
101. Froehlich, J.D. and Kubiak, C.P., *The Homogeneous Reduction of CO<sub>2</sub> by [Ni(cyclam)](+): Increased Catalytic Rates with the Addition of a CO Scavenger*. Journal of the American Chemical Society (2015), **137**: p. 3565-3573.
102. Sharma, H.N., Sharma, V., Mhadeshwar, A.B., and Ramprasad, R., *Why Pt Survives but Pd Suffers From SO<sub>x</sub> Poisoning?* The journal of physical chemistry letters (2015), **6**: p. 1140-1148.
103. Tymoczko, J., Calle-Vallejo, F., Colic, V., Koper, M.T.M., Schuhmann, W., and Bandarenka, A.S., *Oxygen Reduction at a Cu-Modified Pt(111) Model Electrocatalyst in Contact with Nafion Polymer*. ACS Catalysis (2014), **4**: p. 3772-3778.
104. Tymoczko, J., Schuhmann, W., and Bandarenka, A.S., *Position of Cu Atoms at the Pt(111) Electrode Surfaces Controls Electrosorption of (H)SO<sub>4</sub>(<sup>2-</sup>) from H<sub>2</sub>SO<sub>4</sub> Electrolytes*. Chemelectrochem (2014), **1**: p. 213-219.
105. Ganassin, A., Colic, V., Tymoczko, J., Bandarenka, A.S., and Schuhmann, W., *Non-covalent interactions in water electrolysis: influence on the activity of Pt(111) and iridium oxide catalysts in acidic media*. Phys Chem Chem Phys (2015), **17**: p. 8349-55.
106. Prieto, F., Navarro, I., and Rueda, M., *Impedance analysis of the mechanism for nitromethane reduction in aqueous solutions: The influence of pH*. Journal of Physical Chemistry (1996), **100**: p. 16346-16355.
107. Takashima, T., Hashimoto, K., and Nakamura, R., *Mechanisms of pH-dependent activity for water oxidation to molecular oxygen by MnO<sub>2</sub> electrocatalysts*. J Am Chem Soc (2012), **134**: p. 1519-27.
108. Blizanac, B.B., Lucas, C.A., Gallagher, M.E., Arenz, M., Ross, P.N., and Markovic, N.M., *Anion adsorption, CO oxidation, and oxygen reduction reaction on a Au(100) surface: The pH effect*. Journal of Physical Chemistry B (2004), **108**: p. 625-634.
109. Zhong, Y.Q., Ueno, K., Mori, Y., Oshikiri, T., and Misawa, H., *Cocatalyst Effects on Hydrogen Evolution in a Plasmon-Induced Water-Splitting System*. Journal of Physical Chemistry C (2015), **119**: p. 8889-8897.
110. Tarasevich, M.R. and Korchagin, O.V., *Electrocatalysis and pH (a review)*. Russian Journal of Electrochemistry (2013), **49**: p. 600-618.
111. Murphy, B.J., Sargent, F., and Armstrong, F.A., *Transforming an oxygen-tolerant [NiFe] uptake hydrogenase into a proficient, reversible hydrogen producer*. Energy & Environmental Science (2014), **7**: p. 1426-1433.
112. Bockris, J.O. and Parsons, R., *The Kinetics of the Hydrogen Evolution Reaction at Mercury Cathodes - the Effect of Temperature, Ph, and Pressure on Hydrogen Overpotential in Aqueous, Mixed and Methanolic Solutions*. Transactions of the Faraday Society (1949), **45**: p. 916-928.

113. Zeng, M. and Li, Y.G., *Recent advances in heterogeneous electrocatalysts for the hydrogen evolution reaction*. Journal of Materials Chemistry A (2015), **3**: p. 14942-14962.
114. Rostrup-Nielsen, J.R. and Rostrup-Nielsen, T., *Large-scale hydrogen production*. Cattech (2002), **6**: p. 150-159.
115. Esposito, D.V. and Chen, J.G., *Monolayer platinum supported on tungsten carbides as low-cost electrocatalysts: opportunities and limitations*. Energy & Environmental Science (2011), **4**: p. 3900-3912.
116. Esposito, D.V., Hunt, S.T., Stottlemeyer, A.L., Dobson, K.D., McCandless, B.E., Birkmire, R.W., and Chen, J.G., *Low-Cost Hydrogen-Evolution Catalysts Based on Monolayer Platinum on Tungsten Monocarbide Substrates*. Angewandte Chemie International Edition (2010), **49**: p. 9859-9862.
117. Esposito, D.V., Hunt, S.T., Kimmel, Y.C., and Chen, J.G., *A new class of electrocatalysts for hydrogen production from water electrolysis: metal monolayers supported on low-cost transition metal carbides*. Journal of the American Chemical Society (2012), **134**: p. 3025-3033.
118. Kelly, T.G., Lee, K.X., and Chen, J.G., *Pt-modified molybdenum carbide for the hydrogen evolution reaction: From model surfaces to powder electrocatalysts*. Journal of Power Sources (2014), **271**: p. 76-81.
119. Greeley, J., Jaramillo, T.F., Bonde, J., Chorkendorff, I.B., and Norskov, J.K., *Computational high-throughput screening of electrocatalytic materials for hydrogen evolution*. Nat Mater (2006), **5**: p. 909-13.
120. Santos, D.M., Sequeira, C.A., and Figueiredo, J.L., *Hydrogen production by alkaline water electrolysis*. Química Nova (2013), **36**: p. 1176-1193.
121. Rommal, H. and Morgan, P., *The Role of Absorbed Hydrogen on the Voltage-Time Behavior of Nickel Cathodes in Hydrogen Evolution*. Journal of The Electrochemical Society (1988), **135**: p. 343-346.
122. Soares, D., Teschke, O., and Torriani, I., *Hydride effect on the kinetics of the hydrogen evolution reaction on nickel cathodes in alkaline media*. Journal of The Electrochemical Society (1992), **139**: p. 98-105.
123. Lohrberg, K. and Kohl, P., *Preparation and use of Raney-Ni activated cathodes for large scale hydrogen production*. Electrochimica Acta (1984), **29**: p. 1557-1561.
124. Los, P., Rami, A., and Lasia, A., *Hydrogen evolution reaction on Ni-Al electrodes*. Journal of applied electrochemistry (1993), **23**: p. 135-140.
125. Raj, I.A. and Vasu, K., *Transition metal-based hydrogen electrodes in alkaline solution—electrocatalysis on nickel based binary alloy coatings*. Journal of applied electrochemistry (1990), **20**: p. 32-38.
126. Subbaraman, R., Tripkovic, D., Strmcnik, D., Chang, K.-C., Uchimura, M., Paulikas, A.P., Stamenkovic, V., and Markovic, N.M., *Enhancing hydrogen evolution activity in water splitting by tailoring Li<sup>+</sup>-Ni(OH)<sub>2</sub>-Pt interfaces*. Science (2011), **334**: p. 1256-1260.
127. Danilovic, N., Subbaraman, R., Strmcnik, D., Chang, K.C., Paulikas, A., Stamenkovic, V., and Markovic, N.M., *Enhancing the alkaline hydrogen evolution reaction activity through the bifunctionality of Ni(OH)<sub>2</sub>/metal catalysts*. Angewandte Chemie (2012), **124**: p. 12663-12666.
128. Deng, J., Ren, P., Deng, D., and Bao, X., *Enhanced electron penetration through an ultrathin graphene layer for highly efficient catalysis of the hydrogen evolution reaction*. Angewandte Chemie International Edition (2015), **54**: p. 2100-2104.

129. Tavakkoli, M., Kallio, T., Reynaud, O., Nasibulin, A.G., Johans, C., Sainio, J., Jiang, H., Kauppinen, E.I., and Laasonen, K., *Single-Shell Carbon-Encapsulated Iron Nanoparticles: Synthesis and High Electrocatalytic Activity for Hydrogen Evolution Reaction*. *Angewandte Chemie* (2015), **127**: p. 4618-4621.
130. Morales-Guio, C.G., Stern, L.-A., and Hu, X., *Nanostructured hydrotreating catalysts for electrochemical hydrogen evolution*. *Chemical Society Reviews* (2014), **43**: p. 6555-6569.
131. Merki, D. and Hu, X., *Recent developments of molybdenum and tungsten sulfides as hydrogen evolution catalysts*. *Energy & Environmental Science* (2011), **4**: p. 3878-3888.
132. Laursen, A.B., Kegnæs, S., Dahl, S., and Chorkendorff, I., *Molybdenum sulfides—efficient and viable materials for electro-and photoelectrocatalytic hydrogen evolution*. *Energy & Environmental Science* (2012), **5**: p. 5577-5591.
133. Yan, Y., Xia, B., Xu, Z., and Wang, X., *Recent development of molybdenum sulfides as advanced electrocatalysts for hydrogen evolution reaction*. *Acs Catalysis* (2014), **4**: p. 1693-1705.
134. Chhowalla, M., Shin, H.S., Eda, G., Li, L.-J., Loh, K.P., and Zhang, H., *The chemistry of two-dimensional layered transition metal dichalcogenide nanosheets*. *Nature chemistry* (2013), **5**: p. 263-275.
135. Tributsch, H. and Bennett, J., *Electrochemistry and photochemistry of MoS<sub>2</sub> layer crystals. I*. *Journal of Electroanalytical Chemistry and Interfacial Electrochemistry* (1977), **81**: p. 97-111.
136. Hinnemann, B., Moses, P.G., Bonde, J., Jørgensen, K.P., Nielsen, J.H., Horch, S., Chorkendorff, I., and Nørskov, J.K., *Biomimetic hydrogen evolution: MoS<sub>2</sub> nanoparticles as catalyst for hydrogen evolution*. *Journal of the American Chemical Society* (2005), **127**: p. 5308-5309.
137. Jaramillo, T.F., Jorgensen, K.P., Bonde, J., Nielsen, J.H., Horch, S., and Chorkendorff, I., *Identification of active edge sites for electrochemical H<sub>2</sub> evolution from MoS<sub>2</sub> nanocatalysts*. *Science* (2007), **317**: p. 100-2.
138. Tenne, R. and Redlich, M., *Recent progress in the research of inorganic fullerene-like nanoparticles and inorganic nanotubes*. *Chemical Society Reviews* (2010), **39**: p. 1423-1434.
139. Margulis, L., Salitra, G., Tenne, R., and Tallanker, M., *Nested fullerene-like structures*. *Nature* (1993), **365**: p. 113-114.
140. Kibsgaard, J., Chen, Z., Reinecke, B.N., and Jaramillo, T.F., *Engineering the surface structure of MoS<sub>2</sub> to preferentially expose active edge sites for electrocatalysis*. *Nature materials* (2012), **11**: p. 963.
141. Xie, J., Zhang, H., Li, S., Wang, R., Sun, X., Zhou, M., Zhou, J., Lou, X.W.D., and Xie, Y., *Defect-rich MoS<sub>2</sub> ultrathin nanosheets with additional active edge sites for enhanced electrocatalytic hydrogen evolution*. *Advanced materials* (2013), **25**: p. 5807-5813.
142. Kong, D., Wang, H., Cha, J.J., Pasta, M., Koski, K.J., Yao, J., and Cui, Y., *Synthesis of MoS<sub>2</sub> and MoSe<sub>2</sub> films with vertically aligned layers*. *Nano letters* (2013), **13**: p. 1341-1347.
143. Li, Y., Wang, H., Xie, L., Liang, Y., Hong, G., and Dai, H., *MoS<sub>2</sub> nanoparticles grown on graphene: an advanced catalyst for the hydrogen evolution reaction*. *Journal of the American Chemical Society* (2011), **133**: p. 7296-7299.

144. Brorson, M., Carlsson, A., and Topsøe, H., *The morphology of MoS<sub>2</sub>, WS<sub>2</sub>, Co–Mo–S, Ni–Mo–S and Ni–W–S nanoclusters in hydrodesulfurization catalysts revealed by HAADF-STEM*. *Catalysis today* (2007), **123**: p. 31-36.
145. Bonde, J., Moses, P.G., Jaramillo, T.F., Nørskov, J.K., and Chorkendorff, I., *Hydrogen evolution on nano-particulate transition metal sulfides*. *Faraday discussions* (2009), **140**: p. 219-231.
146. Tsai, C., Chan, K., Abild-Pedersen, F., and Nørskov, J.K., *Active edge sites in MoSe<sub>2</sub> and WSe<sub>2</sub> catalysts for the hydrogen evolution reaction: a density functional study*. *Physical Chemistry Chemical Physics* (2014), **16**: p. 13156-13164.
147. Faber, M.S., Lukowski, M.A., Ding, Q., Kaiser, N.S., and Jin, S., *Earth-abundant metal pyrites (FeS<sub>2</sub>, CoS<sub>2</sub>, NiS<sub>2</sub>, and their alloys) for highly efficient hydrogen evolution and polysulfide reduction electrocatalysis*. *The Journal of Physical Chemistry C* (2014), **118**: p. 21347-21356.
148. Faber, M.S., Dzedzic, R., Lukowski, M.A., Kaiser, N.S., Ding, Q., and Jin, S., *High-performance electrocatalysis using metallic cobalt pyrite (CoS<sub>2</sub>) micro- and nanostructures*. *Journal of the American Chemical Society* (2014), **136**: p. 10053-10061.
149. Carim, A.I., Saadi, F.H., Soriaga, M.P., and Lewis, N.S., *Electrocatalysis of the hydrogen-evolution reaction by electrodeposited amorphous cobalt selenide films*. *Journal of Materials Chemistry A* (2014), **2**: p. 13835-13839.
150. Peng, S., Li, L., Han, X., Sun, W., Srinivasan, M., Mhaisalkar, S.G., Cheng, F., Yan, Q., Chen, J., and Ramakrishna, S., *Cobalt sulfide nanosheet/graphene/carbon nanotube nanocomposites as flexible electrodes for hydrogen evolution*. *Angewandte Chemie International Edition* (2014), **53**: p. 12594-12599.
151. Zhang, H., Yang, B., Wu, X., Li, Z., Lei, L., and Zhang, X., *Polymorphic CoSe<sub>2</sub> with mixed orthorhombic and cubic phases for highly efficient hydrogen evolution reaction*. *ACS applied materials & interfaces* (2015), **7**: p. 1772-1779.
152. Chen, W.-F., Muckerman, J.T., and Fujita, E., *Recent developments in transition metal carbides and nitrides as hydrogen evolution electrocatalysts*. *Chemical Communications* (2013), **49**: p. 8896-8909.
153. Kitchin, J.R., Nørskov, J.K., Barteau, M.A., and Chen, J.G., *Trends in the chemical properties of early transition metal carbide surfaces: A density functional study*. *Catalysis Today* (2005), **105**: p. 66-73.
154. Chen, J.G., *Carbide and nitride overlayers on early transition metal surfaces: preparation, characterization, and reactivities*. *Chemical reviews* (1996), **96**: p. 1477-1498.
155. Levy, R. and Boudart, M., *Platinum-like behavior of tungsten carbide in surface catalysis*. *science* (1973), **181**: p. 547-549.
156. Stottlemeyer, A.L., Weigert, E.C., and Chen, J.G., *Tungsten carbides as alternative electrocatalysts: from surface science studies to fuel cell evaluation*. *Industrial & Engineering Chemistry Research* (2010), **50**: p. 16-22.
157. Garcia-Esparza, A.T., Cha, D., Ou, Y., Kubota, J., Domen, K., and Takahashi, K., *Tungsten carbide nanoparticles as efficient cocatalysts for photocatalytic overall water splitting*. *ChemSusChem* (2013), **6**: p. 168-181.
158. Hunt, S.T., Nimmanwudipong, T., and Román-Leshkov, Y., *Engineering Non-sintered, Metal-Terminated Tungsten Carbide Nanoparticles for Catalysis*. *Angewandte Chemie International Edition* (2014), **53**: p. 5131-5136.

159. Lavrenko, V., Yagupol'skaya, L., and Kuznetsova, L., *Kinetics of electrolytic hydrogen evolution at some transition metal borides*. *Ehlektrokhimiya* (1974), **10**: p. 1078-1081.
160. Los, P. and Lasia, A., *Electrocatalytic properties of amorphous nickel boride electrodes for hydrogen evolution reaction in alkaline solution*. *Journal of Electroanalytical Chemistry* (1992), **333**: p. 115-125.
161. Adan, C., Perez-Alonso, F., Rojas, S., Pena, M., and Fierro, J., *Enhancement of electrocatalytic activity towards hydrogen evolution reaction by boron-modified nickel nanoparticles*. *international journal of hydrogen energy* (2012), **37**: p. 14984-14991.
162. Ndzebet, E. and Savadogo, O., *The hydrogen evolution reaction in 3M KOH on nickel boride electrodeposited with and without SiW12O404-*. *International journal of hydrogen energy* (1994), **19**: p. 687-691.
163. Borodzinski, J. and Lasia, A., *Electrocatalytic properties of doped nickel boride based electrodes for the hydrogen evolution reaction*. *Journal of applied electrochemistry* (1994), **24**: p. 1267-1275.
164. Oyama, S.T., Gott, T., Zhao, H.Y., and Lee, Y.K., *Transition metal phosphide hydroprocessing catalysts: A review*. *Catalysis Today* (2009), **143**: p. 94-107.
165. Alexander, A.M. and Hargreaves, J.S., *Alternative catalytic materials: carbides, nitrides, phosphides and amorphous boron alloys*. *Chem Soc Rev* (2010), **39**: p. 4388-401.
166. Daems, N., Sheng, X., Vankelecom, I.F.J., and Pescarmona, P.P., *Metal-free doped carbon materials as electrocatalysts for the oxygen reduction reaction*. *Journal of Materials Chemistry A* (2014), **2**: p. 4085-4110.
167. Zheng, Y., Jiao, Y., Li, L.H., Xing, T., Chen, Y., Jaroniec, M., and Qiao, S.Z., *Toward design of synergistically active carbon-based catalysts for electrocatalytic hydrogen evolution*. *ACS Nano* (2014), **8**: p. 5290-6.
168. Ito, Y., Cong, W., Fujita, T., Tang, Z., and Chen, M., *High catalytic activity of nitrogen and sulfur co-doped nanoporous graphene in the hydrogen evolution reaction*. *Angew Chem Int Ed Engl* (2015), **54**: p. 2131-6.
169. Cui, W., Liu, Q., Cheng, N., Asiri, A.M., and Sun, X., *Activated carbon nanotubes: a highly-active metal-free electrocatalyst for hydrogen evolution reaction*. *Chem Commun (Camb)* (2014), **50**: p. 9340-2.
170. Li, Y., Zhou, W., Wang, H., Xie, L., Liang, Y., Wei, F., Idrobo, J.C., Pennycook, S.J., and Dai, H., *An oxygen reduction electrocatalyst based on carbon nanotube-graphene complexes*. *Nat Nanotechnol* (2012), **7**: p. 394-400.
171. Li, Y. and Dai, H., *Recent advances in zinc-air batteries*. *Chem Soc Rev* (2014), **43**: p. 5257-75.
172. Shalom, M., Gimenez, S., Schipper, F., Herraiz-Cardona, I., Bisquert, J., and Antonietti, M., *Controlled carbon nitride growth on surfaces for hydrogen evolution electrodes*. *Angew Chem Int Ed Engl* (2014), **53**: p. 3654-8.
173. Zheng, Y., Jiao, Y., Zhu, Y., Li, L.H., Han, Y., Chen, Y., Du, A., Jaroniec, M., and Qiao, S.Z., *Hydrogen evolution by a metal-free electrocatalyst*. *Nat Commun* (2014), **5**: p. 3783.
174. Nørskov, J.K., Rossmeisl, J., Logadottir, A., Lindqvist, L., Kitchin, J.R., Bligaard, T., and Jónsson, H., *Origin of the Overpotential for Oxygen Reduction at a Fuel-Cell Cathode*. *The Journal of Physical Chemistry B* (2004), **108**: p. 17886-17892.
175. Lee, I., Delbecq, F., Morales, R., Albitter, M.A., and Zaera, F., *Tuning selectivity in catalysis by controlling particle shape*. *Nat Mater* (2009), **8**: p. 132-8.
176. Viswanathan, V., Hansen, H.A., Rossmeisl, J., and Nørskov, J.K., *Universality in Oxygen Reduction Electrocatalysis on Metal Surfaces*. *Acs Catalysis* (2012), **2**: p. 1654-1660.

177. Vojvodic, A. and Norskov, J.K., *New design paradigm for heterogeneous catalysts*. National Science Review (2015), **2**: p. 140-143.
178. Bockris, R. and John, O., 'M., *Volume 1: Modern Electrochemistry, edited by JO Bockris*. 1998, Springer US.
179. Ge, X.M., Sumboja, A., Wu, D., An, T., Li, B., Goh, F.W.T., Hor, T.S.A., Zong, Y., and Liu, Z.L., *Oxygen Reduction in Alkaline Media: From Mechanisms to Recent Advances of Catalysts*. Acs Catalysis (2015), **5**: p. 4643-4667.
180. Anastasijević, N., Vesović, V., and Adžić, R., *Determination of the kinetic parameters of the oxygen reduction reaction using the rotating ring-disk electrode: Part I. Theory*. Journal of electroanalytical chemistry and interfacial electrochemistry (1987), **229**: p. 305-316.
181. Seh, Z.W., Kibsgaard, J., Dickens, C.F., Chorkendorff, I., Norskov, J.K., and Jaramillo, T.F., *Combining theory and experiment in electrocatalysis: Insights into materials design*. Science (2017), **355**.
182. Markovic, N.M., Adzic, R.R., Cahan, B.D., and Yeager, E.B., *Structural Effects in Electrocatalysis - Oxygen Reduction on Platinum Low-Index Single-Crystal Surfaces in Perchloric-Acid Solutions*. Journal of Electroanalytical Chemistry (1994), **377**: p. 249-259.
183. Chen, Z., Waje, M., Li, W., and Yan, Y., *Supportless Pt and PtPd Nanotubes as Electrocatalysts for Oxygen-Reduction Reactions*. Angewandte Chemie International Edition (2007), **46**: p. 4060-4063.
184. Zhang, L., Roling, L.T., Wang, X., Vara, M., Chi, M., Liu, J., Choi, S.I., Park, J., Herron, J.A., Xie, Z., Mavrikakis, M., and Xia, Y., *NANOCATALYSTS. Platinum-based nanocages with subnanometer-thick walls and well-defined, controllable facets*. Science (2015), **349**: p. 412-6.
185. Wang, C., Daimon, H., Lee, Y., Kim, J., and Sun, S., *Synthesis of monodisperse Pt nanocubes and their enhanced catalysis for oxygen reduction*. Journal of the American Chemical Society (2007), **129**: p. 6974-+.
186. Stamenkovic, V., Mun, B.S., Mayrhofer, K.J., Ross, P.N., Markovic, N.M., Rossmeisl, J., Greeley, J., and Norskov, J.K., *Changing the activity of electrocatalysts for oxygen reduction by tuning the surface electronic structure*. Angew Chem Int Ed Engl (2006), **45**: p. 2897-901.
187. Stamenkovic, V.R., Mun, B.S., Arenz, M., Mayrhofer, K.J., Lucas, C.A., Wang, G., Ross, P.N., and Markovic, N.M., *Trends in electrocatalysis on extended and nanoscale Pt-bimetallic alloy surfaces*. Nat Mater (2007), **6**: p. 241-7.
188. Escudero-Escribano, M., Malacrida, P., Hansen, M.H., Vej-Hansen, U.G., Velazquez-Palenzuela, A., Tripkovic, V., Schiotz, J., Rossmeisl, J., Stephens, I.E., and Chorkendorff, I., *Tuning the activity of Pt alloy electrocatalysts by means of the lanthanide contraction*. Science (2016), **352**: p. 73-6.
189. Calle-Vallejo, F., Pohl, M.D., Reinisch, D., Loffreda, D., Sautet, P., and Bandarenka, A.S., *Why conclusions from platinum model surfaces do not necessarily lead to enhanced nanoparticle catalysts for the oxygen reduction reaction*. Chemical Science (2017), **8**: p. 2283-2289.
190. Shao, M., Chang, Q., Dodelet, J.P., and Chenitz, R., *Recent Advances in Electrocatalysts for Oxygen Reduction Reaction*. Chem Rev (2016), **116**: p. 3594-657.
191. Shao, M., *Palladium-based electrocatalysts for hydrogen oxidation and oxygen reduction reactions*. Journal of Power Sources (2011), **196**: p. 2433-2444.

192. Kondo, S., Nakamura, M., Maki, N., and Hoshi, N., *Active Sites for the Oxygen Reduction Reaction on the Low and High Index Planes of Palladium*. Journal of Physical Chemistry C (2009), **113**: p. 12625-12628.
193. Shao, M., Yu, T., Odell, J.H., Jin, M., and Xia, Y., *Structural dependence of oxygen reduction reaction on palladium nanocrystals*. Chem Commun (Camb) (2011), **47**: p. 6566-8.
194. Yan, Y., Zhan, F., Du, J., Jiang, Y., Jin, C., Fu, M., Zhang, H., and Yang, D., *Kinetically-controlled growth of cubic and octahedral Rh-Pd alloy oxygen reduction electrocatalysts with high activity and durability*. Nanoscale (2015), **7**: p. 301-7.
195. Pires, F.I. and Villullas, H.M., *Pd-based catalysts: Influence of the second metal on their stability and oxygen reduction activity*. International Journal of Hydrogen Energy (2012), **37**: p. 17052-17059.
196. Savadogo, O., Lee, K., Oishi, K., Mitsushima, S., Kamiya, N., and Ota, K.-I., *New palladium alloys catalyst for the oxygen reduction reaction in an acid medium*. Electrochemistry communications (2004), **6**: p. 105-109.
197. Son, J., Cho, S., Lee, C., Lee, Y., and Shim, J.H., *Spongelike nanoporous Pd and Pd/Au structures: facile synthesis and enhanced electrocatalytic activity*. Langmuir (2014), **30**: p. 3579-88.
198. Xiong, L., Huang, Y.X., Liu, X.W., Sheng, G.P., Li, W.W., and Yu, H.Q., *Three-dimensional bimetallic Pd-Cu nanodendrites with superior electrochemical performance for oxygen reduction reaction*. Electrochimica Acta (2013), **89**: p. 24-28.
199. Ishihara, A., Ohgi, Y., Matsuzawa, K., Mitsushima, S., and Ota, K., *Progress in non-precious metal oxide-based cathode for polymer electrolyte fuel cells*. Electrochimica Acta (2010), **55**: p. 8005-8012.
200. Ota, K.-i. and Ishihara, A., *Metal Oxide-based compounds as electrocatalysts for Oxygen reduction reaction*, in *Electrocatalysis in Fuel Cells*. 2013, Springer. p. 391-416.
201. Ota, K., Ohgi, Y., Nam, K.D., Matsuzawa, K., Mitsushima, S., and Ishihara, A., *Development of group 4 and 5 metal oxide-based cathodes for polymer electrolyte fuel cell*. Journal of Power Sources (2011), **196**: p. 5256-5263.
202. Ishihara, A., Imai, H., and Ota, K.i., *Transition Metal Oxides, Carbides, Nitrides, Oxynitrides, and Carbonitrides for O<sub>2</sub> Reduction Reaction Electrocatalysts for Acid PEM Fuel Cells*. Non-Noble Metal Fuel Cell Catalysts (2014): p. 183-204.
203. Asahi, R., Morikawa, T., Ohwaki, T., Aoki, K., and Taga, Y., *Visible-light photocatalysis in nitrogen-doped titanium oxides*. Science (2001), **293**: p. 269-71.
204. Fang, C.M., Orhan, E., de Wijs, G.A., Hintzen, H.T., de Groot, R.A., Marchand, R., Saillard, J.Y., and de With, G., *The electronic structure of tantalum (oxy)nitrides TaON and Ta<sub>3</sub>N<sub>5</sub>*. Journal of Materials Chemistry (2001), **11**: p. 1248-1252.
205. Maekawa, Y., Ishihara, A., Kim, J.H., Mitsushima, S., and Ota, K.I., *Catalytic activity of zirconium oxynitride prepared by reactive sputtering for ORR in sulfuric acid*. Electrochemical and Solid State Letters (2008), **11**: p. B109-B112.
206. Easton, E.B., Bonakdarpour, A., Yang, R., Stevens, D.A., and Dahn, J.R., *Magnetron sputtered Fe-C-N, Fe-C, and C-N based oxygen reduction electrocatalysts*. Journal of the Electrochemical Society (2008), **155**: p. B547-B557.
207. Yang, R.Z., Bonakdarpour, A., Easton, E.B., Stoffyn-Egli, P., and Dahn, J.R., *Co-C-N oxygen reduction catalysts prepared by combinatorial magnetron sputter deposition*. Journal of the Electrochemical Society (2007), **154**: p. A275-A282.

208. Kim, J.-H., Ishihara, A., Mitsushima, S., Kamiya, N., and Ota, K.-i., *Oxygen reduction reaction of Cr-CN prepared using reactive sputtering with heat treatment*. Chem. Lett (2007), **36**: p. 514-515.
209. Kim, J.-H., Ishihara, A., Mitsushima, S., Kamiya, N., and Ota, K.-i., *Oxygen reduction reaction of Ta-CN prepared by reactive sputtering with heat treatment*. Electrochemistry (2007), **75**: p. 166-168.
210. Chao, Y.S., Tsai, D.S., Wu, A.P., Tseng, L.W., and Huang, Y.S., *Cobalt selenide electrocatalyst supported by nitrogen-doped carbon and its stable activity toward oxygen reduction reaction*. International Journal of Hydrogen Energy (2013), **38**: p. 5655-5664.
211. Higgins, D.C., Hassan, F.M., Seo, M.H., Choi, J.Y., Hoque, M.A., Lee, D.U., and Chen, Z., *Shape-controlled octahedral cobalt disulfide nanoparticles supported on nitrogen and sulfur-doped graphene/carbon nanotube composites for oxygen reduction in acidic electrolyte*. Journal of Materials Chemistry A (2015), **3**: p. 6340-6350.
212. Zheng, Q., Cheng, X., Jao, T.-C., Weng, F.-B., Su, A., and Chiang, Y.-C., *Microwave assisted synthesis of high performance Ru 85 Se 15/MWCNTs cathode catalysts for PEM fuel cell applications*. international journal of hydrogen energy (2011), **36**: p. 14599-14607.
213. Liu, G., Zhang, H., and Hu, J., *Novel synthesis of a highly active carbon-supported Ru 85 Se 15 chalcogenide catalyst for the oxygen reduction reaction*. Electrochemistry Communications (2007), **9**: p. 2643-2648.
214. Babu, P.K., Lewera, A., Chung, J.H., Hunger, R., Jaegermann, W., Alonso-Vante, N., Wieckowski, A., and Oldfield, E., *Selenium becomes metallic in Ru-Se fuel cell catalysts: an EC-NMR and XPS investigation*. J Am Chem Soc (2007), **129**: p. 15140-1.
215. Alonso-Vante, N., Malakhov, I.V., Nikitenko, S.G., Savinova, E.R., and Kochubey, D.I., *The structure analysis of the active centers of Ru-containing electrocatalysts for the oxygen reduction. An in situ EXAFS study*. Electrochimica Acta (2002), **47**: p. 3807-3814.
216. Malakhov, I.V., Nikitenko, S.G., Savinova, E.R., Kochubey, D.I., and Alonso-Vante, N., *In situ EXAFS study to probe active centers of Ru chalcogenide electrocatalysts during oxygen reduction reaction*. Journal of Physical Chemistry B (2002), **106**: p. 1670-1676.
217. Cao, D.X., Wieckowski, A., Inukai, J., and Alonso-Vante, N., *Oxygen reduction reaction on ruthenium and rhodium nanoparticles modified with selenium and sulfur*. Journal of the Electrochemical Society (2006), **153**: p. A869-A874.
218. Ma, J.Y., Ai, D.S., Xie, X.F., and Guo, J.W., *Novel methanol-tolerant Ir-S/C chalcogenide electrocatalysts for oxygen reduction in DMFC fuel cell*. Particuology (2011), **9**: p. 155-160.
219. Baresel, D., Sarholz, W., Scharner, P., and Schmitz, J., *Transition-Metal Chalcogenides as Oxygen Catalysts for Fuel-Cells*. Berichte Der Bunsen-Gesellschaft-Physical Chemistry Chemical Physics (1974), **78**: p. 608-611.
220. Feng, Y., He, T., and Alonso-Vante, N., *In situ free-surfactant synthesis and ORR-electrochemistry of carbon-supported Co<sub>3</sub>S<sub>4</sub> and CoSe<sub>2</sub> nanoparticles*. Chemistry of Materials (2007), **20**: p. 26-28.
221. Liu, G. and Zhang, H., *Facile synthesis of carbon-supported Ir<sub>x</sub>Se<sub>y</sub> chalcogenide nanoparticles and their electrocatalytic activity for the oxygen reduction reaction*. The Journal of Physical Chemistry C (2008), **112**: p. 2058-2065.

222. Behret, H., Binder, H., and Sandstede, G., *Electrocatalytic oxygen reduction with thiospinels and other sulphides of transition metals*. *Electrochimica Acta* (1975), **20**: p. 111-117.
223. Vesborg, P.C.K. and Jaramillo, T.F., *Addressing the terawatt challenge: scalability in the supply of chemical elements for renewable energy*. *Rsc Advances* (2012), **2**: p. 7933-7947.
224. Jaouen, F., Proietti, E., Lefevre, M., Chenitz, R., Dodelet, J.P., Wu, G., Chung, H.T., Johnston, C.M., and Zelenay, P., *Recent advances in non-precious metal catalysis for oxygen-reduction reaction in polymer electrolyte fuel cells*. *Energy & Environmental Science* (2011), **4**: p. 114-130.
225. Bezerra, C.W.B., Zhang, L., Lee, K.C., Liu, H.S., Marques, A.L.B., Marques, E.P., Wang, H.J., and Zhang, J.J., *A review of Fe-N/C and Co-N/C catalysts for the oxygen reduction reaction*. *Electrochimica Acta* (2008), **53**: p. 4937-4951.
226. Koper, M.T., *Structure sensitivity and nanoscale effects in electrocatalysis*. *Nanoscale* (2011), **3**: p. 2054-73.
227. Bandarenka, A.S., Varela, A.S., Karamad, M., Calle-Vallejo, F., Bech, L., Perez-Alonso, F.J., Rossmeisl, J., Stephens, I.E.L., and Chorkendorff, I., *Design of an Active Site towards Optimal Electrocatalysis: Overlayers, Surface Alloys and Near-Surface Alloys of Cu/Pt(111)*. *Angewandte Chemie International Edition* (2012), **51**: p. 11845-11848.
228. Ehteshami, S.M.M. and Chan, S.H., *A review of electrocatalysts with enhanced CO tolerance and stability for polymer electrolyte membrane fuel cells*. *Electrochimica Acta* (2013), **93**: p. 334-345.
229. Pohl, M.D., Colic, V., Scieszka, D., and Bandarenka, A.S., *Elucidation of adsorption processes at the surface of Pt(331) model electrocatalysts in acidic aqueous media*. *Physical Chemistry Chemical Physics* (2016), **18**: p. 10792-10799.
230. Tian, B., *Preparation and characterization of iron oxide electrode materials for lithium-ion batteries by electrochemical and spectroscopic (XPS, ToF-SIMS) methods*. 2014, Université Pierre et Marie Curie-Paris VI.
231. Reinisch, D., *Influence of Alkali Metal Cations on the Activity of Model Pt Electrocatalysts towards the Oxygen Reduction Reaction*, in *Physics of Energy Conversion and Storage*. 2016, Technische Universität München.
232. Villullas, H. and Teijelo, M.L., *The hanging-meniscus rotating disk (HMRD) Part 1. Dependence of hydrodynamic behavior on experimental variables*. *Journal of Electroanalytical Chemistry* (1995), **384**: p. 25-30.
233. Xing, W., Yin, G., and Zhang, J., *Rotating electrode methods and oxygen reduction electrocatalysts*. 2014, Amsterdam: Elsevier. ISBN: 0444633286
234. Cahan, B.D. and Villullas, H.M., *The Hanging Meniscus Rotating-Disk (Hmrd)*. *Journal of Electroanalytical Chemistry* (1991), **307**: p. 263-268.
235. Villullas, H. and Teijelo, M.L., *The hanging meniscus rotating disk (HMRD) Part 2. Application to simple charge transfer reaction kinetics*. *Journal of Electroanalytical Chemistry* (1995), **385**: p. 39-44.
236. Villullas, H. and Teijelo, M.L., *The hanging meniscus rotating disk (HMRD) Part 3. Application to a charge transfer preceded by a chemical reaction in equilibrium*. *Journal of Electroanalytical Chemistry* (1996), **418**: p. 159-165.
237. Rizo, R., Herrero, E., and Feliu, J.M., *Oxygen reduction reaction on stepped platinum surfaces in alkaline media*. *Phys Chem Chem Phys* (2013), **15**: p. 15416-25.
238. Ragoisha, G.A. and Bondarenko, A.S., *Potentiodynamic electrochemical impedance spectroscopy*. *Electrochimica acta* (2005), **50**: p. 1553-1563.

239. Chang, B.Y. and Park, S.M., *Electrochemical impedance spectroscopy*. Annu Rev Anal Chem (Palo Alto Calif) (2010), **3**: p. 207-29.
240. Barsukov, Y. and Macdonald, J.R., *Electrochemical impedance spectroscopy. Characterization of Materials*. 2012, Hoboken: John Wiley & Sons, Inc. ISBN: 0471266965
241. Park, S.-M. and Yoo, J.-S., *Peer reviewed: electrochemical impedance spectroscopy for better electrochemical measurements*. Anal Chem (2003), **75**: p. 455A-461A.
242. Taguchi, S. and Feliu, J.M., *Electrochemical reduction of nitrate on Pt(S)[n(111) x (111)] electrodes in perchloric acid solution*. Electrochimica Acta (2007), **52**: p. 6023-6033.
243. Srejjic, I., Smiljanic, M., Rakocevic, Z., and Strbac, S., *Oxygen Reduction on Polycrystalline Pt and Au Electrodes in Perchloric Acid Solution in the Presence of Acetonitrile*. International Journal of Electrochemical Science (2011), **6**: p. 3344-3354.
244. Rossmeis, J., Karlberg, G.S., Jaramillo, T., and Nørskov, J.K., *Steady state oxygen reduction and cyclic voltammetry*. Faraday discussions (2009), **140**: p. 337-346.
245. Bondarenko, A.S., *Analysis of large experimental datasets in electrochemical impedance spectroscopy*. Anal Chim Acta (2012), **743**: p. 41-50.
246. Boukamp, B.A., *A Linear Kronig-Kramers Transform Test for Immittance Data Validation*. Journal of the electrochemical society (1995), **142**: p. 1885-1894.
247. Schiller, C.A., Richter, F., Gulzow, E., and Wagner, N., *Validation and evaluation of electrochemical impedance spectra of systems with states that change with time*. Physical Chemistry Chemical Physics (2001), **3**: p. 374-378.
248. Berkes, B.B., Maljus, A., Schuhmann, W., and Bondarenko, A.S., *Simultaneous Acquisition of Impedance and Gravimetric Data in a Cyclic Potential Scan for the Characterization of Nonstationary Electrode/Electrolyte Interfaces*. Journal of Physical Chemistry C (2011), **115**: p. 9122-9130.
249. Berkes, B.B., Henry, J.B., Huang, M., and Bondarenko, A.S., *Electrochemical characterisation of copper thin-film formation on polycrystalline platinum*. Chemphyschem (2012), **13**: p. 3210-7.
250. Dolin, P. and Ershler, B., *The kinetics of discharge and ionization of hydrogen adsorbed at Pt-electrode*. Zh. Fiz. Khim (1940), **14**: p. 886.
251. Randles, J.E.B., *Kinetics of Rapid Electrode Reactions*. Discussions of the Faraday Society (1947), **1**: p. 11-19.
252. Lasia, A., *Electrochemical impedance spectroscopy and its applications*. 1999, Springer. p. XV, 420.
253. Lasia, A., *Electrochemical impedance spectroscopy and its applications*, in *Modern aspects of electrochemistry*. 2002, Springer. p. 143-248.
254. Conway, B.E., Barber, J., and Morin, S., *Comparative evaluation of surface structure specificity of kinetics of UPD and OPD of H at single-crystal Pt electrodes*. Electrochimica Acta (1998), **44**: p. 1109-1125.
255. Morin, S., Dumont, H., and Conway, B.E., *Evaluation of the effect of two-dimensional geometry of Pt single-crystal faces on the kinetics of upd of H using impedance spectroscopy*. Journal of Electroanalytical Chemistry (1996), **412**: p. 39-52.
256. Sibert, E., Faure, R., and Durand, R., *High frequency impedance measurements on Pt(111) in sulphuric and perchloric acids*. Journal of Electroanalytical Chemistry (2001), **515**: p. 71-81.
257. Colic, V., Tymoczko, J., Maljus, A., Ganassin, A., Schuhmann, W., and Bandarenka, A.S., *Experimental Aspects in Benchmarking of the Electrocatalytic Activity*. Chemelectrochem (2015), **2**: p. 143-149.

258. Kurth, S., Perdew, J.P., and Blaha, P., *Molecular and solid-state tests of density functional approximations: LSD, GGAs, and meta-GGAs*. International Journal of Quantum Chemistry (1999), **75**: p. 889-909.
259. Hammer, B. and Norskov, J.K., *Theoretical surface science and catalysis - Calculations and concepts*. Advances in Catalysis, Vol 45 (2000), **45**: p. 71-129.
260. Schnur, S. and Gross, A., *Strain and coordination effects in the adsorption properties of early transition metals: A density-functional theory study*. Physical Review B (2010), **81**: p. 033402.
261. Hofmann, T., Yu, T.H., Folse, M., Weinhardt, L., Bar, M., Zhang, Y.F., Merinov, B.V., Myers, D.J., Goddard, W.A., and Heske, C., *Using Photoelectron Spectroscopy and Quantum Mechanics to Determine d-Band Energies of Metals for Catalytic Applications*. Journal of Physical Chemistry C (2012), **116**: p. 24016-24026.
262. Greeley, J. and Norskov, J.K., *Large-scale, density functional theory-based screening of alloys for hydrogen evolution*. Surface Science (2007), **601**: p. 1590-1598.
263. Nørskov, J.K., Bligaard, T., Logadottir, A., Kitchin, J., Chen, J.G., Pandelov, S., and Stimming, U., *Trends in the exchange current for hydrogen evolution*. Journal of The Electrochemical Society (2005), **152**: p. J23-J26.
264. Skúlason, E., Tripkovic, V., Björketun, M.E., Gudmundsdottir, S., Karlberg, G., Rossmeis, J., Bligaard, T., Jónsson, H., and Nørskov, J.K., *Modeling the electrochemical hydrogen oxidation and evolution reactions on the basis of density functional theory calculations*. The Journal of Physical Chemistry C (2010), **114**: p. 18182-18197.
265. Hoshi, N., Nakamura, M., Sakata, O., Nakahara, A., Naito, K., and Ogata, H., *Surface X-ray scattering of stepped surfaces of platinum in an electrochemical environment: Pt(331) = 3(111)-(111) and Pt(511) = 3(100)-(111)*. Langmuir (2011), **27**: p. 4236-42.
266. Marković, N., Grgur, B., Lucas, C., and Ross, P., *Surface electrochemistry of CO on Pt(110)-(1×2) and Pt(110)-(1×1) surfaces*. Surface Science (1997), **384**: p. L805-L814.
267. Attard, G.A., Brew, A., Hunter, K., Sharman, J., and Wright, E., *Specific adsorption of perchlorate anions on Pt{hkl} single crystal electrodes*. Phys Chem Chem Phys (2014), **16**: p. 13689-98.
268. Ledezma-Yanez, I., Wallace, W.D.Z., Sebastian-Pascual, P., Climent, V., Feliu, J.M., and Koper, M.T.M., *Interfacial water reorganization as a pH-dependent descriptor of the hydrogen evolution rate on platinum electrodes*. Nature Energy (2017), **2**: p. 17031.
269. Tymoczko, J., Calle-Vallejo, F., Schuhmann, W., and Bandarenka, A.S., *Making the hydrogen evolution reaction in polymer electrolyte membrane electrolyzers even faster*. Nat Commun (2016), **7**: p. 10990.
270. Kajiwar, R., Asami, Y., Nakamura, M., and Hoshi, N., *Active sites for the hydrogen oxidation and the hydrogen evolution reactions on the high index planes of Pt*. Journal of Electroanalytical Chemistry (2011), **657**: p. 61-65.
271. Markovic, N.M., Grgur, B.N., and Ross, P.N., *Temperature-dependent hydrogen electrochemistry on platinum low-index single-crystal surfaces in acid solutions*. Journal of Physical Chemistry B (1997), **101**: p. 5405-5413.
272. Crabtree, G.W., Dresselhaus, M.S., and Buchanan, M.V., *The hydrogen economy*. Physics Today), **57**: p. 39-44.
273. Gasteiger, H.A., Kocha, S.S., Sompalli, B., and Wagner, F.T., *Activity benchmarks and requirements for Pt, Pt-alloy, and non-Pt oxygen reduction catalysts for PEMFCs*. Applied Catalysis B-Environmental (2005), **56**: p. 9-35.
274. Gasteiger, H.A. and Markovic, N.M., *Chemistry. Just a dream--or future reality?* Science (2009), **324**: p. 48-9.

275. Zhang, J., *PEM fuel cell electrocatalysts and catalyst layers: fundamentals and applications*. 2008, Berlin: Springer Science & Business Media. ISBN: 978184800-9363
276. Markovic, N.M. and Ross, P.N., *Electrocatalysts by design: from the tailored surface to a commercial catalyst*. *Electrochimica Acta* (2000), **45**: p. 4101-4115.
277. Larminie, J., Dicks, A., and McDonald, M.S., *Fuel cell systems explained*. Vol. 2. 2003, Hoboken: John Wiley & Sons Ltd. ISBN: 9780470848579
278. Bandarenka, A.S. and Koper, M.T.M., *Structural and electronic effects in heterogeneous electrocatalysis: Toward a rational design of electrocatalysts*. *Journal of Catalysis* (2013), **308**: p. 11-24.
279. Stamenkovic, V.R., Mun, B.S., Mayrhofer, K.J., Ross, P.N., and Markovic, N.M., *Effect of surface composition on electronic structure, stability, and electrocatalytic properties of Pt-transition metal alloys: Pt-skin versus Pt-skeleton surfaces*. *J Am Chem Soc* (2006), **128**: p. 8813-9.
280. Holton, O.T. and Stevenson, J.W., *The Role of Platinum in Proton Exchange Membrane Fuel Cells Evaluation of platinum's unique properties for use in both the anode and cathode of a proton exchange membrane fuel cell*. *Platinum Metals Review* (2013), **57**: p. 259-271.
281. Nie, Y., Li, L., and Wei, Z., *Recent advancements in Pt and Pt-free catalysts for oxygen reduction reaction*. *Chem Soc Rev* (2015), **44**: p. 2168-201.
282. Kocha, S., *Chapter 3-Electrochemical Degradation: Electrocatalyst and Support Durability A2-Veziroglu, Matthew M. MenchEmin Caglan KumburT. Nejat*. *Polymer Electrolyte Fuel Cell Degradation*: p. 89-214.
283. Yu, X.W. and Ye, S.Y., *Recent advances in activity and durability enhancement of Pt/C catalytic cathode in PEMFC - Part II: Degradation mechanism and durability enhancement of carbon supported platinum catalyst*. *Journal of Power Sources* (2007), **172**: p. 145-154.
284. Dillich, S., Ramsden, T., and Melina, M., *DOE Hydrogen and Fuel Cells Program Record*. Department of Energy (DOE) (2012).
285. Rice, C.A., Urchaga, P., Pistono, A.O., McFerrin, B.W., McComb, B.T., and Hu, J.W., *Platinum Dissolution in Fuel Cell Electrodes: Enhanced Degradation from Surface Area Assessment in Automotive Accelerated Stress Tests*. *Journal of the Electrochemical Society* (2015), **162**: p. F1175-F1180.
286. Pinto, L.M., Quaino, P., Arce, M.D., Santos, E., and Schmickler, W., *Electrochemical adsorption of OH on Pt(111) in alkaline solutions: combining DFT and molecular dynamics*. *Chemphyschem* (2014), **15**: p. 2003-9.
287. Kleis, J., Greeley, J., Romero, N.A., Morozov, V.A., Falsig, H., Larsen, A.H., Lu, J., Mortensen, J.J., Dulak, M., Thygesen, K.S., Norskov, J.K., and Jacobsen, K.W., *Finite Size Effects in Chemical Bonding: From Small Clusters to Solids*. *Catalysis Letters* (2011), **141**: p. 1067-1071.
288. Shustorovich, E. and Sellers, H., *The UBI-QEP method: a practical theoretical approach to understanding chemistry on transition metal surfaces*. *Surface Science Reports* (1998), **31**: p. 5-119.
289. Groß, A., *Adsorption at nanostructured surfaces from first principles*. *Journal of Computational and Theoretical Nanoscience* (2008), **5**: p. 894-922.
290. Peterson, A.A., Grabow, L.C., Brennan, T.P., Shong, B.G., Ooi, C.C., Wu, D.M., Li, C.W., Kushwaha, A., Medford, A.J., Mbuga, F., Li, L., and Norskov, J.K., *Finite-Size Effects in O and CO Adsorption for the Late Transition Metals*. *Topics in Catalysis* (2012), **55**: p. 1276-1282.

291. Norskov, J.K., Bligaard, T., Rossmeisl, J., and Christensen, C.H., *Towards the computational design of solid catalysts*. Nat Chem (2009), **1**: p. 37-46.
292. Strasser, P., Koh, S., and Greeley, J., *Voltammetric surface dealloying of Pt bimetallic nanoparticles: an experimental and DFT computational analysis*. Phys Chem Chem Phys (2008), **10**: p. 3670-83.
293. Topalov, A.A., Katsounaros, I., Auinger, M., Cherevko, S., Meier, J.C., Klemm, S.O., and Mayrhofer, K.J., *Dissolution of platinum: limits for the deployment of electrochemical energy conversion?* Angew Chem Int Ed Engl (2012), **51**: p. 12613-5.
294. Johnson, D., Napp, D., and Bruckenstein, S., *A ring-disk electrode study of the current/potential behaviour of platinum in 1.0 M sulphuric and 0.1 M perchloric acids*. Electrochimica Acta (1970), **15**: p. 1493-1509.
295. Koper, M.T. and Lukkien, J.J., *Modeling the butterfly: the voltammetry of ( $\sqrt{3} \times \sqrt{3}$ ) R30 and p ( $2 \times 2$ ) overlayers on (111) electrodes*. Journal of Electroanalytical Chemistry (2000), **485**: p. 161-165.
296. Huang, Y.F., Kooyman, P.J., and Koper, M.T., *Intermediate stages of electrochemical oxidation of single-crystalline platinum revealed by in situ Raman spectroscopy*. Nat Commun (2016), **7**: p. 12440.
297. Bondarenko, A.S., Stephens, I.E.L., Hansen, H.A., Perez-Alonso, F.J., Tripkovic, V., Johansson, T.P., Rossmeisl, J., Norskov, J.K., and Chorkendorff, I., *The Pt(111)/Electrolyte Interface under Oxygen Reduction Reaction Conditions: An Electrochemical Impedance Spectroscopy Study*. Langmuir (2011), **27**: p. 2058-2066.
298. Subbaraman, R., Strmcnik, D., Paulikas, A.P., Stamenkovic, V.R., and Markovic, N.M., *Oxygen Reduction Reaction at Three-Phase Interfaces*. ChemPhysChem (2010), **11**: p. 2825-2833.
299. Subbaraman, R., Strmcnik, D., Stamenkovic, V., and Markovic, N.M., *Three phase interfaces at electrified metal– solid electrolyte systems 1. Study of the Pt (hkl)– Nafion interface*. The Journal of Physical Chemistry C (2010), **114**: p. 8414-8422.
300. Escudero-Escribano, M., Verdaguer-Casadevall, A., Malacrida, P., Gronbjerg, U., Knudsen, B.P., Jepsen, A.K., Rossmeisl, J., Stephens, I.E.L., and Chorkendorff, I., *Pt5Gd as a Highly Active and Stable Catalyst for Oxygen Electroreduction*. Journal of the American Chemical Society (2012), **134**: p. 16476-16479.
301. Suntivich, J., Gasteiger, H.A., Yabuuchi, N., Nakanishi, H., Goodenough, J.B., and Shao-Horn, Y., *Design principles for oxygen-reduction activity on perovskite oxide catalysts for fuel cells and metal-air batteries*. Nat Chem (2011), **3**: p. 546-50.
302. Lebedeva, N., Koper, M., Herrero, E., Feliu, J., and Van Santen, R., *Cooxidation on stepped Pt [ $n(111) \times (111)$ ] electrodes*. Journal of Electroanalytical Chemistry (2000), **487**: p. 37-44.
303. Schouten, K.J., van der Niet, M.J., and Koper, M.T., *Impedance spectroscopy of H and OH adsorption on stepped single-crystal platinum electrodes in alkaline and acidic media*. Phys Chem Chem Phys (2010), **12**: p. 15217-24.
304. Markovic, N.M. and Ross, P.N., *Surface science studies of model fuel cell electrocatalysts*. Surface Science Reports (2002), **45**: p. 121-229.
305. Van der Niet, M.J., Garcia-Araez, N., Hernández, J., Feliu, J.M., and Koper, M.T., *Water dissociation on well-defined platinum surfaces: The electrochemical perspective*. Catalysis Today (2013), **202**: p. 105-113.
306. Greeley, J., Rossmeisl, J., Hellman, A., and Norskov, J.K., *Theoretical trends in particle size effects for the oxygen reduction reaction*. Zeitschrift Fur Physikalische Chemie-

- International Journal of Research in Physical Chemistry & Chemical Physics (2007), **221**: p. 1209-1220.
307. Kimmel, G.A., Petrik, N.G., Dohnalek, Z., and Kay, B.D., *Crystalline ice growth on Pt(111): observation of a hydrophobic water monolayer*. Phys Rev Lett (2005), **95**: p. 166102.
308. Codorniu-Hernández, E. and Kusalik, P.G., *Mobility mechanism of hydroxyl radicals in aqueous solution via hydrogen transfer*. Journal of the American Chemical Society (2011), **134**: p. 532-538.
309. Picolin, A., Busse, C., Redinger, A., Morgenstern, M., and Michely, T., *Desorption of H<sub>2</sub>O from flat and stepped Pt (111)*. The Journal of Physical Chemistry C (2008), **113**: p. 691-697.
310. Climent, V., Markovic, N.M., and Ross, P.N., *Kinetics of oxygen reduction on an epitaxial film of palladium on Pt(111)*. Journal of Physical Chemistry B (2000), **104**: p. 3116-3120.
311. Clavilier, J., El Achi, K., and Rodes, A., *In situ characterization of the Pt (S)-[n (111)/sx (111)] electrode surfaces using electrosorbed hydrogen for probing terrace and step sites*. Journal of electroanalytical chemistry and interfacial electrochemistry (1989), **272**: p. 253-261.
312. Clavilier, J. and Rodes, A., *Electrochemical Detection and Characterization at Pt(N,N,N-2) Oriented Electrodes of Multiatomic Step Formation Induced by Quenching at High-Temperatures*. Journal of Electroanalytical Chemistry (1993), **348**: p. 247-264.
313. Berkes, B.z.B., Inzelt, G.r., Schuhmann, W., and Bondarenko, A.S., *Influence of Cs<sup>+</sup> and Na<sup>+</sup> on specific adsorption of \*OH, \*O, and \*H at platinum in acidic sulfuric media*. The Journal of Physical Chemistry C (2012), **116**: p. 10995-11003.
314. Bondarenko, A.S., Stephens, I.E.L., Bech, L., and Chorkendorff, I., *Probing adsorption phenomena on a single crystal Pt-alloy surface under oxygen reduction reaction conditions*. Electrochimica Acta (2012), **82**: p. 517-523.
315. Tymoczko, J., Colic, V., Bandarenka, A.S., and Schuhmann, W., *Detection of 2D phase transitions at the electrode/electrolyte interface using electrochemical impedance spectroscopy*. Surface Science (2015), **631**: p. 81-87.
316. Karlberg, G.S., *Adsorption trends for water, hydroxyl, oxygen, and hydrogen on transition-metal and platinum-skin surfaces*. Physical Review B (2006), **74**: p. 153414.
317. Casalongue, H.S., Kaya, S., Viswanathan, V., Miller, D.J., Friebel, D., Hansen, H.A., Nørskov, J.K., Nilsson, A., and Ogasawara, H., *Direct observation of the oxygenated species during oxygen reduction on a platinum fuel cell cathode*. Nature Communications (2013), **4**: p. 2817.
318. Li, H.J., Li, Y.D., Koper, M.T.M., and Calle-Vallejo, F., *Bond-Making and Breaking between Carbon, Nitrogen, and Oxygen in Electrocatalysis*. Journal of the American Chemical Society (2014), **136**: p. 15694-15701.
319. Kolb, M.J., Calle-Vallejo, F., Juurlink, L.B., and Koper, M.T., *Density functional theory study of adsorption of H<sub>2</sub>O, H, O, and OH on stepped platinum surfaces*. J Chem Phys (2014), **140**: p. 134708.
320. Peng, G. and Mavrikakis, M., *Adsorbate diffusion on transition metal nanoparticles*. Nano Lett (2015), **15**: p. 629-34.
321. Lucas, C.A., Markovic, N.M., and Ross, P.N., *Surface structure and relaxation at the Pt(110)/electrolyte interface*. Physical Review Letters (1996), **77**: p. 4922-4925.
322. Attard, G.A. and Brew, A., *Cyclic voltammetry and oxygen reduction activity of the Pt{110}-(1 x 1) surface*. Journal of Electroanalytical Chemistry (2015), **747**: p. 123-129.

323. Biener, J., Wittstock, A., Baumann, T.F., Weissmuller, J., Baumer, M., and Hamza, A.V., *Surface Chemistry in Nanoscale Materials*. Materials (2009), **2**: p. 2404-2428.
324. Perez-Alonso, F.J., McCarthy, D.N., Nierhoff, A., Hernandez-Fernandez, P., Strebel, C., Stephens, I.E., Nielsen, J.H., and Chorkendorff, I., *The effect of size on the oxygen electroreduction activity of mass-selected platinum nanoparticles*. Angew Chem Int Ed Engl (2012), **51**: p. 4641-3.
325. Shao, M., Peles, A., and Shoemaker, K., *Electrocatalysis on platinum nanoparticles: particle size effect on oxygen reduction reaction activity*. Nano Lett (2011), **11**: p. 3714-9.
326. Tripkovic, V., Cerri, I., Bligaard, T., and Rossmeisl, J., *The Influence of Particle Shape and Size on the Activity of Platinum Nanoparticles for Oxygen Reduction Reaction: A Density Functional Theory Study*. Catalysis Letters (2014), **144**: p. 380-388.
327. Tritsarlis, G.A., Greeley, J., Rossmeisl, J., and Norskov, J.K., *Atomic-Scale Modeling of Particle Size Effects for the Oxygen Reduction Reaction on Pt*. Catalysis Letters (2011), **141**: p. 909-913.
328. Nesselberger, M., Roefzaad, M., Hamou, R.F., Biedermann, P.U., Schweinberger, F.F., Kunz, S., Schloegl, K., Wiberg, G.K., Ashton, S., Heiz, U., Mayrhofer, K.J., and Arenz, M., *The effect of particle proximity on the oxygen reduction rate of size-selected platinum clusters*. Nat Mater (2013), **12**: p. 919-24.
329. Kang, Y., Ye, X., Chen, J., Cai, Y., Diaz, R.E., Adzic, R.R., Stach, E.A., and Murray, C.B., *Design of Pt-Pd binary superlattices exploiting shape effects and synergistic effects for oxygen reduction reactions*. J Am Chem Soc (2013), **135**: p. 42-5.
330. Chen, C., Kang, Y., Huo, Z., Zhu, Z., Huang, W., Xin, H.L., Snyder, J.D., Li, D., Herron, J.A., Mavrikakis, M., Chi, M., More, K.L., Li, Y., Markovic, N.M., Somorjai, G.A., Yang, P., and Stamenkovic, V.R., *Highly crystalline multimetallic nanoframes with three-dimensional electrocatalytic surfaces*. Science (2014), **343**: p. 1339-43.
331. Dubau, L., Lopez-Haro, M., Durst, J., Guetaz, L., Bayle-Guillemaud, P., Chatenet, M., and Maillard, F., *Beyond conventional electrocatalysts: hollow nanoparticles for improved and sustainable oxygen reduction reaction activity*. Journal of Materials Chemistry A (2014), **2**: p. 18497-18507.
332. Becknell, N., Kang, Y., Chen, C., Resasco, J., Kornienko, N., Guo, J., Markovic, N.M., Somorjai, G.A., Stamenkovic, V.R., and Yang, P., *Atomic Structure of Pt<sub>3</sub>Ni Nanoframe Electrocatalysts by in Situ X-ray Absorption Spectroscopy*. J Am Chem Soc (2015), **137**: p. 15817-24.
333. Gan, L., Cui, C., Heggen, M., Dionigi, F., Rudi, S., and Strasser, P., *Element-specific anisotropic growth of shaped platinum alloy nanocrystals*. Science (2014), **346**: p. 1502-6.
334. Kibsgaard, J., Gorlin, Y., Chen, Z., and Jaramillo, T.F., *Meso-structured platinum thin films: active and stable electrocatalysts for the oxygen reduction reaction*. J Am Chem Soc (2012), **134**: p. 7758-65.
335. Badwal, S.P.S., Giddey, S., Kulkarni, A., Goel, J., and Basu, S., *Direct ethanol fuel cells for transport and stationary applications - A comprehensive review*. Applied Energy (2015), **145**: p. 80-103.
336. Steele, B.C. and Heinzel, A., *Materials for fuel-cell technologies*. Nature (2001), **414**: p. 345-52.
337. Semelsberger, T.A., Borup, R.L., and Greene, H.L., *Dimethyl ether (DME) as an alternative fuel*. Journal of Power Sources (2006), **156**: p. 497-511.

338. Lebedeva, N.P., Koper, M.T.M., Feliu, J.M., and van Santen, R.A., *Role of crystalline defects in electrocatalysis: Mechanism and kinetics of CO adlayer oxidation on stepped platinum electrodes*. *Journal of Physical Chemistry B* (2002), **106**: p. 12938-12947.
339. Farias, M.J.S., Cheuquepan, W., Camara, G.A., and Feliu, J.M., *Disentangling Catalytic Activity at Terrace and Step Sites on Selectively Ru-Modified Well-Ordered Pt Surfaces Probed by CO Electro-oxidation*. *Acs Catalysis* (2016), **6**: p. 2997-3007.
340. Calle-Vallejo, F., Tymoczko, J., Colic, V., Vu, Q.H., Pohl, M.D., Morgenstern, K., Loffreda, D., Sautet, P., Schuhmann, W., and Bandarenka, A.S., *Finding optimal surface sites on heterogeneous catalysts by counting nearest neighbors*. *Science* (2015), **350**: p. 185-189.
341. Villegas, I. and Weaver, M.J., *Carbon monoxide adlayer structures on platinum (111) electrodes: A synergy between in-situ scanning tunneling microscopy and infrared spectroscopy*. *The Journal of chemical physics* (1994), **101**: p. 1648-1660.
342. Malacrida, P., Casalongue, H.G., Masini, F., Kaya, S., Hernandez-Fernandez, P., Deiana, D., Ogasawara, H., Stephens, I.E., Nilsson, A., and Chorkendorff, I., *Direct observation of the dealloying process of a platinum-yttrium nanoparticle fuel cell cathode and its oxygenated species during the oxygen reduction reaction*. *Phys Chem Chem Phys* (2015), **17**: p. 28121-8.
343. Wang, C., Markovic, N.M., and Stamenkovic, V.R., *Advanced Platinum Alloy Electrocatalysts for the Oxygen Reduction Reaction*. *Acs Catalysis* (2012), **2**: p. 891-898.
344. Wang, C., Chi, M.F., Li, D.G., van der Vliet, D., Wang, G.F., Lin, Q.Y., Mitchell, J.F., More, K.L., Markovic, N.M., and Stamenkovic, V.R., *Synthesis of Homogeneous Pt-Bimetallic Nanoparticles as Highly Efficient Electrocatalysts*. *Acs Catalysis* (2011), **1**: p. 1355-1359.
345. Paulus, U.A., Wokaun, A., Scherer, G.G., Schmidt, T.J., Stamenkovic, V., Markovic, N.M., and Ross, P.N., *Oxygen reduction on high surface area Pt-based alloy catalysts in comparison to well defined smooth bulk alloy electrodes*. *Electrochimica Acta* (2002), **47**: p. 3787-3798.
346. Stamenkovic, V., Schmidt, T.J., Ross, P.N., and Markovic, N.M., *Surface composition effects in electrocatalysis: Kinetics of oxygen reduction on well-defined Pt<sub>3</sub>Ni and Pt<sub>3</sub>Co alloy surfaces*. *Journal of Physical Chemistry B* (2002), **106**: p. 11970-11979.
347. Antolini, E., Salgado, J.R., and Gonzalez, E.R., *The stability of Pt-M (M= first row transition metal) alloy catalysts and its effect on the activity in low temperature fuel cells: a literature review and tests on a Pt-Co catalyst*. *Journal of Power Sources* (2006), **160**: p. 957-968.
348. Wu, J.F., Yuan, X.Z., Martin, J.J., Wang, H.J., Zhang, J.J., Shen, J., Wu, S.H., and Merida, W., *A review of PEM fuel cell durability: Degradation mechanisms and mitigation strategies*. *Journal of Power Sources* (2008), **184**: p. 104-119.
349. Pedersen, A.F., Ulrikkeholm, E.T., Escudero-Escribano, M., Johansson, T.P., Malacrida, P., Pedersen, C.M., Hansen, M.H., Jensen, K.D., Rossmeis, J., Friebel, D., Nilsson, A., Chorkendorff, I., and Stephens, I.E.L., *Probing the nanoscale structure of the catalytically active overlayer on Pt alloys with rare earths*. *Nano Energy* (2016), **29**: p. 249-260.
350. Vej-Hansen, U., Escudero-Escribano, M., Velázquez-Palenzuela, A., Malacrida, P., Rossmeis, J., Stephens, I., Chorkendorff, I., and Schiøtz, J., *New Platinum Alloy Catalysts for Oxygen Electroreduction Based on Alkaline Earth Metals*. *Electrocatalysis* (2017): p. 1-11.

351. Cohen, J.L., Volpe, D.J., and Abruna, H.D., *Electrochemical determination of activation energies for methanol oxidation on polycrystalline platinum in acidic and alkaline electrolytes*. *Phys Chem Chem Phys* (2007), **9**: p. 49-77.
352. Kunimatsu, K., Samant, M., and Seki, H., *In-situ FT-IR spectroscopic study of bisulfate and sulfate adsorption on platinum electrodes: Part 1. Sulfuric acid*. *Journal of electroanalytical chemistry and interfacial electrochemistry* (1989), **258**: p. 163-177.
353. Schmidt, T.J., Stamenkovic, V., Ross, P.N., and Markovic, N.M., *Temperature dependent surface electrochemistry on Pt single crystals in alkaline electrolyte - Part 3. The oxygen reduction reaction*. *Physical Chemistry Chemical Physics* (2003), **5**: p. 400-406.
354. Schmidt, T.J., Stamenkovic, V., Arenz, M., Markovic, N.M., and Ross, P.N., *Oxygen electrocatalysis in alkaline electrolyte: Pt(hkl), Au(hkl) and the effect of Pd-modification*. *Electrochimica Acta* (2002), **47**: p. 3765-3776.